



ANALYSIS STUDY OF THE AXIAL TRANSPORT AND HEAT TRANSFER OF A FLIGHTED ROTARY DRUM OPERATED AT OPTIMUM LOADING

Dissertation
zur Erlangung des akademischen Grades

Doktoringenieur
(Dr.-Ing.)

von M.Sc. Mohamed Ahmed Mahmoud Karali
geboren am: 01. Dezember 1979 in Kalyobiya, Ägypten

genehmigt durch die Fakultät für Verfahrens- und Systemtechnik
der Otto-von-Guericke-Universität Magdeburg

Gutachter:

Prof. Dr.-Ing. Eckehard Specht Institute of Fluid Dynamics and Thermodynamics, Universität Magdeburg, Germany.	(Betreuer und Gutachter)
JProf. Dr.-Ing. Fabian Herz Institute of Fluid Dynamics and Thermodynamics, Universität Magdeburg, Germany.	(Gutachter)
Dr.-Ing. Jochen Mellmann Department of post harvest technology, ATB Potsdam, Germany.	(Gutachter)

Eingereicht am: 07.07.2015

Promotionskolloquium am: 20.08.2015

This work is dedicated to...

my father Ahmed, my mother Samia, my wife Alaa and my son Malek

Preface

This dissertation is submitted to Otto von Guericke University, Magdeburg for the degree of Doctor of Philosophy. The research described herein was conducted under the supervision of Prof. Ekehard Specht between October 2012 and July 2015. To the best of my knowledge, this work is original, except where suitable references are made to previous works. Neither this, nor any substantially similar dissertation has been submitted for any degree, diploma or qualification at any other university or institution.

Mohamed A. Karali

Magdeburg, 06.07.2015

Think of it as having a wide target selection, where success is a journey; not a destination.

Acknowledgements

I would like to express my profound gratitude and sincere appreciation to my supervisor Prof. Dr.-Ing. Eckehard Specht for his inspiration, indispensable guidance and for teaching me invaluable knowledge throughout the course of my study. With his initial support, this great dream of mine can finally turn to reality, and with his endless guidance throughout the study, I was able to navigate the arduous path down to the very end. I am sure that whatever I have learned while working with him will be very useful in my future endeavors. He has been a great mentor.

I would like to express my thanks to the reviewers of this work JProf. Dr.-Ing. Fabian Herz and Dr.-Ing. Jochen Mellmann for accepting reviewing my work, providing ideas and text modifications to reshape the current work to be much better. One more time my thanks goes to JProf. Dr.-Ing. Fabian Herz for his continuous encouragement and help during my experimental work in the lab.

I am in deep gratitude to the Future University in Egypt (my main affiliation) for the financial support of my PhD study in Germany. First of all, I should mention Dr. Hassan Azazy the founder of this great establishment. After him I would like to send my thanks and greetings to Mr. Khaled Hassan Azazy, the chairman of the board of trustees of the Future University, for supporting the sending of researchers abroad to complete their studies. Believing in the idea that this kind of cooperation between universities will be beneficial to the Future University and also to our beloved Egypt. I would like to express my deepest gratitude to all people working at the Future University in Egypt. Special thanks to Prof. Dr. Adel Sakr, Prof. Dr.-Ing. Mohamad A. Badr and Prof. Dr.-Ing. Mahmoud Abdelrasheed, for their continued encouragement and valuable advices during all stages in the preparation of this work.

I would like to express my gratitude and thanks to the following people close to me: Herr. Tino Redemann for his continued help and kind, useful discussions. My office-mate Dr.-Ing. Koteswara Rao Sunkara for the useful scientific discussions where his work was a good guide for my PhD. All of our group members for every nice moment spent together, especially Dr.Ing. Janan Al-Karawi, Mr. Ali Mohsan, Mr. Abdelkader Abdelwahab, Mr. Bassam Hallak, Mr. Adnan Tuaamah and Ms. Ainaa Nafsun. My Thanks to our institute secretary Frau. Christin Hasemann for her help with the administrations of my work. Also my thanks goes to all the workers and technicians in the lab, especially to Herr.Timpe for his help and perfect work.

It is my duty to thank the people who worked on the Mathworks - Matlab Center web site (www.mathworks.com) for their great efforts in connecting people searching for solving engineering problems with the most experienced people working in these fields.

I cannot leave without acknowledging all of my Egyptian colleagues in Magdeburg, where without their support and help from the first moment I arrived Germany, It would have been very hard for me to manage my life: Dr.-Ing. Essam Elgendy, Dr.-Ing. Ahmed Hassan and Dr.-Ing. Hassanain Refay. Special thanks from the bottom of my heart to Dr.-Ing. Abouelmagd H. Abdelsamie who helped me with many things including my study.

I am indebted to my parents who grown me up with the good manners that has credited all the successes in my life. My beloved wife Alaa, she always supported me in the hardest times I encountered during this work. She and my son Malek are the most beautiful things in my life.

Finally, I would like to express my gratitude to everyone who helped me shape the ideas explored in this dissertation, either by giving technical advice or encouraging and supporting my work in many other ways. This dissertation would not have come into existence without their hands-on advice and motivation.

Abstract

The objective of the present work is to study the performance of a flighted rotary drum operated at optimum loading (design loading). A lot of experiments were carried out on a 0.5 m diameter and 0.15 m length batch rotary drum furnished internally with rectangular flights to assess the design loading. Different loadings were examined through two image analysis methods (manual and automated) of the recorded videos from under loading to over loading, including design loading. Many solid materials (free flowing) with different particle diameters and angles of repose, varied rotational speeds (from 1 to 5 rpm), two numbers of flights (12 and 18), and two flight length ratios (0.375 and 0.75) were researched. The automated method of the image analysis showed significant time saving for the extraction process of the data from the experimental work. However some problems were found when applying the automated method on the current experimental work images. Indicating that a new experimental technique should be developed to facilitate both manual and automated methods. An extension for the experimental work was conducted using a bigger drum of 1.0 m diameter and 0.3 m length. This extension was based on using a new experimental technique by modifying the location of both the camera and light. The discharge characteristics of the drum were studied in order to get information about the flights holdups, cascading rate and the curtain's height of fall.

A comparison was conducted between the experimental results and some available design loading models from literature and a new fitting factor was proposed. A correlation in terms of the filling degree of design loading conditions and function of all operating parameters was developed.

A novel mathematical model was proposed to study the axial transport of solids along the rotary drum using the available experimental results presented in the current work with the application of a case study. This model is able to predict the

mean residence time of the solid along the drum. The calculated mean residence time is compared with models available from literature and a new fitting factor was proposed.

A mathematical model was developed to describe the heat transfer mechanism in a flighted rotary cooler with application from industry. The results from the heat transfer model gives information about the temperature profiles of the solid and the air along the drum. Two approaches were introduced to calculate the heat transfer area in a flighted rotary drum. New factors for Nusselt correlations of the two approaches were proposed.

Zusammenfassung

Das Ziel der vorliegenden Arbeit ist die Untersuchung des Verhaltens der Partikelbewegung in Drehrohren mit rechteckigen Hubschaufeln. Zur Beurteilung einer optimalen Beladung dieser Hubschaufeln wurden eine Vielzahl von Experimenten an einer Drehtrommel mit einem Durchmesser von 0.5 m und einer Länge von 0.15 m durchgeführt. Dabei wurde stets der stationäre Arbeitspunkt der Partikelbewegung in dieser Drehtrommel betrachtet. Betriebszustände von zu geringer Beladung, optimaler Beladung bis hin zu einer Überladung der Trommel wurden untersucht. Die Schüttgutbewegung wurde mit einer hochauflösenden Kamera aufgezeichnet und mit Hilfe zwei verschiedener Auswertemethoden (manuell und automatisch) analysiert. Für die Versuche wurden Materialien (trocken und monodispers) mit unterschiedlichem Partikeldurchmesser und somit verschiedenem Böschungswinkel verwendet. Dabei wurden die Umdrehungsgeschwindigkeit (von 1 bis 5 U/min), die Anzahl der Hubschaufeln (12 und 18) und das Längenverhältnis der Hubschaufelkanten (0.375 and 0.75) variiert. Durch die Einführung der automatischen Auswertemethode des Bildmaterials konnte der Zeitaufwand der Datenanalyse signifikant reduziert werden.

Der Entleerungsvorgang der Hubschaufeln wurde untersucht, um Aussagen über den Beladungszustand, die Ausflussrate und die Höhe der Partikelschleier zu erhalten. Es wurde ein Vergleich angestellt zwischen den erhaltenen experimentellen Ergebnissen und den verfügbaren Modellen in der Literatur, die den optimalen Beladungszustand beschreiben. Aufgrund der gewonnenen Erkenntnisse wird ein neuer Anpassungsparameter für die bestehenden Modelle vorgeschlagen. Die Auswirkung einer Maßstabsvergrößerung auf den Beladungszustand der Hubschaufeln wurde

anhand von Versuchen an einer Drehtrommel mit dem Durchmesser von 1.0 m und einer Länge von 0.3 m untersucht. Dabei konnte das experimentelle Vorgehen so angepasst werden, dass die manuelle sowie automatische Auswertemethode des Bildmaterials erleichtert wurde.

Des Weiteren wurde ein mathematisches Modell entwickelt, das den Wärmeübergangsmechanismus im Drehrohr auf Basis der mittleren Verweilzeit für das genannte Fallbeispiel beschreibt. Ferner kann dieses Modell zur Vorhersage der axialen Temperaturprofile des Schüttbettes und der damit in Kontakt stehenden Gasatmosphäre genutzt werden.

Nomenclature

A	drum cross section area	[m ²]
A _{sur}	heat transfer surface area (Ch. 6)	[m ²]
a	acceleration	[m/s ²]
a ₁	constant in Eq. (5.5)	
C _D	drag coefficient	[-]
c _p	specific heat at constant pressure	[kJ/kg·K]
c _s	specific heat of solid material	[kJ/kg·K]
D	drum diameter	[m]
d _p	particle diameter	[m]
f	filling degree	[%]
F	force	[N]
Fr	Froude number, $Fr = \omega^2 R / g$	[-]
g	gravitational acceleration	[m/s ²]
h	solid height of fall	[m]
H	holdup	[m ³ /m or cm ²]
h _{conv}	convection heat transfer coefficient (Ch. 6)	[W/m ³ ·K]
K	coefficient in Eq. (5.6)	
k	coefficient in Eq. (5.8)	
k	thermal conductivity (Ch. 6)	[W/m·K]
L	drum length	[m]
l ₁	flight radial length	[m]
l ₂	flight tangential length	[m]
LMTD	Logarithmic temperature difference	[°C]
m	mass	[kg]
N	rotational speed	[rpm]

n_F	total number of flights	[-]
Nu	Nusselt number, $Nu = h_{conv} L / k$	[-]
Pr	Prandtl number	[-]
Q	heat rate	[W]
R	drum radius	[m]
Re	Reynolds number	[-]
r_H	effective radial distance of the flight	[m]
$RMSD$	root mean square deviation	
S	gas borne phase to flight borne phase ratio	[-]
t	time	[s]
T	temperature	[°C]
u	velocity	[m/s]
U_e	overall heat transfer loss coefficient	[W/m ² ·K]
U_v	volumetric overall heat transfer coefficient between solid and air	[W/m ³ ·K]
V	drum volume	[m ³]
x	axial position presented in Ch. 6	[m]
X	particle axial advance	[m]
Y	particle falling height	[m]
z	dimensionless length presented in Ch. 6	[-]

Greek letters

α	flight tangential angle	[°]
β	inclination angle of the drum	[°]
γ	kinetic angle of repose of solid reside inside the flight	[°]
δ	flight tip angle	[°]
Θ_A	solid dynamic angle of repose	[°]
μ	dynamic viscosity	[m ² /s]
ρ	density	[kg/m ³]
τ	mean residence time	[s]
ω	angular velocity	[rad/s]

Subscripts

A	angle of repose
a	air
avg	average
b	solid bulk (consolidated)
d	drum
design	design loading conditions
F	flight
FUF	first unloading flight
g	gas
i	directional coordinates implies the flights
L	final discharge angle
LUF	last unloading flight
p	particle
r	relative
s	solid material
Tot	total
x	directional coordinates implies the axial direction
y	directional coordinates implies falling direction
e	heat loss
sa	solid-air
sw	solid- drum wall
wa	drum wall-air

Contents

Preface	iii
Acknowledgements	v
Abstract	vii
Zusammenfassung	ix
Nomenclature	xi
Contents	xv
1 Introduction	1
1.1 Granular materials	1
1.2 Granular material flows	2
1.3 Rotary drums	5
1.3.1 Principles	5
1.3.2 Rotary kilns	5
1.3.3 Rotary dryers	7
1.4 Flights	8
1.5 Loading of flighted rotary drums	11
1.6 Thesis outline	16
2 Experimental determination of the optimum loading of a flighted rotary drum	17
2.1 Experimental setup	17
2.1.1 Experimental test rig	17
2.2.2 Experimental procedures	19
2.2.3 Experimental program	20
2.3 Data Processing	21

2.3.1	Design loading determination criterion	21
2.3.2	Data extraction sequence	21
2.3.3	Image analysis	24
2.3.4	Manual method	26
2.3.5	Automated method	27
2.3.6	Automated method validation	31
2.4	Data fitting	32
2.5	Results and Discussions	32
2.5.1	Influence of number of flights	32
2.5.2	Influence of flight length ratio	35
2.5.3	Influence of Material properties	37
2.5.4	Discharge angle	38
2.6	Comparisons with models from literature	39
3	New experimental technique and scale up	43
3.1	Background	43
3.2	New innovative experimental technique	43
3.3	New experimental work and scaling up the drum size	46
3.4	Results and discussions	48
3.4.1	Influence of number of flights	48
3.4.2	Influence of flight length ratio	50
3.4.3	Comparisons with models from literature	51
3.4.4	Scaling up the drum size	53
3.5	Correlation development	54
4	Determination of the discharge characteristics	57
4.1	Overview	57
4.2	Geometrical parameters	58
4.3	Kinetic angle of repose of the solid residing inside the flight	58
4.4	Flight holdup	63
4.5	Final discharge angle of flight	65
4.6	Flight cascading rate	68
4.7	Curtains height of fall	70

4.7.1	Measured height of fall	70
4.7.2	Mean height of fall	72
5	Axial transport	75
5.1	Introduction	75
5.2	Physical description of the axial transport in a rotary drum	76
5.3	Models from literature	76
5.3	Current work model description	81
5.3.1	Model assumptions	81
5.3.2	Equationing	81
5.4	Case study	85
5.4.1	Given data	85
5.4.2	Results	86
5.5	Direct application of the model (using in industry)	90
6	Heat transfer	91
6.1	Introduction	91
6.2	Model description	95
6.3	Case study	99
6.3.1	Case study description	99
6.3.2	Results	100
6.4	Defining the heat transfer area	102
6.4.1	First approach (flow over flat plate)	103
6.4.2	Second approach (flow over a spherical particle)	103
6.4.3	New suggested factors for Nusselt correlations	105
7	Conclusions and Outlook	107
7.1	Conclusions	107
7.2	Outlook	109
	Bibliography	111
	Internet web links	123
	List of publications of the current work	124
	Curriculum Vitae	125

Chapter 1

Introduction

1.1 Granular materials

A granular material is defined as a collection of discrete macroscopic particles of sizes larger than $1\ \mu\text{m}$ (**Rodhes, 1997, Duran, 1999** and **Gennes, 1999**). Many basic products in our daily life including a variety of building materials, chemicals, pharmaceuticals and food are granular, such as: sand, sugar, corn, wheat, salt, peanuts, flour, cement, limestone, fertilizers, wood chips, pills etc., see Fig. 1.1 (a). Although the granular particle is of solid nature it can flows like liquids as the sand do in an hourglass (see Fig. 1.1 (b)), or when a cereal flows from silos, also it takes the shape of its container (**Menon and Durian, 1997, Kadanoff, 1999, Midi, 2004, Job et al., 2006, Bierwisch, 2009**). Thus granular materials can be categorized as a new form of matter with quit different properties than solids, liquids and gases. Granular materials are characterized by forming such heaps or piles when resting on a surface (see Fig. 1.1 (c)), by adding more material the pile will grow until its slope reaches a critical angle (the critical angle of repose), determined by the size and stickiness of the grains. Beyond the critical angle, there is some sort of avalanches will happen (**Evesque, 1992, Jaeger and Nagel, 1992** and **Frette et al., 1996**). Wet sand can be formed into sandcastles and even, as shown in Fig. 1.1 (d), stable arches. But adding too much water weakens the sand, so it is no longer can support itself.



(a) Examples of granular materials



(b) Sand hourglass



(c) Different sand piles



(d) Wet sand arches

Figure 1.1: Different granular material characteristics - photos from internet [1].

1.2 Granular material flows

Typical flows of granular materials are illustrated in Fig. 1.2 (**Forterre and Pouliquen, 2008** and **Sunkara, 2013**). The granular materials flows can be classified into two categories: the flow confined between two surfaces (Fig. 1.2 (a)-(c)) and the free surface flows (Fig. 1.2 (d)-(f)). Free surface flows develop a flowing layer on top of a static bed which is slightly inclined to the horizontal. They have diverse applications in various industries as well as in the geological practice (**Khakhar et al., 2001**).

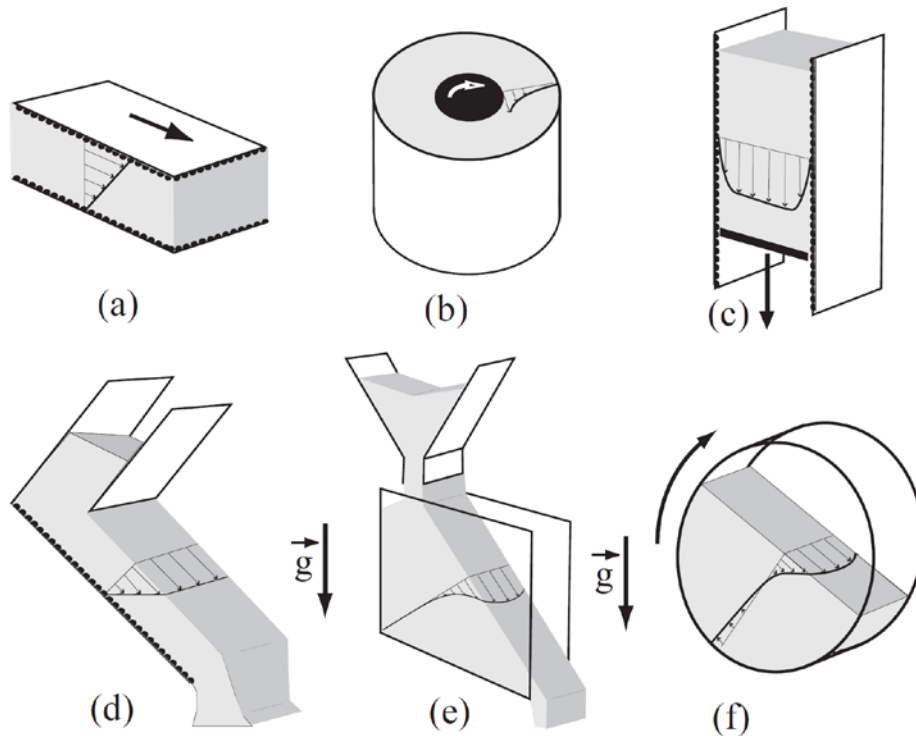


Figure 1.2: Typical flows of granular material (a) plane shear, (b) annular shear, (c) vertical-chute flows, (d) inclined plane, (e) heap flow, (f) rotating drum (**Forterre and Pouliquen, 2008** and **Sunkara, 2013**).

For the flow of granular material in rotating cylinders (rotary drums, will described in section 1.3) the material is stable till the inclination of the free surface is less than the dynamic angle of repose (Θ_A) (see Fig. 1.3). Increasing beyond this angle leads to change the stability of the system and a continuous flow of the material is possible only after the maximum angle of stability. Distinct motion behaviors were identified for the granular matter in the transverse section of a rotating drum: slipping, slumping, rolling, cascading, cataracting, and centrifuging (**Henein, 1983, Mellmann, 2001, Mellmann et al., 2001** and **Longo and Lamberti, 2002**). The kind of motion depends on the nature of the material, drum speed, filling degree, and roughness of the drum walls. The most common modes of motion behaviors for the industrial rotary drums are slumping and rolling (**Mellmann, 1989, Perron and Bui, 1992, Elperin and Vikhansky, 1998** and **Boateng, 1998**). During the slumping mode the material oscillates between two angles, upper and lower angles of repose for every avalanche (**Liu et al., 2005**). However, the avalanches are not continuous in this case. Increasing the drum speed progressively, increases the frequency of avalanches

which then leads to rolling motion by rolling down the particles continuously. The surface of the material becomes nearly flat for such motion behavior. This is the desired mode of operation in the industries for a better performance of the drums. Due to the fast renewal of the surface the mixing behavior improves. In rotary drums the filling degree, and the characteristics of the material changes along the length of the drum. As a result, the rolling and slumping modes occur at different sections of the drum depending on the filling degree.

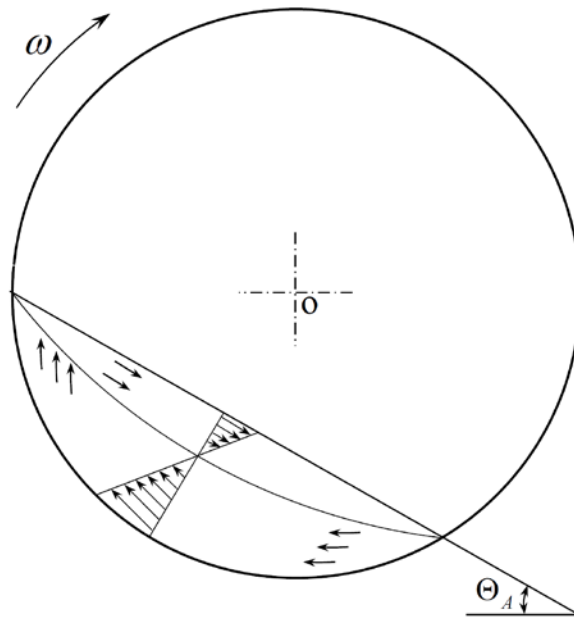


Figure 1.3: Transverse motion of a granular material in a rotating drum (Sunkara, 2013).

1.3 Rotary drums

1.3.1 Principles

Rotary drums are essential in industry for the manufacturing and the processing of different granular materials with free flowing or cohesive nature. Rotary kilns, rotary dryers and rotary coolers are the most commonly used types of rotary drums within industry. A rotary drum consists of a long cylinder inclined to the horizontal and have the possibility to rotate around its axis. The solid granular feed is introduced into the upper end of the drum by various methods including inclined chutes, overhung screw conveyors and slurry pipes. The charge then travels down along the kiln by axial and circumferential movements, due to the drum's inclination and rotation. During the travelling of the solid it interacts with a processing gas along the drum specially in the gas-borne area for a certain process, in either counter or co-current flow directions (**Friedman and Marshall, 1949**), until the processed solid discharged from the other end of the drum. In the following are more description of the rotary drums applications.

1.3.2 Rotary kilns

The rotary kiln is one of the most widely used industrial reactors for high temperature processes (will presented below) involving solids. Thus Its metal cylinder always lined with bricks or refractory. The kiln inclination depends on the process with a typical range of values from 1.1° - 3.6° . Different rotational speeds are used depending on the process and kiln size from very low, i.e., a peripheral speed of 1 rpm, for a TiO_2 pigment kiln, to 1.4 rpm for a cement kiln, to 4 rpm for a unit calcining phosphate material. The sizes of industrial kilns range from 1.7 m (Internal diameter) x 11.8 m long for firing light weight aggregate, to 5.9 m x 125 m for iron ore direct reduction. Direct firing or indirect heating may be used, and the kiln can operate in either co-current or counter-current flow. Solids may be fed either in the dry state, or as a wet state (**Sullivan et al., 1927, Tscheng, 1978 and Henein, 1983**).

The main uses of rotary kilns are in the processes of calcining, fusing, nodulizing, roasting, incinerating, and reducing of solid materials. Lime, magnesia and alumina are calcined to release carbon dioxide and water, at temperatures in the ranges of 1260-1500 K. The nodulizing process is applied to phosphate rock and certain iron ores with temperatures, 1500 to 1600 K. Roasting occurs at temperatures between 800 K and 1600 K, to oxidize and drive off sulfur and arsenic from various ores, including gold, silver, iron, etc. The rotary kiln is successfully used as a pre-combustion reactor for incineration of plastics wastes. The temperatures in this process are in the range of 570-970 K. Iron ore reduction is typical of reducing processes carried out in rotary kilns. The reaction temperatures are around 1300 K. A considerable portion of the kiln length may be used to dry solids and bring them up to reaction temperature. In a typical wet process cement kiln, 60% of the 137 meter kiln length is required to dry the slurry and heat solids to 1100 K (Tscheng, 1978). An schematic diagram of a rotary kiln arrangement is shown in Fig. 1.4.

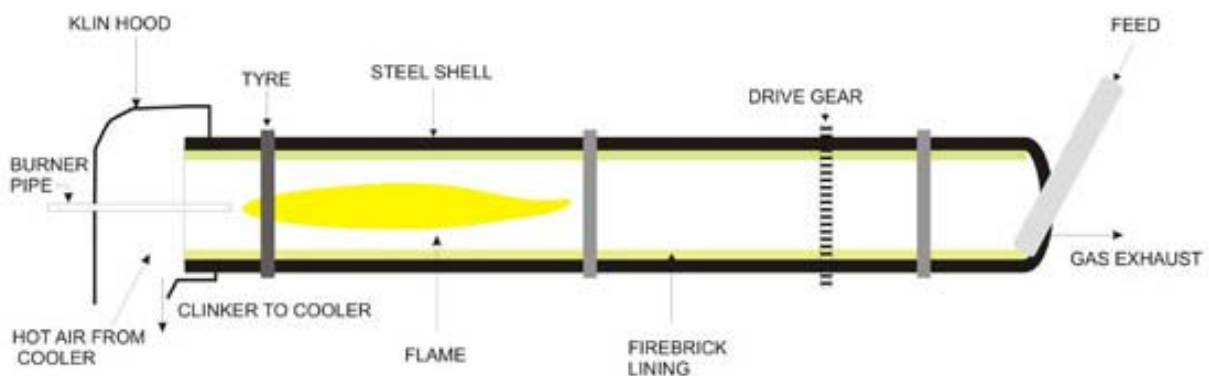


Figure 1.4: Rotary kiln arrangement - photos from internet [2].

1.3.3 Rotary dryers

It is worth to define the term drying or dehydration at the beginning, as it refers to removal of moisture from the matter by evaporation under controlled condition (**Miskell and Marshall, 1965**). Some reports suggested that 7-15% of the industrial energy is concentrated in drying operations for countries like United States, UK, Canada, and France, whereas countries like Germany, Denmark is further extended to 15-20% (**Raghavan et al., 2005**). Since the significance of energy has been rising, it is necessary to develop the optimal solutions by providing minimum energy requirements. Drying techniques can be classified as; natural drying or industrial drying (**Smith, 1942** and **Van't Land, 1991**). Natural Drying, is the oldest method and most common form of food processing and preservation employed by humankind. Traditionally, the sun's energy was used for drying of agricultural and food products. It is the most widely practiced form of drying in the world because it is cheap, easy, and convenient. Even though sun drying requires little capital or expertise, there are many problems in using this method for drying of food products; large space requirement, long (exposure) drying time, extremely weather dependent, lack of sufficient control during drying, undesirable changes in the quality of food products, contamination of the product with soil and dust and non uniformity of drying products. Whereas the artificial or industrial Drying it overcomes all of the disadvantages of the natural drying. Nowadays, dryers have an important position in industry for processing and preservation of different foods and industrial materials. A lot of dryer types can be found in industry among them, rotary dryers are presented with its potentials for drying of granular materials.

Rotary dryers are normally employed in the chemical and pharmaceutical industry, but also are used to dry agricultural products and by - products alfalfa and beet pulp. i.e; fertilizers, pharmaceuticals, mineral concentrates, cement, sugar, soybean meal, corn meal, plastics and many others (**Williams, 1971, Shirley et al., 1982, Gerhartz, 1985, Savaresi, 2001, Song et al., 2003, Geng et al., 2009** and **Abbasfard, 2013**). Drying of these by - products and its utilization as animal feed (cattle), soil conditioner or even as a source of protein is a promising alternative to its incineration or accumulation in garbage dumps. By its characteristics, this type of dryers is suitable for the drying of vegetable by - products since it allows the handling

of heterogeneous or sticky products and products that flow with difficulty. Rotary dryer is a very complicated process that implies not only thermal drying but also movement of particles with the dryer.

The direction of the gas flow through the cylinder relative to the solids is dictated mainly by the properties of the proposed material; Con-current flow is used for heat sensitive materials even for high inlet gas temperature due to the rapid cooling of the gas during initial evaporation of surface moisture. Whereas for other materials counter-current flow is desirable in order to take the advantages of higher thermal efficiency that can be achieved in this way (**Krokida, 2007**). Rotary dryers are classified according to its heating type as: direct, indirect and special types. Direct heating type (**Shene, 1996**): heat is added or removed from the solids by direct exchange between gas and solids (here, heat exchange is by convection and radiation). such kind of dryers required flights to help for the lifting and showering of the granular material through the gas-borne area. Also, there should be a perfect insulation to the dryer shell. Indirect heating type (**Kröll, 1978** and **Canales, 2001**): the heating medium separated from contact with the solids by a metal wall or tube (here, heat is dominated by contact heat transfer between the metal wall and solids). In a special type, Indirect steam tube dryer: one or more rows of steam tubes are installed longitudinally in its interior, it is suitable for operation up to the available steam temperature or in process requiring water cooling of the tubes. Typical ammonium nitrate rotary dryer plant (**Abbasfard,2013**) is shown in Fig. 1.5. Rotary coolers in principle of operation are the same like rotary dryers. Except for the purpose, here is just focused on cooling the granular material to a certain temperature using a cold gas stream. Fig. 1.6 shows an industrial rotary tube cooler.

1.4 Flights

Rotary drums interior wall is usually furnished with longitudinal flights (extended surfaces or fins) as shown in Fig. 1.7, which lifts the granular material from the bottom bed then cascade and showers it developing a series of curtains through the gas-borne area (Revol et al., 2001; Krokida et al., 2007; Lee and Sheehan, 2010; Sunkara et al., 2013a and Sunkara, 2015).

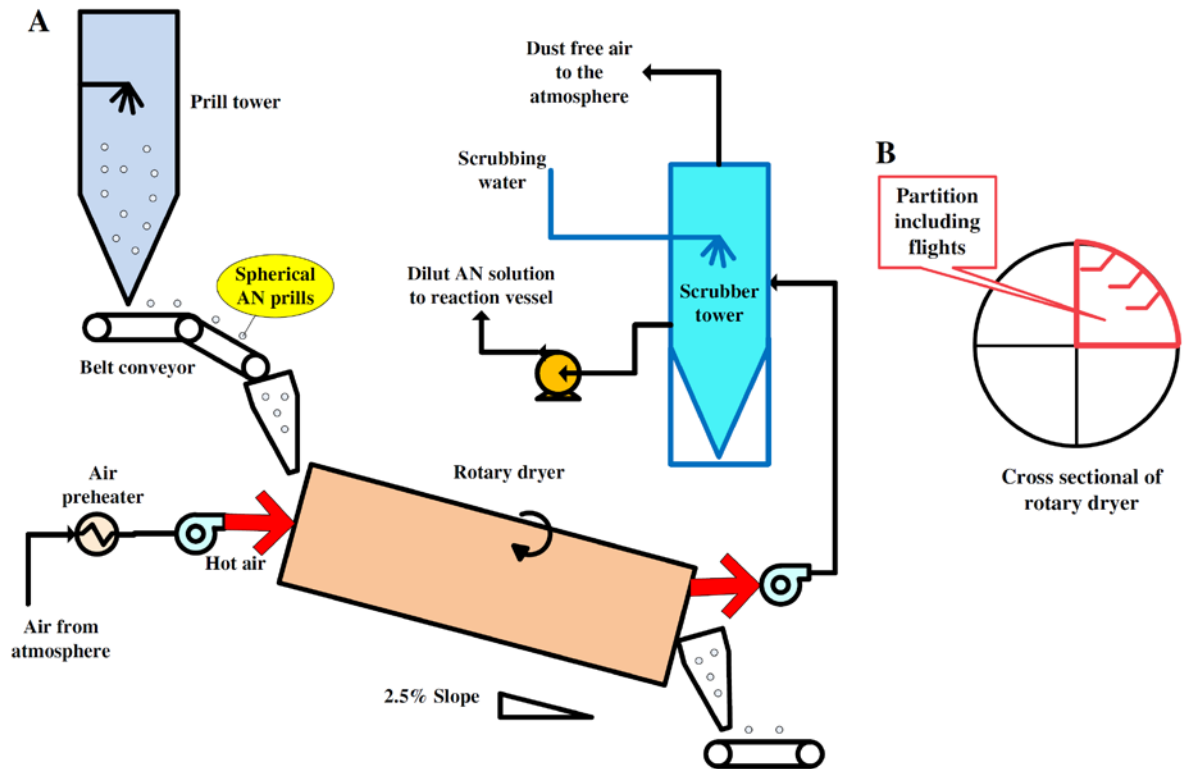


Figure 1.5: Typical ammonium nitrate rotary dryer plant (co-current flow type) (Abbasfard,2013).

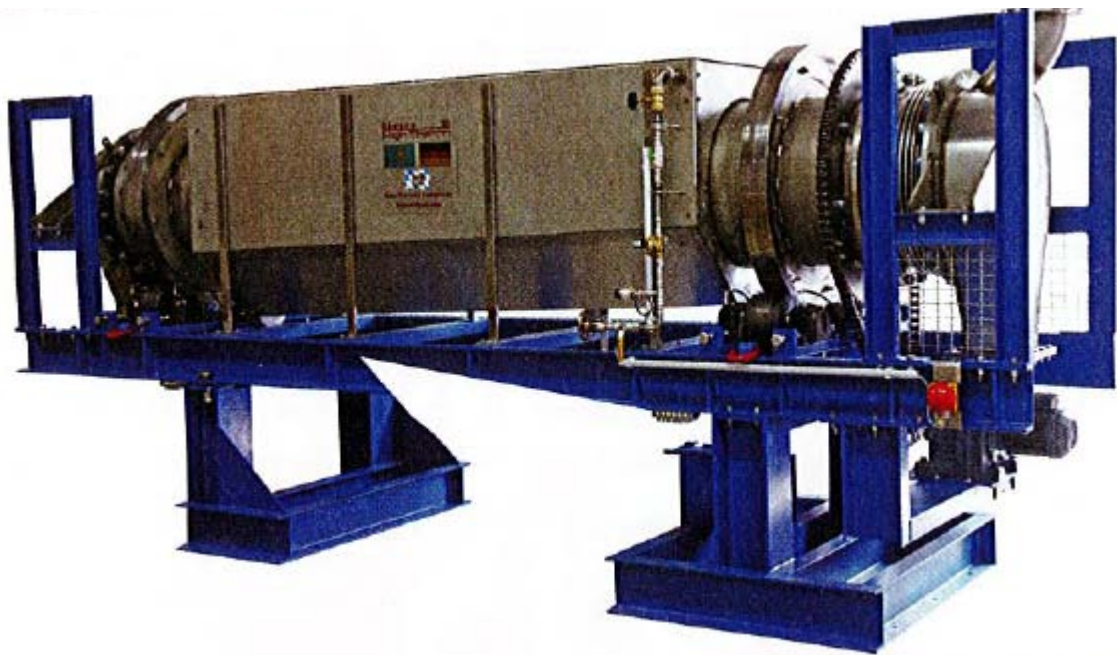


Figure 1.6: Rotary tube cooler (Linn High Therm GmbH, Eschenfelden Germany).

The material falling from the flight is advanced to a specific distance in each cascade depending on the gas flow type and velocity and various flight actions such as bouncing and kilning. Due to the inclination of the drum and the action of the flights, the material is transported to the other end of the drum. The material within the drum has been exposed to three different phases during the process; the dense phase at the bottom of the drum, the flight phase (passive), and the gas-borne phase (active) where the material is exposed to the gas. The effectiveness of the flighted rotary drum greatly depends on the extent and uniformity of the gas-solid contact and the residence time of the material in the drum, which in turn depends on the number, size and shape of the flights. The selection of the shape of the flight is largely governed by the behavior of flow of the particulates. The most commonly used flight profiles are shown in Fig. 1.8. In general, rectangular flights are mostly used for free flowing bulk materials. Radial flights are used for sticky materials and circular flights are applicable for developing a uniform distribution of the particulates (**Moyers, 1997**).



Figure 1.7: Cross sectional view of an industrial rotary dryer showing flights (Feeco, Inc., Wisconsin, USA).

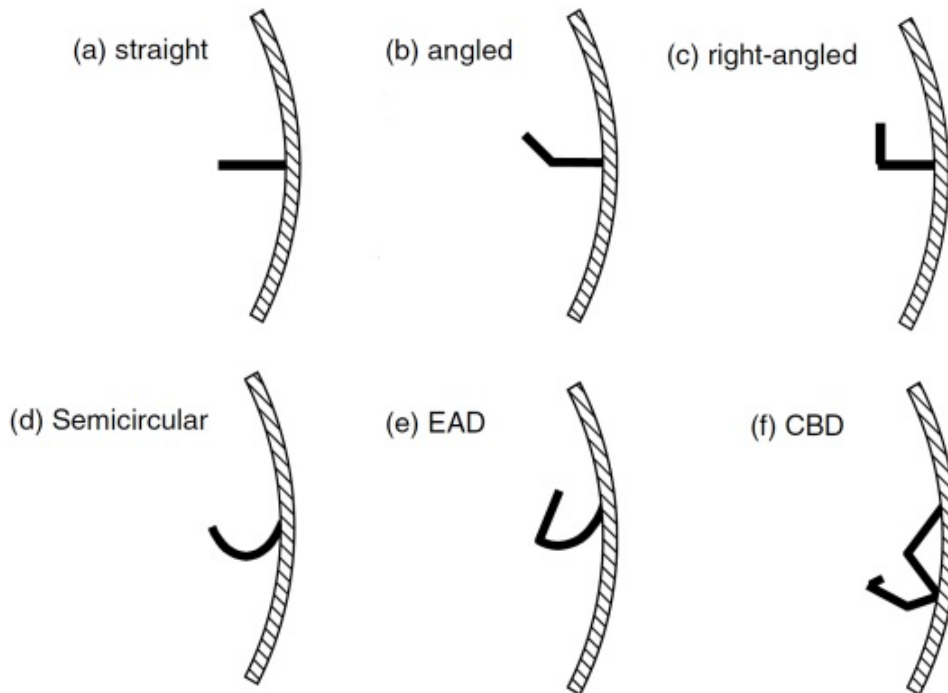


Figure 1.8: Common flight profiles used in industry (**Krokida et al., 2007**).

1.5 Loading of flighted rotary drums

The loading of a flighted rotary drum is the total amount of solid material (holdup) fed to the drum. It strongly affects the overall performance as it influences the amount and distribution behavior of the solid in both the gas-borne phase and flight-borne phase. Furthermore, it affects the residence time of transportation along the drum. As a consequence these parameters affects the exchange processes of both heat and mass (**Keey, 1972, Matchett and Baker, 1987**).

Three types of drum loading states can be categorized: under-loading, design-loading (optimum loading), and over-loading which are characterized based on the holdup and the discharge angle of the first unloading flight (FUF) (**Matchett and Baker, 1987; Kelly, 1992; Papadakis et al., 1994; Sherritt et al., 1993, Shahhosseini et al., 2000, Britton et al., 2006**). Full description of these loadings found in **Sunkara et al., 2013b**: "the under-loading: the first unloading flight (FUF) holds less material than its capacity and its discharge angle is in the upper half of the drum laterly than 0° (9 o'clock position), see Fig. 1.9 (a). Under such conditions, the

time spent by the particles in the gas-borne phase is minimum, which can lead to smaller residence time than required. As the drum loading state is gradually increased, the FUF position ultimately becomes lower and the unloading starts when the flight tip is at 9 o'clock position. At this point the drum is said to be at design loading. In this drum the maximum amount of material is distributed in the gas-borne phase where the particles total surface area subjected for heat and mass transfers is substantially increased, hence maximum heat and mass transfers can be expected between the solids and the gas stream, see Fig. 1.9 (b). Further increasing the feed rate does not increase the amount of gas-borne solid, but the flights are completely crowded with the material which is defined as over loading. In this drum the discharge of the material starts immediately as the flight tip detaches from the bed surface, see Fig. 1.9 (c)".

As a conclusion it is proved that, the best performance of a flighted drum occurs when the drum operates at design loading conditions (**Sheehan et al., 2005, Sunkara et al., 2013b**). Therefore, assessing the design-loading of the drum is a critical issue.

Recently, **Ajayi and Sheehan, 2012b** carried out an intensive literature survey about the design loading determination. They performed experimental work on a horizontal pilot scale rotary dryer with a diameter of 0.75 m and a length of 1.15 m fitted internally with angular flights. The design load experiments involved two methods for the image analysis of multiple photographs of the cross sectional area of the solids in the front end of the dryer at increasing loading conditions. Namely; manual analysis using ImageJ software and mix of using ImageJ and Matlab image processing described in **Ajayi and Sheehan, 2012a**. Subsequently, the design load was estimated using conventional criteria based on the saturation of material in the cascading or unloading flights. The proportion of gas-borne to flight-borne solids within the drum was characterized through a combination of photographic analysis coupled with Computational Fluid Dynamics (CFD) simulation.

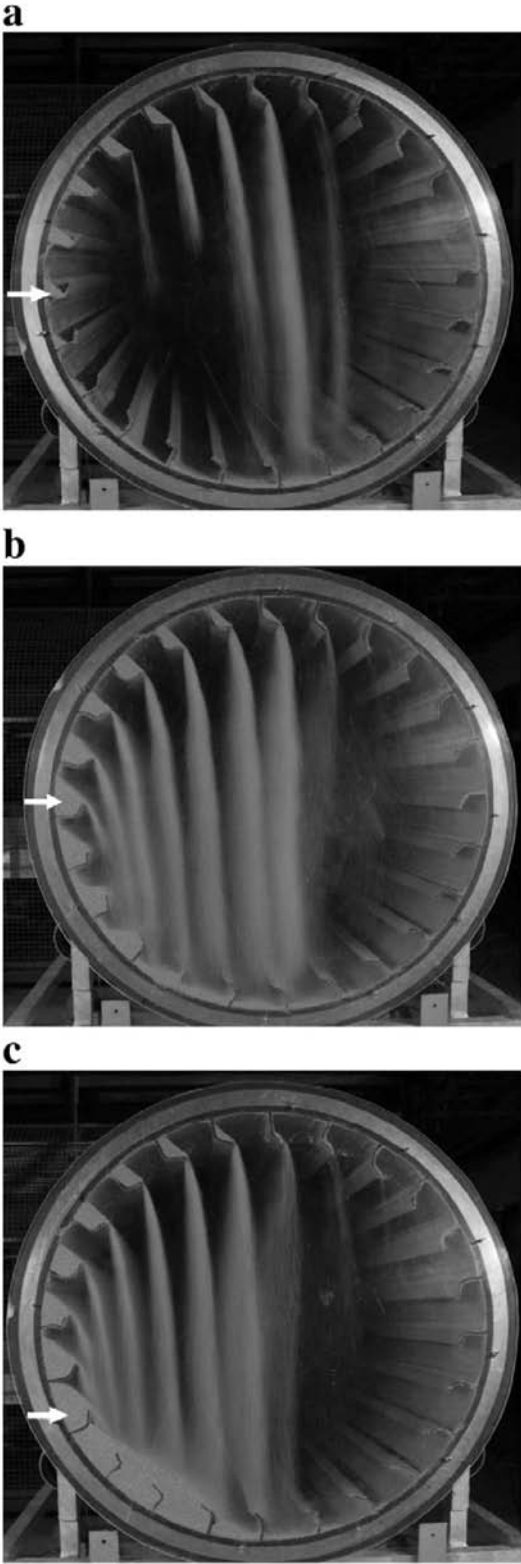


Figure 1.9: Experimental photos from **Ajayi and Sheehan, 2012b**, showing different drum loading: (a) under loading (b) design loading and (c) over loading.

In their work they discussed some available models from literature to calculate the design loading. They argued that none of those models had been validated experimentally and most of these models were non-generic and geometrically developed based on a particular type of flight configurations. Three models were selected for the comparison with experimental results:- namely the models of **Porter (1963)**, **Kelly and O'Donnell (1977)** and **Baker (1988)**. Table 1 summarizes the selected models (Eqs. (1.1) - (1.3)). In addition, they discussed the suitability of using geometric models of flight unloading to predict design loading in flighted rotary dryers and they modified **Baker's (1988)** model - see Table 1 Eq. (1.4).

Table 1.1: Design loading models

Author	Model
Porter (1963):	$H_{Tot} = H_{FUF} \times \frac{n_F}{2} \quad (1.1)$
Kelly and O'Donnell (1977):	$H_{Tot} = H_{FUF} \times \left(\frac{n_F + 1}{2} \right) \quad (1.2)$
Baker (1988):	$H_{Tot, Flights} = \left(2 \times \frac{LUF}{FUF} \sum H_i \right) - H_{FUF} \quad (1.3)$
Ajayi and Sheehan (2012b):	$H_{Tot} = \left(1.24 \times \left(2 \times \frac{LUF}{FUF} \sum H_i \right) - H_{FUF} \right) (1 + S) \quad (1.4)$

In Eqs. (1.1), (1.2) and (1.4), H_{Tot} is the total holdup of the drum at design loading including both gas-borne solid (active) and flight-borne solid (passive). $H_{Tot, Flights}$ in Eq. (1.3) represents the total holdup of the drum at design loading accounting only for the flight-borne solid (passive). In Eqs. (1.1) - (1.4), H_{FUF} is the holdup of solid inside the first unloading flight (FUF), and H_i is the holdup in each loaded flight (i) at design loading starting from the first unloading flight (FUF) to the last unloading flight (LUF). It should be noted that H_{Tot} , $H_{Tot, Flights}$, H_{FUF} and H_i all represent the volumetric holdup of solid per unit length of the drum. It can be expressed in m^3/m (**Glikin, 1978**) or in cm^2 as presented here in the present work (the frontal cross sectional area of the solid assuming uniform solid distribution in the axial direction of the drum). n_F is the total number of flights. (S) is the ratio of gas-borne solid to flight-borne solid at design loading from the experimental work of **Ajayi and Sheehan, 2012b** and

according to their investigated experimental parameters, it has values between 0.042-0.078. In scaling up the experimental results it is more suitable to use the filling degree instead of the total mass as the filling degree is a dimensionless parameter. Eq. (1.5) gives the relation between the drum filling degree and the total solid holdup, here $V_{Tot, solid}$ is the total volume of the solid (total holdup (H_{Tot})) to be fed into the drum in m^3 , V_{drum} is the total drum volume in m^3 , R is the radius of the drum (0.25 m) and L is the length of the drum

$$f_{design} \% = \frac{V_{Tot, solid}}{V_{drum}} = \frac{H_{Tot} L}{\pi R^2 L} \times 100. \quad (1.5)$$

It is worth noting that **Ajayi and Sheehan, 2012b** examined both free flowing and cohesive solids with cohesion being controlled through the addition of low volatility fluid with limited range of dynamic angle of repose from 44.7° to 62.3° . The effect of the drum rotational speed was also examined from 2.5 to 4.5 rpm. Other important drum design parameters were not examined in their study, like flight length ratio and number of flights. Changing these design parameters can drastically change the operation of the drum.

Therefore, in the present work a lot of experiments were carried out to assess the optimum (design) loading of a batch rotary drum equipped with rectangular (right angled) flights. Based on the conventional criterion in determining the design loading, which is the saturation of the FUF with a specific condition where the FUF discharge angle at 9 o'clock position. The experimental work mainly depends on recording videos at different operating conditions and then by means of image analysis tools the results were drawn. Two methods of image analysis were used: manual and automated. Different solid materials (free flowing), rotational speeds, number of flights and flight length ratios were researched, each with wide ranges of use and consequence in industry. The current experimental results were compared with selected design loading models from literature. Based on the experimental results a new fitting factor was proposed and a correlation in terms of the total filling degree was developed. New innovative experimental technique was proposed and used for more experiments performed on a larger size drum. The discharge characteristics of

the flighted drum were studied based on the experimental results. Final aim is to develop a mathematical model describing the axial transport and also the mechanism of heat transfer along the drum essentially based on using the experimental results in order to overall evaluate the whole process within the flighted rotary drum.

1.6 Thesis outline

This dissertation is divided into seven chapters. Chapter 2 reports the analysis of the experimental work carried out in order to assess the optimum loading (design loading) of a flighted rotary drum (with rectangular flights). Through the description of: the experimental test-rig, the experimental procedures, different image analysis techniques used and the results discussions of the design loading. In Chapter 3 the discharge characteristics of the experimental drum are determined and discussed. Chapter 4 represents the results of scaling up the experimental drum and developing a correlation can be used to determine the filling degree at design loading as a function of all of the operating parameters. Chapter 5 reports the development of a mathematical model to study the axial transport along the drum using the experimental results of Chapter 2 with a case study. Chapter 6 is a description for the heat transfer mechanism of a flighted rotary drum with application of the case study from Chapter 5. Finally, Chapter 7 reports the conclusions drawn from the present work and the outlook.

Chapter 2

Experimental determination of the optimum loading of a flighted rotary drum

2.1 Experimental setup

2.1.1 Experimental test rig

Figure 2.1 shows the experimental apparatus. The test rig consists of a 0.5 cm internal diameter and 0.15 m length rotating drum. The drum was directly coupled with an electrical motor and rotated in the clockwise direction. The rotating speed of the motor was controlled by a variable frequency inverter. The drum was set up with zero inclination with respect to the horizontal position on the ground in all directions. In order to maintain uniform solid distribution inside the drum (that means uniform axial flight unloading profiles). A line was stretched horizontally in front of the drum and was located at the center point level of the drum. This line acts as the reference demarcation between under-loaded and over-loaded condition of the drum (0° discharge angle at the 9 o'clock position). Figure 2.2 giving information about the flight profiles used in the experimental work, which are two rectangular flights of the same radial length ($l_1 = 0.05$ m) and two different tangential lengths (l_2) of 0.018 m and 0.037 cm forming two the flight length ratios (l_2/l_1) 0.375 and 0.75.

The drum's front side was covered with a circular glass plate and the rear end with a metal wall. In front of the drum a high definition video camera had been placed perpendicularly to the plane of the glass plate. A Canon 60D still camera was used with attached 18-125 mm focal length lens. The video recording was set with auto exposure, the video quality was set with 1920x1080 pixels and 24 frames per second. The available shortest focal length of lens was adjusted to 18 mm for a wider angle of view. The focal point was focused at the center point of the drum to reduce the video distortion effects and parallax error during the recording of the entire drum object.

For the consistency of light exposure the experiments were performed in a dark room and a light source was placed and directed towards the drum. The position of the light was carefully placed to avoid the reflection of light at the surface of glass which would lead to glaring of the video. Also, the light was distributed equally over the whole drum to facilitate the manual analysis of the experimental images and to reduce eye strain. A black curtain was draped on the back of the drum, to minimize over-exposure of light from the surroundings and back-lit or silhouette effects during video capturing.

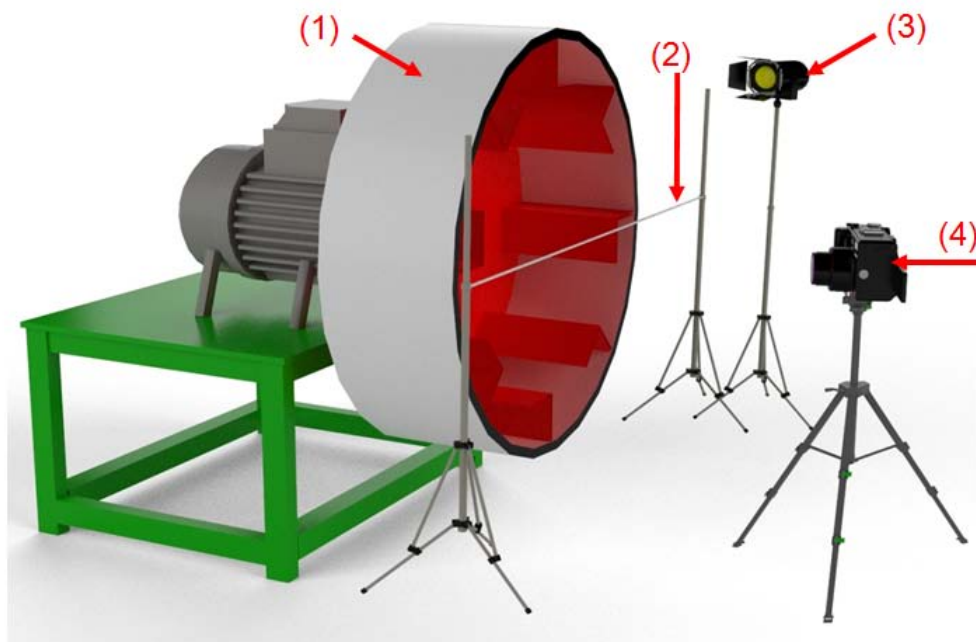


Figure 2.1: Experimental test rig: (1) experimental drum coupled with an electrical motor, (2) horizontal demarcation line, (3) light, and (4) digital FHD camera.

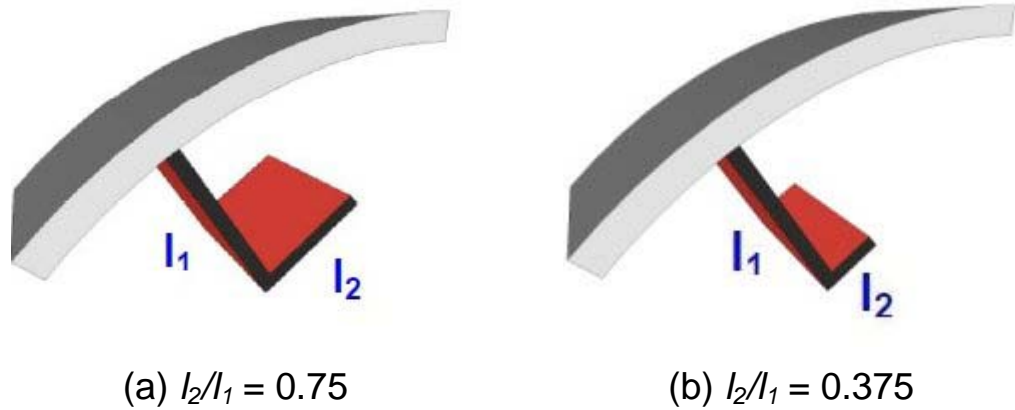


Figure 2.2: Schematic diagram of the flight geometry used in the experimental work (rectangular flight l_2 (tangential length) and l_1 (radial length) = 0.05 m).

2.2.2 Experimental procedures

The experimental procedure after the preparation of experimental setup was as follows: the amount of solid was determined according to the experimental design in terms of drum filling degree and filled into the drum. For example, at a certain desired filling degree the solid holdup (volume $V_{Tot, solid}$ in m^3) was calculated from Eq. (1.5) where V_{drum} is the total drum volume. The calculated solid volume was converted to mass (in kg) using the solid bulk density (measured in laboratory, the solid was weighed for five samples with different volumes and the density was calculated as the mean value). Then weighing out this specified mass of the solid and filling it into the drum. The same procedure was used for incrementing the solid filling degree. As in most cases, the drum filling degree was firstly increased at regular intervals by 1% with respect to the previous reading. When the drum was found to be close to the design loading point (where the FUF discharge angle was nearly at 9 o'clock position), the experiments were repeated before and after this point by small increments of filling degree (depending on experience). Until the design loading point was more precisely determined. With this in mind, some points in between were added to ensure the reliability of the results. The motor was provided with electricity and the frequency control was manipulated to obtain the desired drum rotational speed. After switching on the motor a moment was waited until the material was fully distributed in the drum and a video was recorded for approximately two minutes. Then the motor was stopped for the next experiment with the new filling degree.

2.2.3 Experimental program

A batch rotary drum with 12 and 18 internal flights was used. The flights were fabricated with two flight length ratios (l_2/l_1) of 0.75 and 0.375. Where a total of four different drum profiles were able to be researched. The drum was operated at three different rotational speeds: 1, 3 and 5 rpm. The focus of the experiment was to determine the design loading condition, which is the transition from under-loaded to over-loaded condition. Table 2.1 outlines the specifications of the drum and the operating parameters.

The experiments were performed with three types of materials with different particle size diameters: quartz sand (0.2 mm), glass beads (0.7 mm, 1.0 mm and 2.0 mm) and steel balls (0.8 mm and 2.0 mm). It is worth noting that for all solid materials a sieving test was performed, in order to ensure the required average solid diameter.

For the materials determination of the dynamic angle of repose a similar experimental setup was used. In this case the drum was non-flighted and the dimensions were: a diameter of 600 mm and a length of 150 mm. The drum was operated at 15% filling degree and speed of 3 rpm. Enough care was taken to operate the drum under the rolling motion. The demarcation line was shifted to the bottom of the bed and was used as the horizontal line marking for the dynamic angle of repose measurement. Then, a video was recorded for approximately one minute. All material properties are listed in Table 2.2.

Table 2.1: Specifications of the drum and operating parameters

Drum diameter	0.5 m
Drum length	0.15 m
Flight length ratio	0.75 and 0.375
Number of flights	12 and 18
Rotational Speed	1, 3 and 5 rpm

Table 2.2: Physical properties of materials

Material	d_p (mm)	ρ_b (consolidated) (kg/m ³)	Θ_A (°)
Quartz sand	0.2	1570 ±18	32.4 ±1.1
Glass beads	0.7	1560 ±20	28.0 ±0.6
	1.0	1555 ±22	25.9 ±0.8
	2.0	1549 ±15	25.7 ±1.0
Steel balls	0.8	4630 ±25	28.5 ±0.9
	2.0	4680 ±27	25.5 ±0.7

2.3 Data Processing

2.3.1 Design loading determination criterion

The determination of the design loading filling degree from the experimental results was based on two observations from the recorded videos and images analysis processing. First, that the FUF starts to cascade (discharge) the solid at 9 o'clock position; Second, that the cross sectional area of the first unloading flight (FUF) attained a maximum value or saturation. Figs. 2.3 and 2.4 illustrates samples from the current experimental work at different operating conditions, showing different loadings of the flighted rotary drum including the design loading (see cases (b)).

2.3.2 Data extraction sequence

The sequence of data extraction was as the following: at first the video was recorded during the experiment with a specific material, rotational speed, number of flights, flight length ratio and filling degree of the drum. Then, the video was segmentized using Vlan Player and still images of interest were extracted from the video. Those still images of the first unloading flight were selected and compared side by side in terms of image clarity and positioning of the discharge angle. At least ten images were selected for each operating condition. These selected still images were to be analyzed using a suitable software in order to calculate the FUF area and other parameters as will described in the followings.

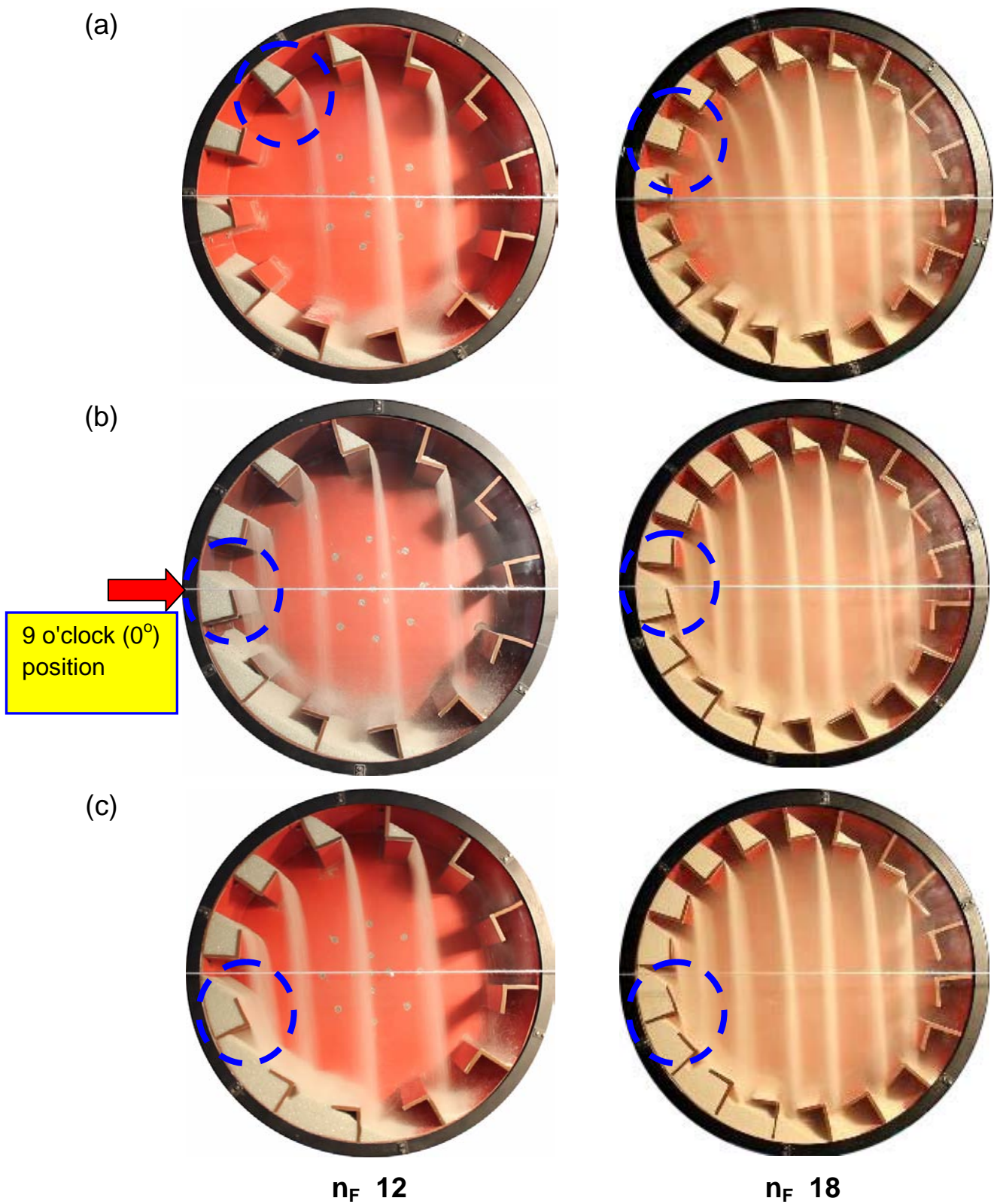


Figure 2.3: Sample photos from our experimental work showing different loadings, dashed circle denoted the FUF; (a) under loading (b) optimum design loading and (c) over loading. For two number of flights 12 and 18.

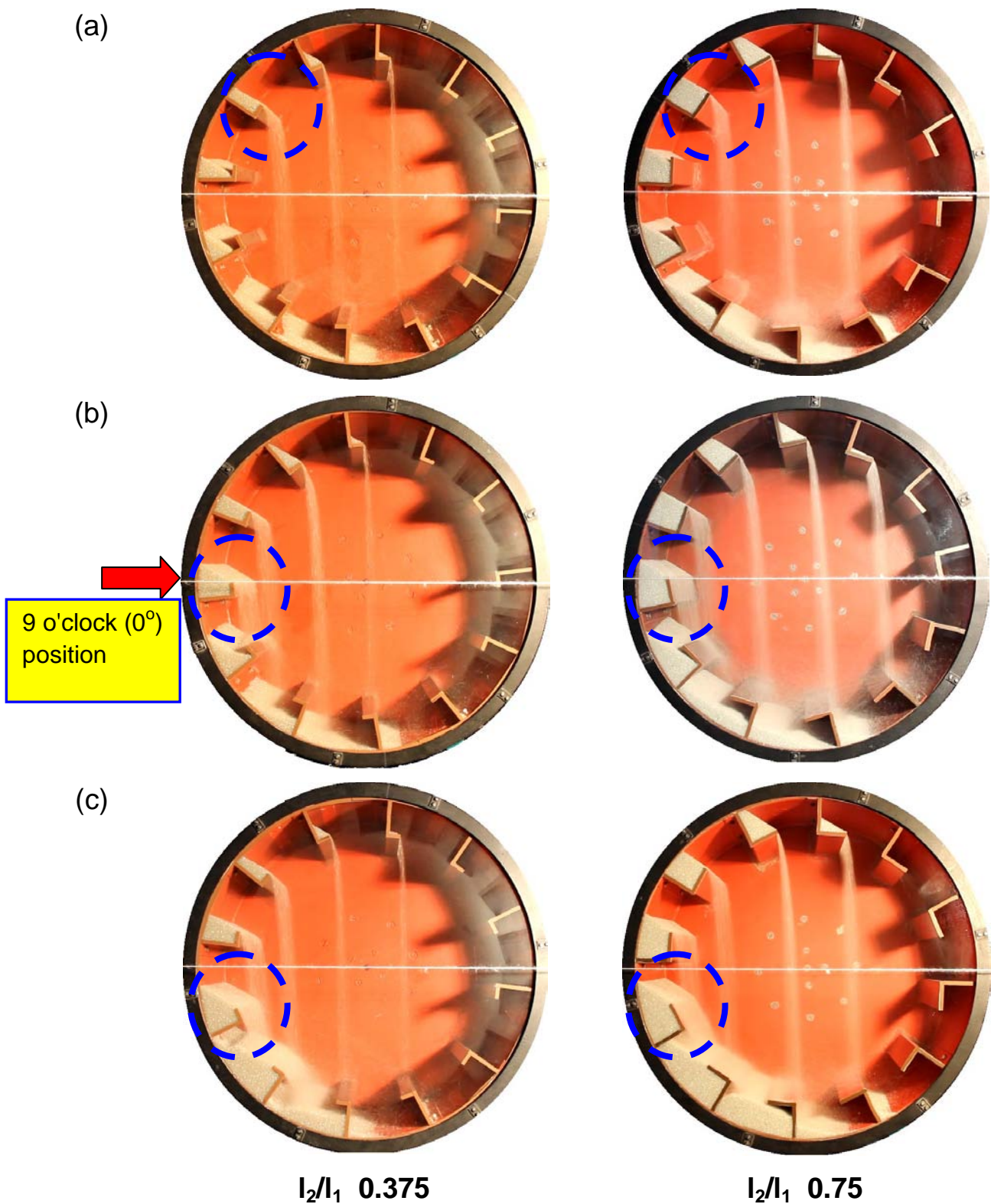


Figure 2.4: Sample photos from our experimental work showing different loadings, for two flight length ratios 0.375 and 0.75.

2.3.3 Image analysis

Image analysis is a powerful tool for solving different engineering problems in particle technology. It is the process of extracting important information from the image; mainly from digital images by means of digital image processing techniques. Most of the scientific publications using the image analysis have been arisen from the biological science fields with application of measuring size and counting the number of bacteria in an image. **MASSANA, et al., 1997**, compared two methods for measuring size and counting the number of Planktonic bacteria represented in different water bodies samples as shown in Fig. 2.5. The first method was by the direct counts, the second was based on computerized image-analysis of epifluorescence preparations, they concluded that the computerized method was the most accurate and simple method to be used. **Heffels, et al., 1996**, studied different possibilities of changing backward light scattering for characterizing dense particle systems. **Obadiat, et al., 1998**, developed an innovative digital image analysis approach to quantify the percentages of voids in mineral aggregates of bituminous mixtures.

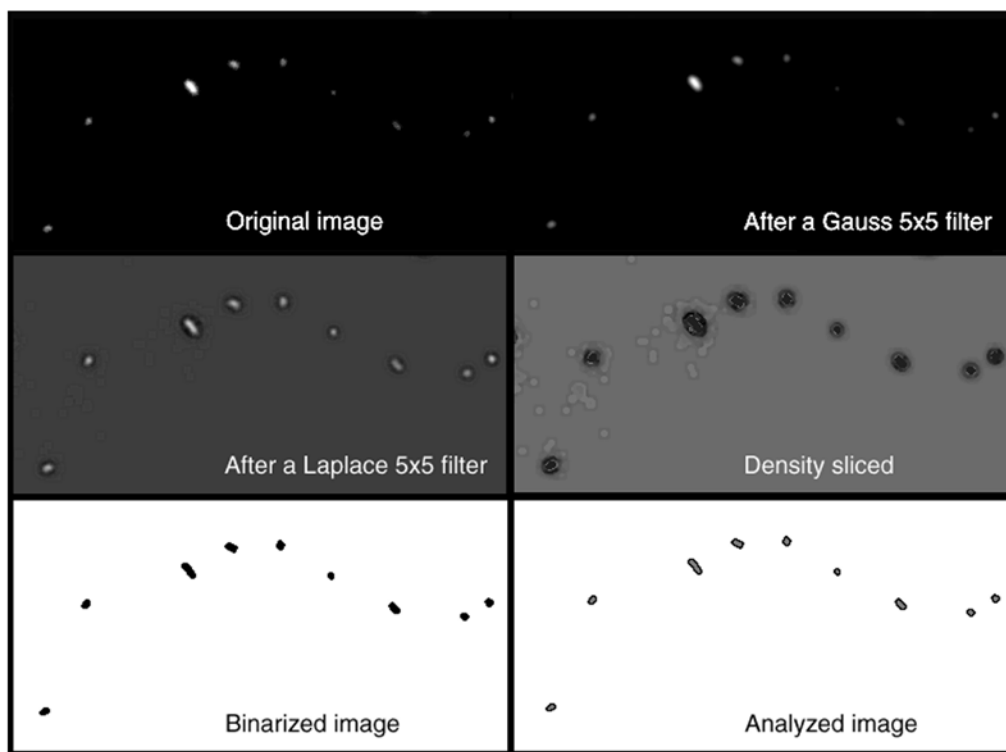


Figure 2.5: Whole process of image processing by **Massana, et al., 1997**, process from the original image to the final binary image. For counting Planktonic bacteria represented in a water body.

The digital image to be analyzed can be defined as a two dimensional array of x and y , where x and y are plane coordinates. A pixel is the smallest element of an image represented on the screen. The address of a pixel corresponds to its physical coordinates (x, y) . The total number of pixels in an image depending on: the device (the camera) used for capturing the digital image or the video where the image is drawn from and the size of the image. There are four basic types of images which can be defined namely:- red-green-blue (RGB or true color) image, indexed image, gray scale image and binary (black and white) image.

In the RGB image each pixel has a color which is described by the amounts of red, green, and blue in it. Each of these components can have a range of values from 0 to 255 giving a total of $255^3 = 16,581,375$ different color possibilities in the image and each pixel in an image corresponds to three values. This leads to deal with a complicated analysis process. The indexed image likes a color map and each pixel with a value does not give its color but an index to its color in the color map. The gray scale image is characterized by shades of gray and the pixel ranges from 0 for black and 255 for white. In the binary image (black and white image) the pixels are either black with value of 0 or white with value of 1. The image analysis technique is much influenced by the type of image to be processed. Where complicated analysis technique is needed for the true color images. The technique becomes easier when using gray scale images and more easier when using binary (black and white) images. Thus, gray scale and binary (black and white) images are predominantly used in image analysis for engineering applications.

Previous studies on rotary drums have used different image analysis methods. As for the studies of particles mixing in rotary drums: **Van Puyvelde, 1999**, describes a new way to determine the mixing rates of solids in a rotating drum through image analysis programming using custom software written in Borland C ++. Recently, **Liu et al., 2015**, conducted a quantitative comparison of image analysis methods namely:- pixel classification, variance method and contact method for studying particle mixing in rotary drums using the image processing toolbox provided by Matlab. Whereas for the studies of rotary drums loading (holdup) and curtains behavior :ImageJ software was used for the image analysis processing by **Lee and Sheehan, 2010** and **Ajayi and Sheehan, 2012a**. Moreover **Ajayi and Sheehan,**

2012a, have used another method which is a combination of ImageJ software and Matlab image processing toolbox.

In the present experimental work, two methods were introduced and compared for the image analysis processing: first, manual method (mainly using ImageJ software); second, automated method (by using a combination of ImageJ software and Matlab image processing toolbox). In the following a full description of the two methods.

2.3.4 Manual method

In the manual method ImageJ software was used. The first process was the scaling of the image, which means identifying a reference length like using the diameter of the drum (50 cm). Then manually selecting the area of interest (like the material residue in a flight). Special care was taken to avoid errors in selection. A multipoint polygon selection was used in order to have an accurate selection of the material without selecting the drum metal parts. Another problem appeared was the difficulty in identifying the separating edges between the material frontal cross section area and its side view (see **Fig. 2.6**). That led to high time consumption and error probability. After selecting the area of interest ImageJ measured the area in cm^2 by counting the number of pixels relying on the predefined scaling factor. Then one by one all the areas of solid materials in all flights were measured.

Another study will depend on measuring the variation of the material frontal cross section area with the change in the discharge angle, in such case the video will be running and by choosing one flight to be traced from the FUF position to the LUF position and captured many images at different positions (different discharge angles, also can be measured by ImageJ). The same processes as mentioned before can be applied to measure the curtains falling height.

As a conclusion, the manual method resulting in significant time consumption which became the major limitation of this image analysis processing method. And it is better to find an automated method to save the significant time consumption.

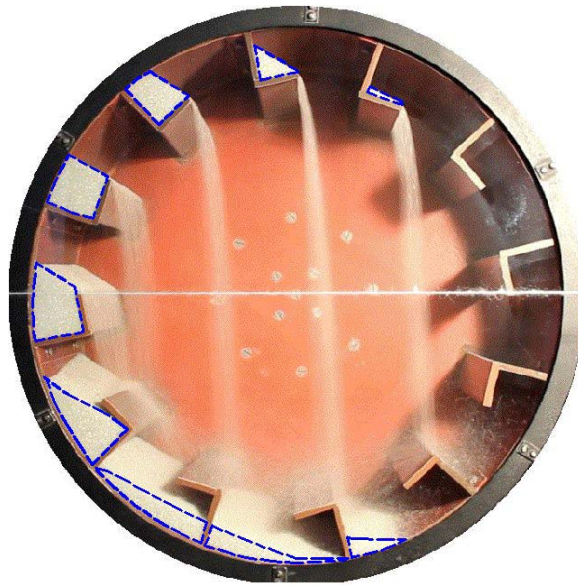


Figure 2.6: Manual selection of solid material residue in the flights.

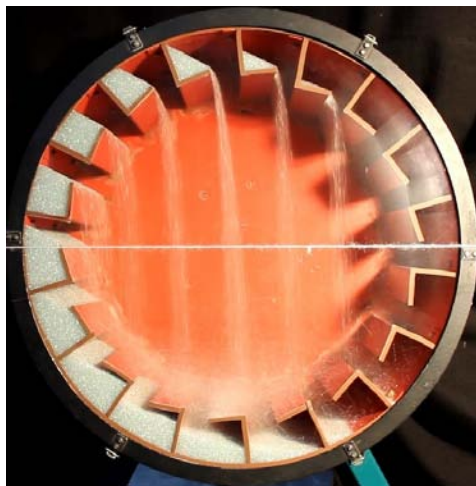
2.3.5 Automated method

The automated method mainly was developed to overcome the disadvantages of the manual method, to save the significant time consumption especially for the analysis of numerous images. The automated method relied on using a combination of ImageJ software and Matlab image processing toolbox. The ImageJ software was used for the pre-processing (enhancement) of the images and then Matlab was used to find all of the required information.

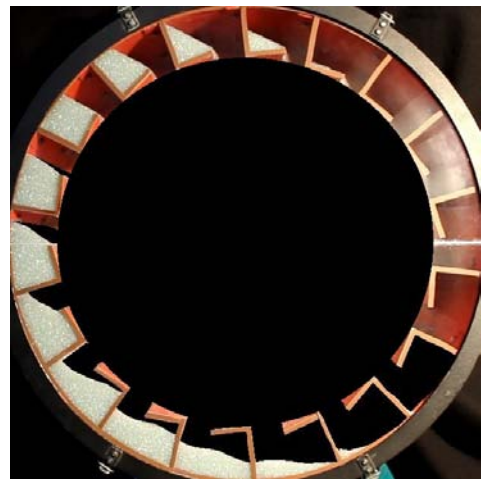
Matlab image process toolbox can read and threshold colors from all images types. The reading process results in giving information about the total number of pixels represented in a specified region for a specified color. In order to simplify the engineering problem (threshold process) the type of image choosed to be analyzed is the binary (black and white) one. The images of the current experimental work were of true color type. Thus it was first transformed to binary type. But it could not be transformed directly due to many problems. First, the appearance of the material's side view in the flight. Second, the existence of the curtains formed by the material cascaded from the upper loaded flights. As these curtains are of the same color as the materials reside in the flights. That leads to a wrong fuzzy selection by imageJ. Third, the lighting intensity (brightness) of the image was horrible for the transformation (this light was settled to make convenience for the manual analysis).

Fourth, there were a large number of images to be pre-processed before analyzed by Matlab which resulted in more time consuming as the manual method. To overcome all of the mentioned problems a Macro code was developed in the ImageJ software for the batch pre-processing of unlimited number of images. But before using this Macro code, the side view's of the material reside inside the flights were to be removed by manual selection (this was only for the current experimental images, but it is recommended in future to extend the experimental work with new technique in avoiding the appearance of the material's side views). The Macro processes were first, the image was cropped to the inner diameter of the drum in order to make all images with the same size. Second, the part where the curtains exist were removed by choosing the inner circle passing by the end point of the tangential length of all flights). Third, the brightness and contrast was adjusted using the built-in function by the ImageJ (depend on the already exist one). Fourth, the true color images were transformed to be in gray scale and then binary (black and white) as shown in **Fig. 2.7**.

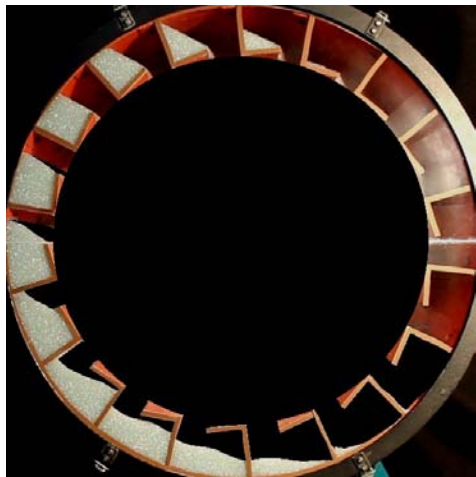
A Matlab code was developed to calculate the total number of white pixels (of the solid) reside in each flight (in a specified region selected by using the function "roipoly" with a special care to avoid the selection of some metal parts of the drum). In order to calculate the actual area of these regions, the total number of the pixels in the whole image (which means with known area of the drum inner diameter circle) was counted first and by normalizing the number of pixels of the selected regions with the total image the area could be calculated. Unlimited number of images can be analyzed with this methodology for any study.



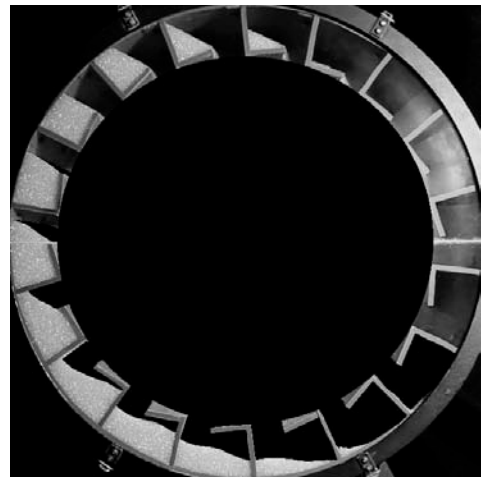
(a) Original image



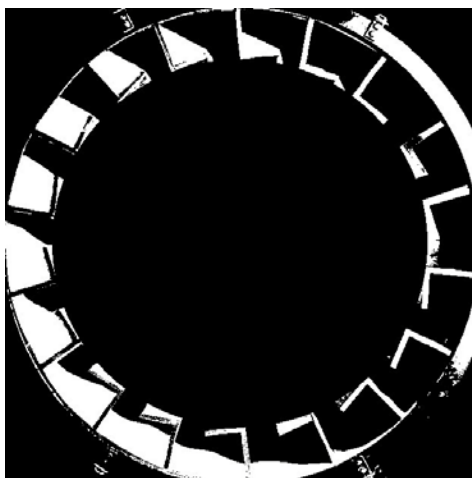
(b) After removing side views and cropping to the inner diameter



(c) After brightness and contrast adjustment

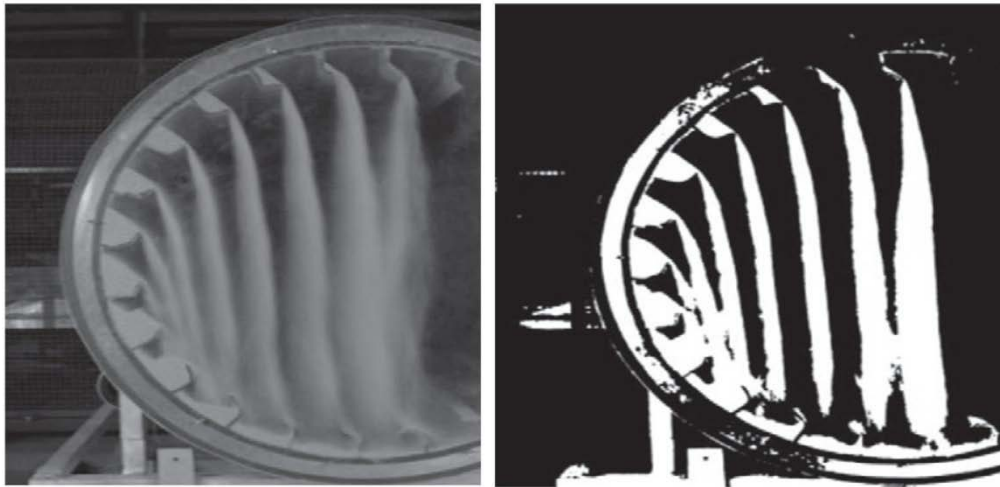


(d) Image in gray scale



(e) Final black and white (BW) image to Matlab

Figure 2.7: Pre-processes of the experimental raw photo using ImageJ.



a) Original image example b) Filtered image example

Figure 2.8: Experimental images from **Ajay and Sheehan, 2012a**.

Ajay and Sheehan, 2012a used similar image analysis technique, as the original image taken by the camera was in grayscale and the camera location was focused at the 9 o'clock position (FUF). But they added some more pre-processes for the images before feeding to Matlab, like using some filters to enable the selection of the material curtains in the air-borne area as well as the material reside in the flights as shown in Fig. 2.8. But on contrary, through the text of their publication they argued the fact that in order to estimate the area of the material reside in the flight, the air-borne area should be removed from the image. Also, they argued that the camera location led to unavoidable difficulties determining the edges of the flight born solids, that makes the use of the naked eye in determining the edges (manually) is more reliable but strainfull.

As a conclusion, the automated method (using combination of ImageJ software and Matlab image processing toolbox) is much time saving for the calculations. But the camera location and lighting location, angle and intensity should be adapted in order to avoid the appearance of the material's side views and also to avoid any reflections on the drum frontal cover glass. That way, the transformations of the true color images (RGB) to the binary (black and white) one will be much easier and does not need much manual processes. Also it should be mentioned that, in order to get

effective use from the automated method (decrease the processing time), the camera location and lighting location, angle and intensity should be the same for all the captured videos of the experimental work. As the batch cropping process will be much easier and precisely. Hence, it is recommended to develop a new experimental technique in future to overcome all the mentioned problems and facilitate both manual and automated methods, as will be described in Ch. 3.

2.3.6 Automated method validation

A comparison was conducted between the manual and the automated methods in order to validate the use of the automated method (Matlab code). The comparison is based on calculating the FUF cross sectional area (or holdup H_{FUF} in cm^2) at the same conditions (only at design loading) using both manual and automated methods (the determination of the design loading points were described later). The comparisons revealed a good matching between both methods for all cases with small error of +3.2% RMSD represented by the shaded area as shown in **Fig. 2.9**.

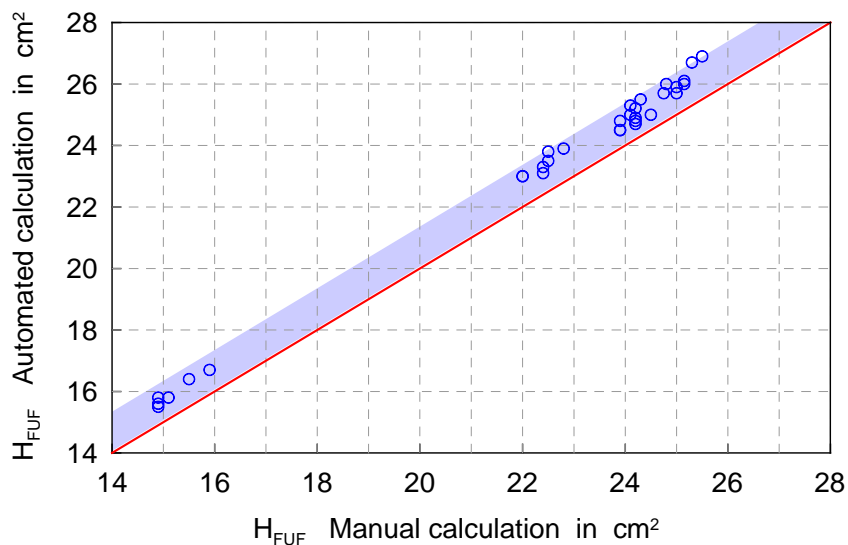


Figure 2.9: Comparison between manual and automated methods based on calculating the H_{FUF} **at the design loading** conditions. the shaded area represents the RMSD.

2.4 Data fitting

In the regression of the experimental data set a simple linear fitting was used. The data set splitted into two groups with breaks in location at the estimated design loading point. These break points were firstly determined by the direct vision as almost all of flights are saturated and starts its cascading when reaching precisely the 9 o'clock position. Then by means of image analysis and calculations of the FUF area over the filling degree these points were verified. After the predetermination of the design loading point filling degree the calculation of the FUF area was focused only at the 9 o'clock position. Otherwise any increase in the filling degree would have caused a case of overloading and introduced a higher FUF area at a lower discharge angle than the 0° . The left side of the break points was fitted linearly with an increasing slope of the H_{FUF} , while the right side of the break points was fitted linearly with zero inclination as the H_{FUF} is remains almost constant here.

The measured average FUF cross sectional area is plotted versus the drum filling degree in the following Figures.

2.5 Results and Discussions

2.5.1 Influence of number of flights

Figure 2.10 shows the influence of the drum filling degree on the measured FUF cross sectional area for rotational speeds of 1, 3 and 5 rpm and the number of flights 12 and 18. It is clearly shown that at any rotational speed an increasing filling degree causes the FUF cross sectional area to increase until it becomes saturated. The point of saturation is considered as the design loading point. It is characterized by a FUF discharge angle at the 9 o'clock position. This is due to the increase of the holdup carried by the flights. For the same number of flights, increasing the rotational speed leads to shift the point of saturation (design loading point) in the direction of an increasing filling degree. Which means higher filling degree is required for the design loading point. This can be attributed to the increased rate of discharge of solid into the gas-borne phase. That requires more material adding to substitute the saturation of the FUF at design loading (see Fig. 2.11). This is further supported by the observed decrease in the slope of the area versus the filling degree line. It is also

shown from Fig. 2.10 increasing the number of flights at the same rotational speed increases the design loading filling degree, this is related to the increase of the total holdup (see Fig. 2.11).

From Fig. 2.10 (a) for quartz sand it can be noted that the saturation (maximum) value of the measured FUF cross sectional area are in the range of 26 cm^2 . For the 12 flights drum the increase in the rotational speed from 1 to 5 rpm causes an increase in the required design loading filling degree from 8.7 to 10%, respectively, which is an increase of 14.9%. For the drum of 18 flights that increase is from 12.7 to 14.8%, a 16.5% increase in the design loading filling degree. By comparing the values of the filling degree required for the design loading points of the 12 flights drum to the 18 flights drum an average increase of 46.5% can be observed.

Figure 2.10 (b) for glass beads shows comparable values of the FUF cross sectional area in the range of 25 cm^2 . For the 12 flights, drum the required filling degree for design loading increased from 8.5 to 10.1% when the rotational speed increased from 1 to 5 rpm, an increase of 18.8%. For the drum with 18 flights, the filling degree varied from 12.8 to 14.7%, which is an increase by 14.8%. In order to achieve design loading conditions using 18 flights, on average 48.1% more material needed to be added when compared with the amount of material used by the 12 flights drum for the same design loading conditions.

From Fig. 2.10 (c) for steel balls it is seen that there are comparable values of the FUF cross sectional area in the range of 25 cm^2 . For the 12 flights drum, the increase in the rotational speed from 1 to 5 rpm caused an increase in the required design loading filling degree from 9.1 to 10.2%, an increase of 12%. For the drum with 18 flights the increase was from 13 to 14.7%, which is a 13% increase. In comparing the values of the filling degree required for the design loading points of the 12 flights drum to the 18 flights drum an average increase of 41.6% was observed.

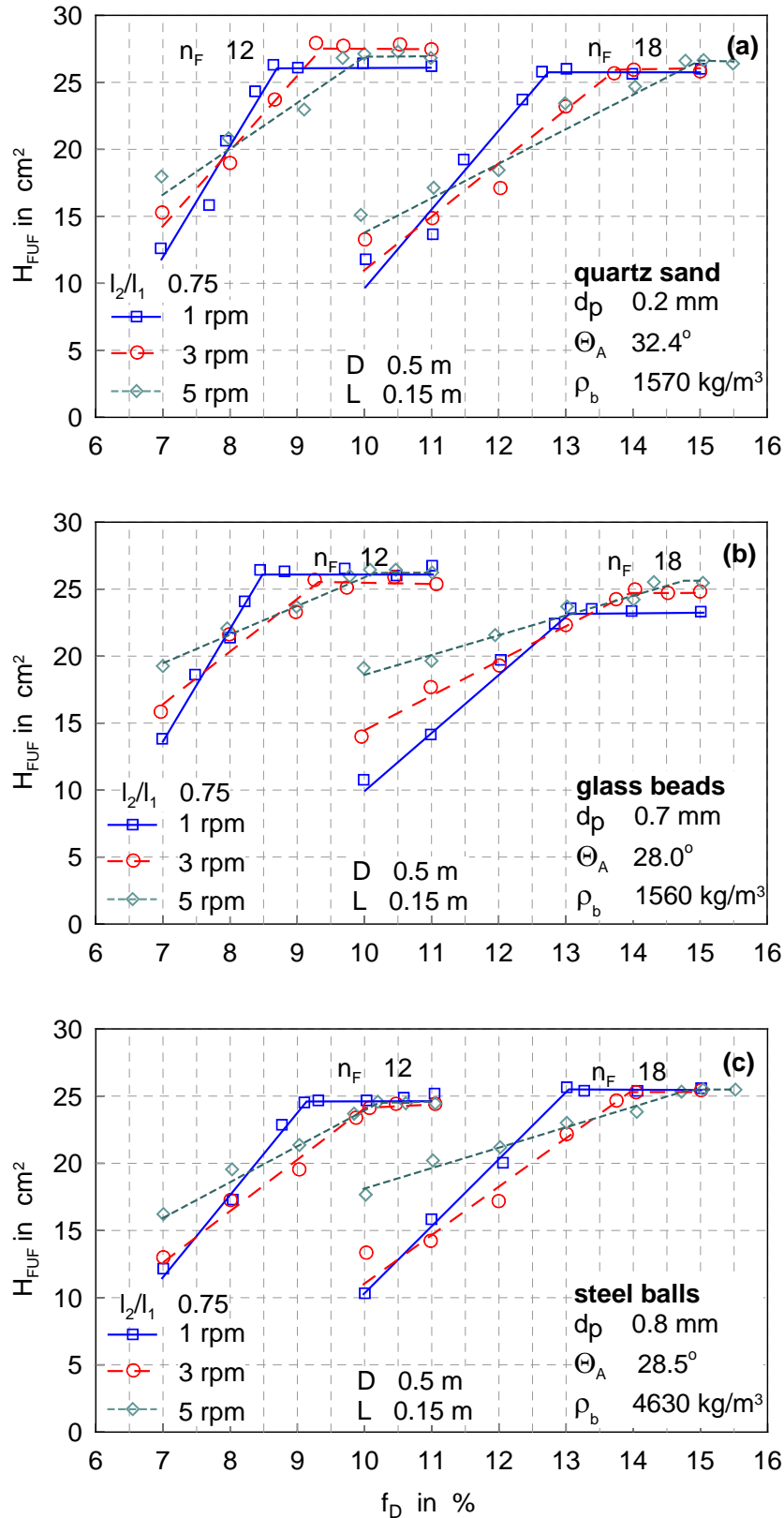


Figure 2.10: Measured FUF cross sectional area versus drum filling degree for various rotational speeds and number of flights (a) quartz sand (b) glass beads (c) steel balls.

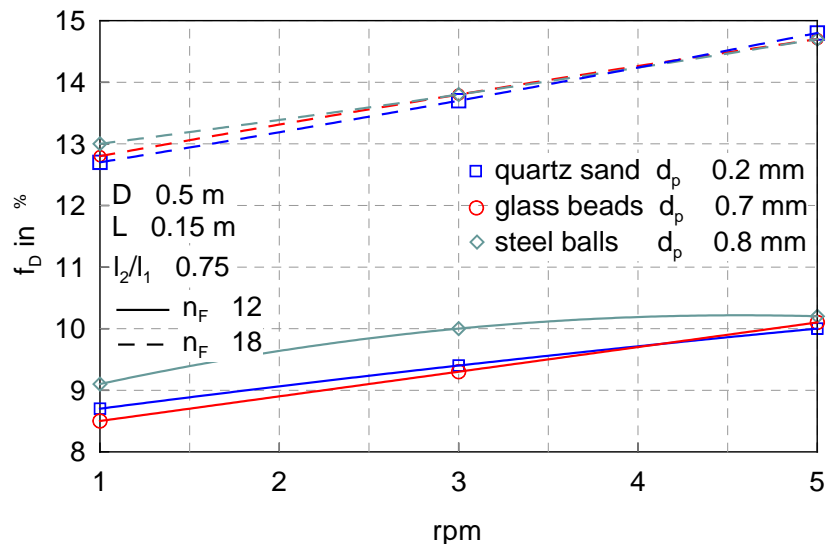


Figure 2.11: Measured design loading filling degree in dependence of rpm for various materials, at two number of flights of 12 and 18 and flight length ratio of 0.75.

2.5.2 Influence of flight length ratio

Figure 2.12 illustrates the variation of the measured FUF cross sectional area versus the drum filling degree for various rotational speeds from 1 to 5 rpm and two flight length ratios of 0.375 and 0.75. It can be seen that increasing the flight length ratio caused an increase in both the FUF cross sectional area and the filling degree required for the design loading point. This is because of the increase of the individual flight holdup and eventually the total holdup. Therefore, flighted rotary drums with longer flight tangential length requires more drum filling degree to reach design loading condition compared to rotary drums with shorter flight tangential length (see Fig. 2.13).

Figure 2.12 (a) for glass beads with particle diameter of 0.7 mm showed an increase in the average measured FUF cross sectional area from 15 to 26 cm² on average while changing the flight length ratio from 0.375 to 0.75 resulted in a percentage increase of 73.3. At a flight length ratio of 0.375 the required drum filling degree for the design point increased from 4.8 to 5.8% when the rpm changes from 1 to 5 which is an increase of 20%. For the flight length ratio of 0.75 an increase was observed from 8.5 to 10.1%, which is a percentage increase of 18.8. Comparing the results of the two flight length ratios it can be seen that the required drum filling degree for the design loading increases by an average of 75.5%.

In Fig. 2.12 (b) for glass beads with particle diameter of 1.0 mm showed an increase in the average measured FUF cross sectional area from 16 to 22.5 cm² while changing the flight length ratio from 0.375 to 0.75 which is a percentage increase of 40.6. At the flight length ratio of 0.375 the required drum filling degree for the design loading point changed from 4.5 to 5.5% when the rpm changes from 1 to 5, which is an increase of 22.2%. For the flight length ratio of 0.75 an increase was observed from 8.1 to 9.4%, which is a percentage increase of 16. Comparing the results of the two flight length ratios it can be seen that the required drum filling degree for the design loading condition increased on average by 77%.

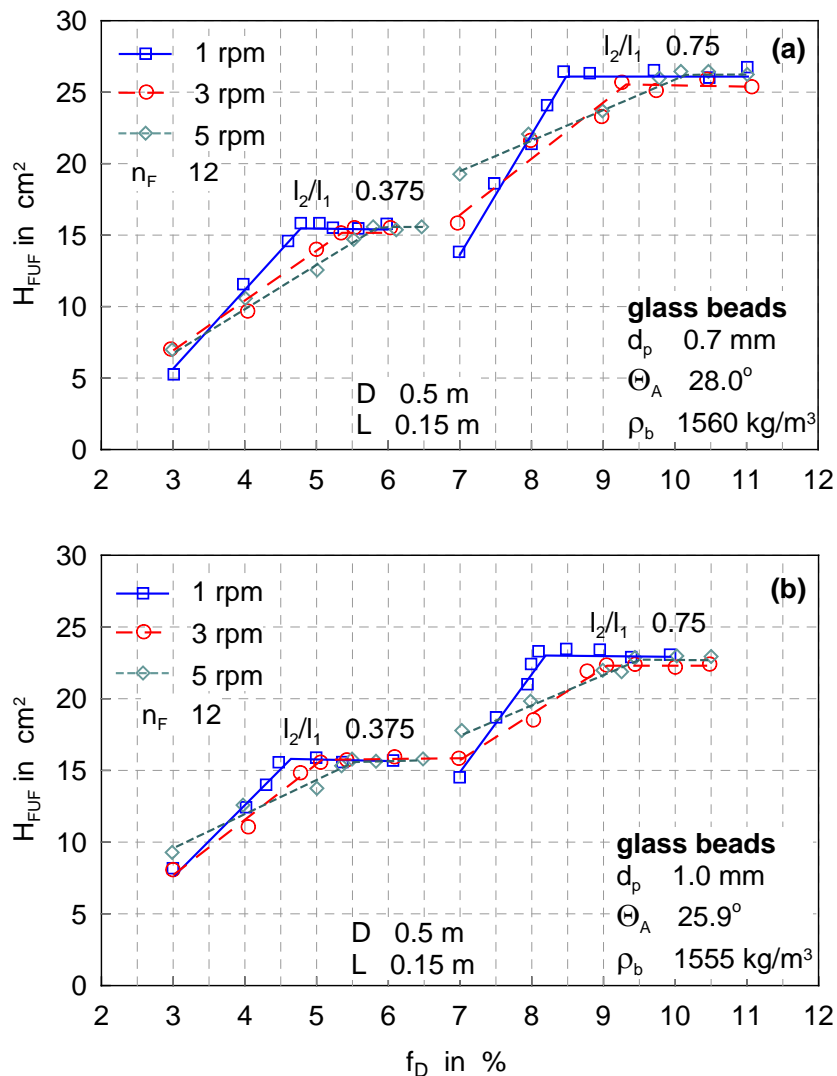


Figure 2.12: Measured FUF cross sectional area versus drum filling degree for various rotational speeds and flight length ratios (a) glass beads 0.7mm (b) glass beads 1.0mm.

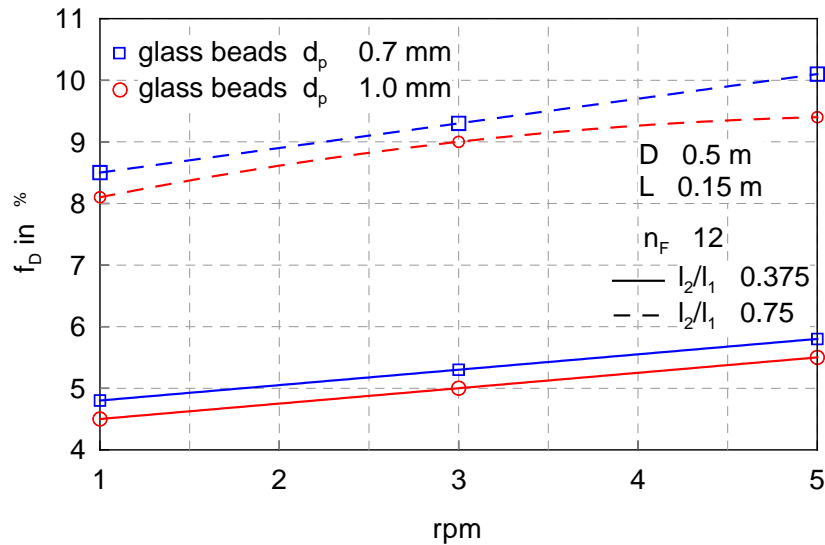


Figure 2.13: Measured design loading filling degree in dependence of rpm for various materials, at two number of flights of 12 and 18 and flight length ratio of 0.75.

2.5.3 Influence of Material properties

Figure 2.13 depicts the variations of the measured FUF cross sectional area versus the drum filling degree for different material properties (particle diameter and dynamic angle of repose). In Fig. 2.13 (a) it is shown that comparable values of FUF cross sectional area is attained of about 25 cm^2 . Also, it can be noted that the design loading filling degree needed for glass beads of 0.7 mm particle diameter and 28° angle of repose is comparable to the one needed for glass beads of 2.0 mm particle diameter and 25.7° angle of repose within a range of 9%.

It can be understood from Fig. 2.13 (b) that the needed filling degree for steel balls of 0.8 mm particle diameter and 28.5° angle of repose is 10%. While the one needed for steel balls of 2.0 mm and 25.5° angle of repose is 9% which is a 11.1% difference. Comparable values of the FUF cross sectional area were attained with a average of 24.5 cm^2 . These unexpected observations maybe related to the error in measuring the dynamic angle of repose.

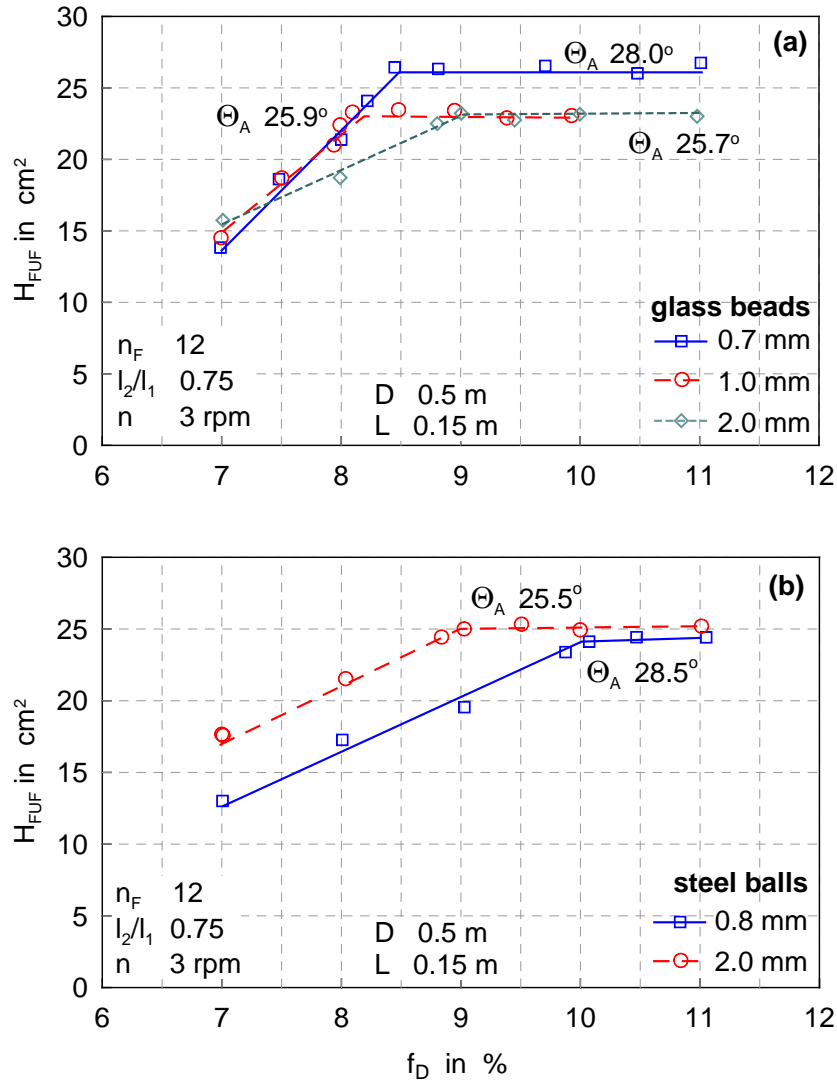


Figure 2.13: Measured FUF cross sectional area versus drum filling degree for various material particle diameters and dynamic angles of repose (a) glass beads (b) steel balls.

2.5.4 Discharge angle

For better understanding of the influence of the drum filling degree on the FUF discharge angle (discussed before in Ch. 1); an example from the experimental results for quartz sand at different rotational speeds is illustrated in Fig. 2.14. As shown from Fig. 2.14 at any rpm (i.e. 1 rpm) an increasing drum filling degree (from the under-loading to the over-loading) leads to lower the FUF discharge angle until it becomes at the 9 o'clock (see Fig. 1). This point considered the design loading of the drum and the corresponding value of the filling degree as shown before in Fig. 2.10 is 8.7%.

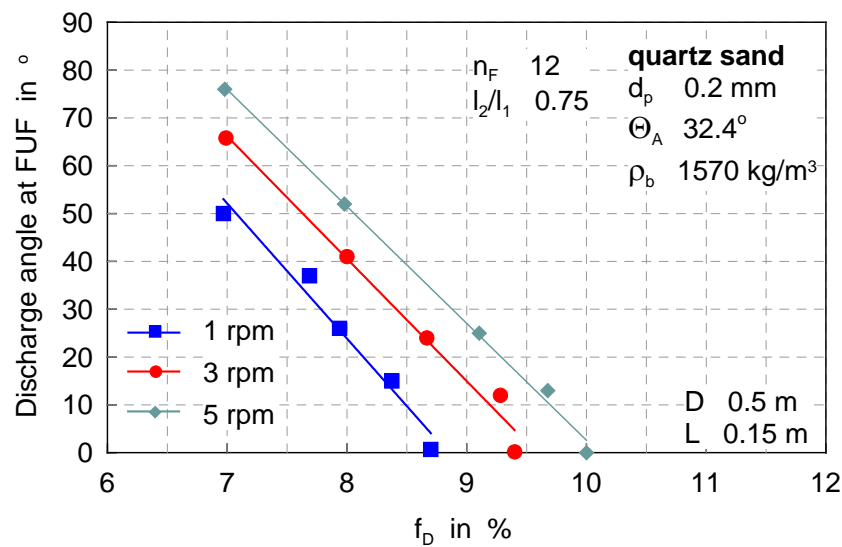


Figure 2.14: FUF discharge angle versus drum filling degree for quartz sand at three rotational speeds.

2.6 Comparisons with models from literature

Table 2.3 outlines the experimental results for different operating conditions, the design loading filling degree and the FUF cross sectional area at the design loading point. The average slandered deviation in measuring the FUF area only at design loading points is also listed in Table 2.3.

Comparisons between the experimental results and some available models from literature (**Porter, 1963; Kelly and O'Donnell, 1977 and Ajayi and Sheehan, 2012b** (modified Baker's model)) were conducted and shown also in Table 2.3. **Ajayi and Sheehan 2012b** showed that the **S** factor values in Eq. (1.4) are small, with a typical range of 0.042-0.078. Due to this, the term in Eq. (1.4) including the factor **S** was neglected in the present work. Consequently the comparison of the current experimental results with the mentioned models will be based on flight-borne data only, as H_{FUF} and H_i were extracted from the photos and used directly in the models. Then the resulted H_{Tot} from the models were converted to filling degree using Eq. (1.5) and finally were compared with one of the current experimental results. The comparisons revealed that no model was able to describe the design loading precisely. The one developed by **Ajayi and Sheehan, 2012b** yields the lowest deviation, especially at lower rotational speeds (10-15%). Based on our experimental

data, the new fitting factor 1.38 can be proposed to modify **Baker's** model, 1988 to give the best fit (when using rectangular flights) as shown in Eq. (2.1).

Present work, model for design loading:

$$H_{Tot} = 1.38 \times \left(2 \times \frac{LUF}{FUF} \sum H_i \right) - H_{FUF} \quad (2.1)$$

Based on the experimental results, it can be suggested that to ensure optimum (design) loading of a rotary drum, the volume occupied by the solid should be between 5-15% of the total drum volume. The range reported by **Perry and Green, 1999** was 10-15%. The reason behind the difference between the two ranges is that the present work studied the influence of the flight length ratio, where the smaller flight length ratio (0.375) reveals that 5% filling degree is required for optimum loading.

Table 2.3: Experimental results and deviations from models

No.	Material used	d_p (mm)	N (rpm)	n_F --	l_2/l_1 --	H_{FUF} (cm^2)	$f_{design\ load}$ (%)	Deviation from models (%)		
								Porter 1963	Kelly and O'Donnell 1977	Ajayi 2012
1	Quartz Sand	0.2	1	12	0.75	26.0 ± 0.4	8.7	11.6	3.0	1.4
2	Quartz Sand	0.2	3	12	0.75	27.1 ± 0.6	9.4	21.5	12.2	10.4
3	Quartz Sand	0.2	5	12	0.75	26.3 ± 0.7	10	30.8	20.8	18.9
4	Glass Beads	0.7	1	12	0.75	25.8 ± 0.6	8.5	12.1	3.5	1.9
5	Glass Beads	0.7	3	12	0.75	24.9 ± 0.4	9.3	22.9	13.4	11.7
6	Glass Beads	0.7	5	12	0.75	25.5 ± 0.7	10.1	36.5	26.0	24.0
7	Steel Balls	0.8	1	12	0.75	24.5 ± 0.4	9.1	24.5	15.0	13.2
8	Steel Balls	0.8	3	12	0.75	23.9 ± 0.5	10	36.9	26.3	24.4
9	Steel Balls	0.8	5	12	0.75	24.4 ± 0.7	10.2	39.6	28.9	26.8
10	Quartz Sand	0.2	1	18	0.75	25.8 ± 1.5	12.7	10.1	4.3	-16.6
11	Quartz Sand	0.2	3	18	0.75	25.7 ± 0.5	13.7	18.8	12.5	-10.1
12	Quartz Sand	0.2	5	18	0.75	26.3 ± 0.6	14.8	29.1	22.3	-2.2
13	Glass Beads	0.7	1	18	0.75	23.1 ± 0.5	12.8	14.9	8.8	-13.0

Table 2.3-continued: Experimental results and deviations from models

No.	Material used	d_p (mm)	N (rpm)	n_F --	l_2/l_1 --	H_{FUF} (cm^2)	$f_{design\ load}$ (%)	Deviation from models (%)		
								Porter 1963	Kelly and O'Donnell 1977	Ajayi 2012
14	Glass Beads	0.7	3	18	0.75	24.5 ±0.3	13.8	24.9	18.3	-5.5
15	Glass Beads	0.7	5	18	0.75	25.1 ±0.6	14.7	33.0	26.0	0.7
16	Steel Balls	0.8	1	18	0.75	25.2 ±0.5	13.0	17.1	11.0	-11.3
17	Steel Balls	0.8	3	18	0.75	25.0 ±0.5	13.8	24.3	17.8	-5.8
18	Steel Balls	0.8	5	18	0.75	25.1 ±0.6	14.7	32.5	25.5	0.3
19	Glass Beads	1.0	1	12	0.75	23.3 ±0.4	8.1	17.8	8.7	7.0
20	Glass Beads	1.0	3	12	0.75	22.8 ±0.5	9.0	33.8	23.5	21.6
21	Glass Beads	1.0	5	12	0.75	22.8 ±0.7	9.4	37.3	26.7	24.7
22	Glass Beads	2.0	3	12	0.75	22.7 ±0.4	9.0	29.1	19.2	17.3
23	Steel Balls	2.0	3	12	0.75	25.1 ±0.5	9.0	20.2	10.9	9.2
24	Glass Beads	0.7	1	12	0.375	15.9 ±0.4	4.8	-1.3	-8.9	-10.3
25	Glass Beads	0.7	3	12	0.375	16.0 ±0.5	5.3	11.8	3.2	1.6
26	Glass Beads	0.7	5	12	0.375	15.8 ±0.3	5.8	25.6	16.0	14.2
27	Glass Beads	1.0	1	12	0.375	15.7 ±0.3	4.5	-1.2	-8.8	-10.2
28	Glass Beads	1.0	3	12	0.375	15.8 ±0.4	5.0	9.8	1.3	-0.3
29	Glass Beads	1.0	5	12	0.375	15.7 ±0.4	5.5	20.7	11.4	9.7

Chapter 3

New experimental technique and scale up

3.1 Background

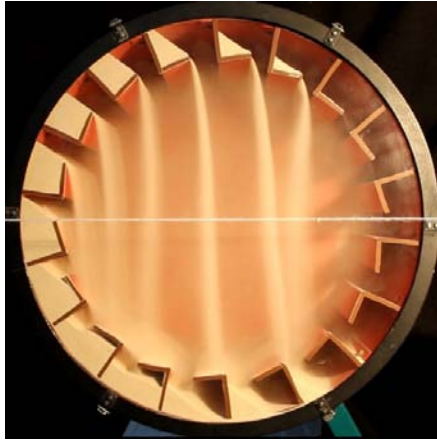
It is concluded in Ch. 2 that the automated method for the image analysis (using combination of ImageJ software and Matlab image processing toolbox) is much time saving. For the calculations and eye strain than the manual method (manual selection using ImageJ). Also the traditional way for recording videos used before in rotary drum studies (see Fig. 2.7 and 2.8) have led to many difficulties in using the automated method. Thus a new technique in recording videos should be developed to overcome all the mentioned problems (in Ch.2).

3.2 New experimental technique

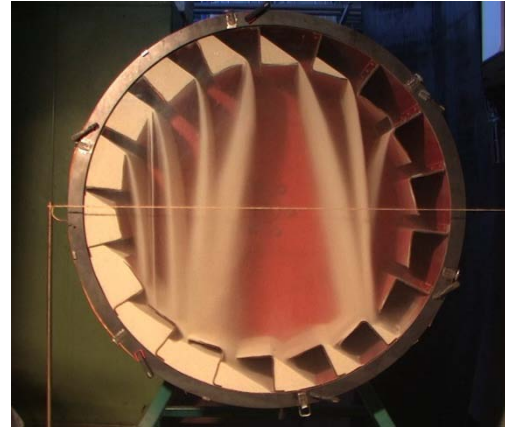
The new technique is mainly developed based on; choosing the best camera position to avoid the appearance of the solid material side views in the axial direction, and choosing the best light intensity and angle to avoid any shadows of the solid materials and reducing the number of pre-processes needed before the transformation in to black and white photo. The most important issue is that, the selected camera position and light intensity and angle must be kept the same for all experiments, where this will make the initial batch processes for large number of photos are much easier and precisely.

Figure 3.1 shows some trials for the selection of the best camera position and light intensity and angle. Where in Fig. 3.1 (b) the camera position kept at the center point of the drum but the light moved to the right side of the drum perpendicularly, as shown the shadows are reduced compared to Fig. 3.1 (a) but it is still exists. In Fig. 3.1 (c) the camera has been moved to the left but at the same elevation of the center point of the drum, and the light is moved also to the right side of the drum perpendicularly, the same happened as before where the shadows are reduced compared to Fig. 3.1 (a) but it is still exist. In Fig. 3.1 (d) the camera has been moved to the down left corner of the drum, also the light moved to the left, it shows maybe this is the best positions where nearly the material side views are no longer exists. But it is found an error in the measurements of the flight tip angels at this camera position of about $2-7^{\circ}$. Thus it is recommended to keep the camera potion at the center point of the drum, but try to handle the light intensity and angle. The case shown in Fig. 3.1 (e) choosed to be the best technique and it is followed for all the coming experimental work.

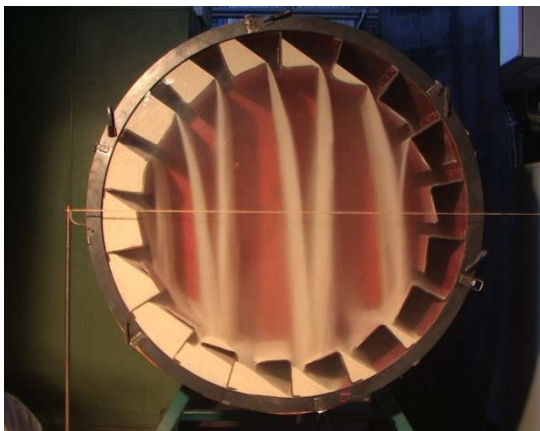
Using this technique will facilitate both the manual and automated methods of image analysis. With the advantage of less pre-processes needed for the photos before the conversion in to black and white photos and the fed to the Matlab code as shown in Fig. 3.2. Where the original photo is converted in to black and white in one step. It is worth to compare Fig. 3.2 with Fig. 2.7 where many pre-processes were needed for the conversion in Fig. 2.7.



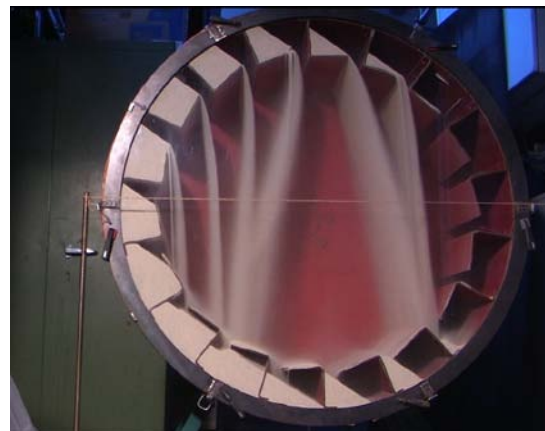
(a) Traditional technique: camera (center)



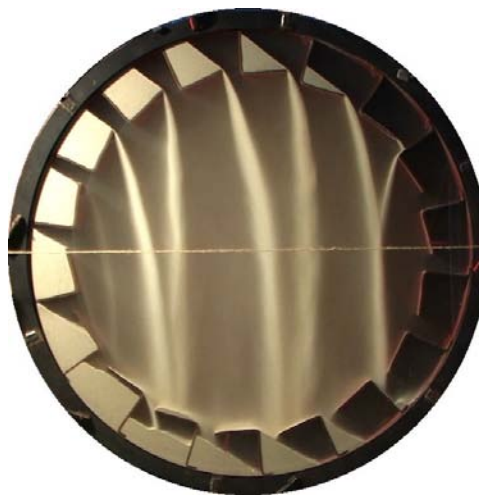
(b) Trial-1: camera (center), light (right-perpendicular)



(c) Trial-2: camera (center-left), light (left-perpendicular)



(d) Trial-3: camera (down-left corner), light (left-perpendicular)



(e) Trial-4: camera (center), light (left angled)

Figure 3.1: New experimental technique trials with different camera positions and light intensity and angle.

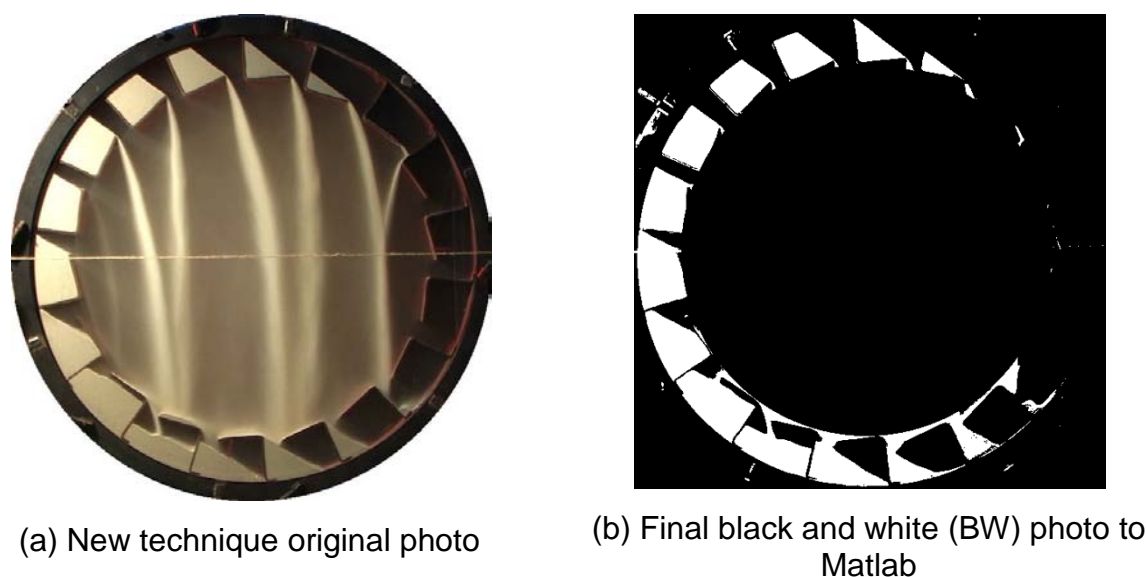


Figure 3.2: Transformation of the new experimental technique photos in black and white.

3.3 New experimental work and scaling up the drum size

In order to verify the use of the new experimental technique, it is planned in this chapter to carry out more experiments using the new technique. Also the drum size was enlarged to be double the drum used for the experiments in Ch. 2. In the present chapter more experiments are to be carried out on a test rig similar to the one described previously in Ch. 2 except for the drum size that will be 1.0 m diameter and 0.3 cm length where the length to the diameter ratio (L/D) kept constant at 0.3. Number of flights are as before 12 and 18. For the flight length ratios, it is planned to study more flight length ratios than before as to be; 0.0, 0.375, 0.75 and 1.0. But It is found during conducting the experiments that, the flight length ratio of 0.0 could only be used for over loading drums. As it is found that the amount of solid needed for the design loading point when using flight length ratio of 0.0 is very less and consequently very early final discharge angle (see Fig. 3.3), because there is no any tangential length of the flight and this will be nonsense to be applied in industry. Thus it is recommended when using flight length ratio of 0.0 the drum should be overloaded. Another observation from the experimental work affected also the selection of the studied flight length ratios, is that the flight length ratio of 1.0 cannot

be used with 18 flights drum. As the spaces between the flights are small and a kind of throttling of the solid happened and a formation of a bed at the bottom of the drum is observed which is inconsistent with the definition of the optimum loading, as shown in Fig. 3.4. Thus the flight length ratios choosed to be 0.375, 0.75 and 1.0 (for 12 flights only). Two materials are to be examined quartz sand of 0.2 mm particle diameter and glass beads of 0.7 mm (back to Table 2.2 for the material properties). For the same range of rotational speeds of 1, 3 and 5 rpm. The new experimental work drum specifications and operating parameters are listed in Table 3.1.

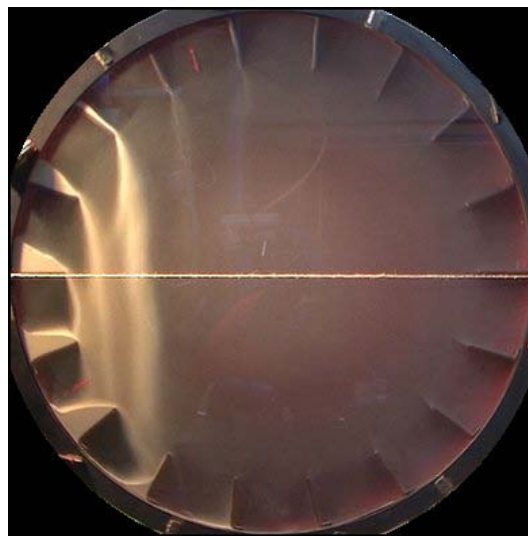
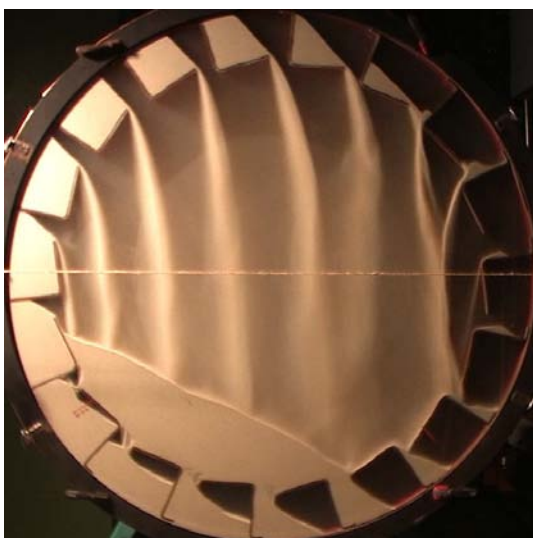
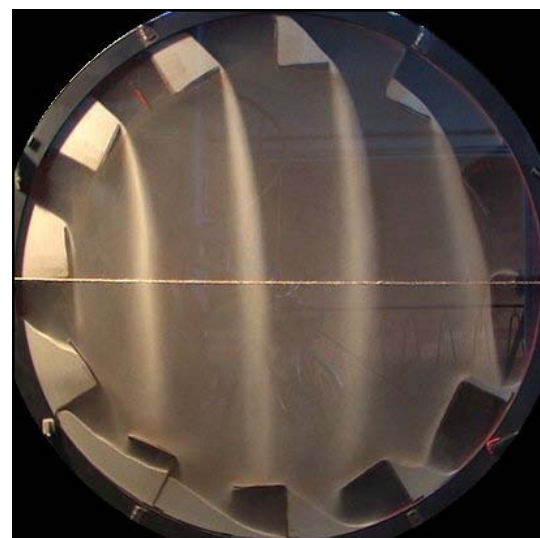


Figure 3.3: Flight length ratio of 0.0 shows very less amount of solid at design loading.



(a) 18 flights (formation of bed)



(b) 12 flights (no bed)

Figure 3.4: Problems when using flight length ratio 1.0 with the 18 flights.

Table 3.1: Specifications of the drum and operating parameters of the new experimental work

Drum diameter	1.0 m
Drum length	0.3 m
Flight length ratio	0.375, 0.75 and 1.0 (12 flights only)
Number of flights	12 and 18
Rotational Speed	1, 3 and 5 rpm

The experimental procedure is the same as discussed in Ch. 2. The data will be extracted based on the automated image analysis method except for the tip angles and curtains falling height measurements, the manual method is used. Same data fitting method for the experimental results used in Ch. 2 is used here in the current work.

3.4 Results and discussions

The measured average FUF cross section area is plotted versus the drum filling degree in the following Figures.

3.4.1 Influence of number of flights

Figure 3.5 shows the influence of the drum filling degree on the measured FUF cross sectional area for rotational speeds of 1, 3 and 5 rpm and the number of flights 12 and 18 at the same flight length ratio of 0.75. From Fig. 3.5 (a) for quartz sand it can be noted that the saturation (maximum) value of the measured FUF cross sectional area are in the range of 105 cm². For the 12 flights drum the increase in the rotational speed from 1 to 5 rpm caused an increase in the required design loading filling degree from 7.5 to 9.5%, respectively, which is an increase of 26.6%. For the drum of 18 flights that increase is from 11 to 13.4 %, a 21.8 % increase in the design loading filling degree. By comparing the values of the filling degree required for the design loading points of the 12 flights drum to the 18 flights drum an average increase of 44% can be observed.

Figure 3.5 (b) for glass beads show comparable values of the FUF cross sectional area in the range of 126 cm². For the 12 flights drum the required filling

degree for design loading increases from 7.3 to 9% when the rotational speed increases from 1 to 5 rpm, respectively, by a percentage increase of 23. For the drum with 18 flights the filling degree varied from 12.3 to 14%, respectively, which is 13.8% increase. In order to achieve design loading conditions using 18 flights, in average 60 % more material should be added when compared with the amount of material used by the 12 flights drum for the same design loading conditions.

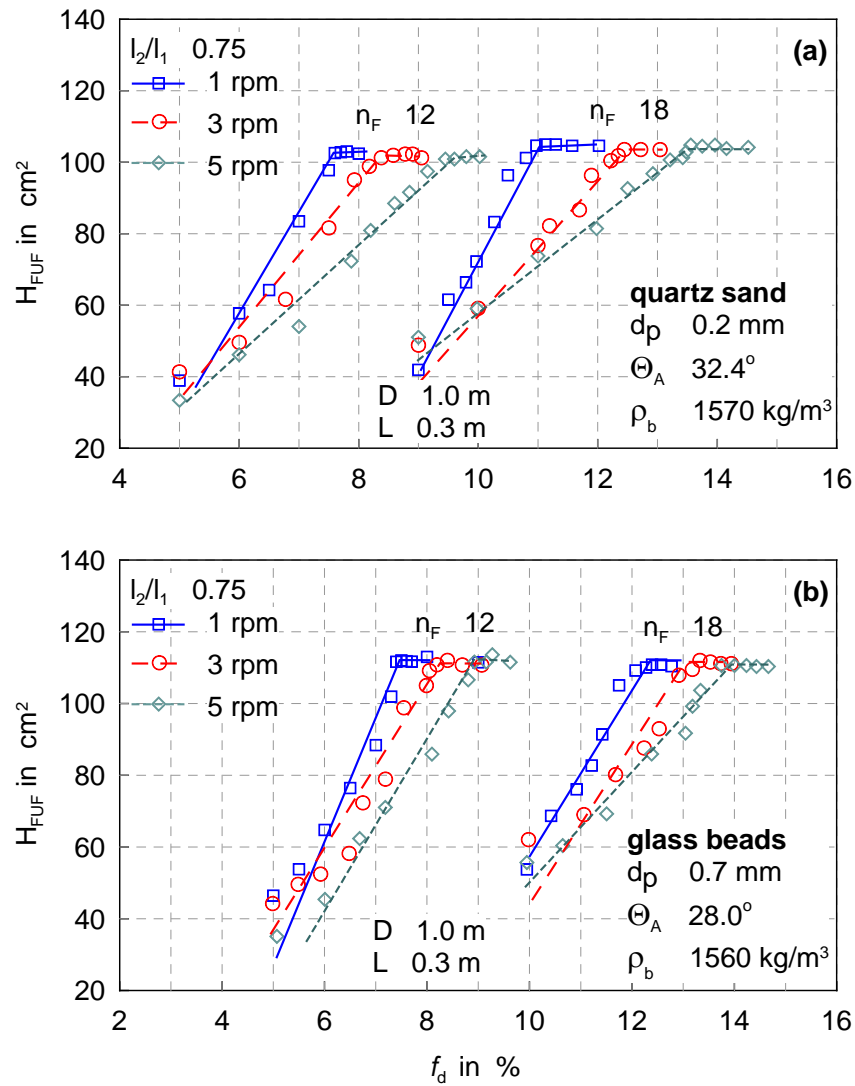


Figure 3.5: Measured FUF cross sectional area versus drum filling degree for various rotational speeds and number of flights (a) quartz sand (b) glass beads.

3.4.2 Influence of flight length ratio

Figure 3.6 illustrates the variation of the measured FUF cross sectional area versus the drum filling degree for various rotational speeds from 1 to 5 rpm and two flight length ratios of 0.375 and 1.0 at the same number of flights of 12.

Figure 3.6 (a) for quartz sand with particle diameter of 0.2 mm showed an increase in the average measured FUF cross sectional area from 70 to 120 cm² on average while changing the flight length ratio from 0.375 to 1.0 resulted in a percentage increase of 71.4. At a flight length ratio of 0.375 the required drum filling degree for the design point increased from 4.1 to 5.3% when the rpm changes from 1 to 5 which is an increase of 29%. For the flight length ratio of 1.0 an increase was observed from 10 to 12.1%, which is a percentage increase of 21. Comparing the results of the two flight length ratios it can be seen that the required drum filling degree for the design loading increases by an average of 120%.

In Fig. (b) 3.6 for glass beads with particle diameter of 0.7 mm showed an increase in the average measured FUF cross sectional area from 70 to 125 cm² while changing the flight length ratio from 0.375 to 1.0 which is a percentage increase of 78. At the flight length ratio of 0.375 the required drum filling degree for the design loading point changed from 4.7 to 5.8% when the rpm changes from 1 to 5, which is an increase of 23.4%. For the flight length ratio of 1.0 an increase was observed from 10 to 12%, which is a percentage increase of 20. Comparing the results of the two flight length ratios it can be seen that the required drum filling degree for the design loading condition increased on average by 120%.

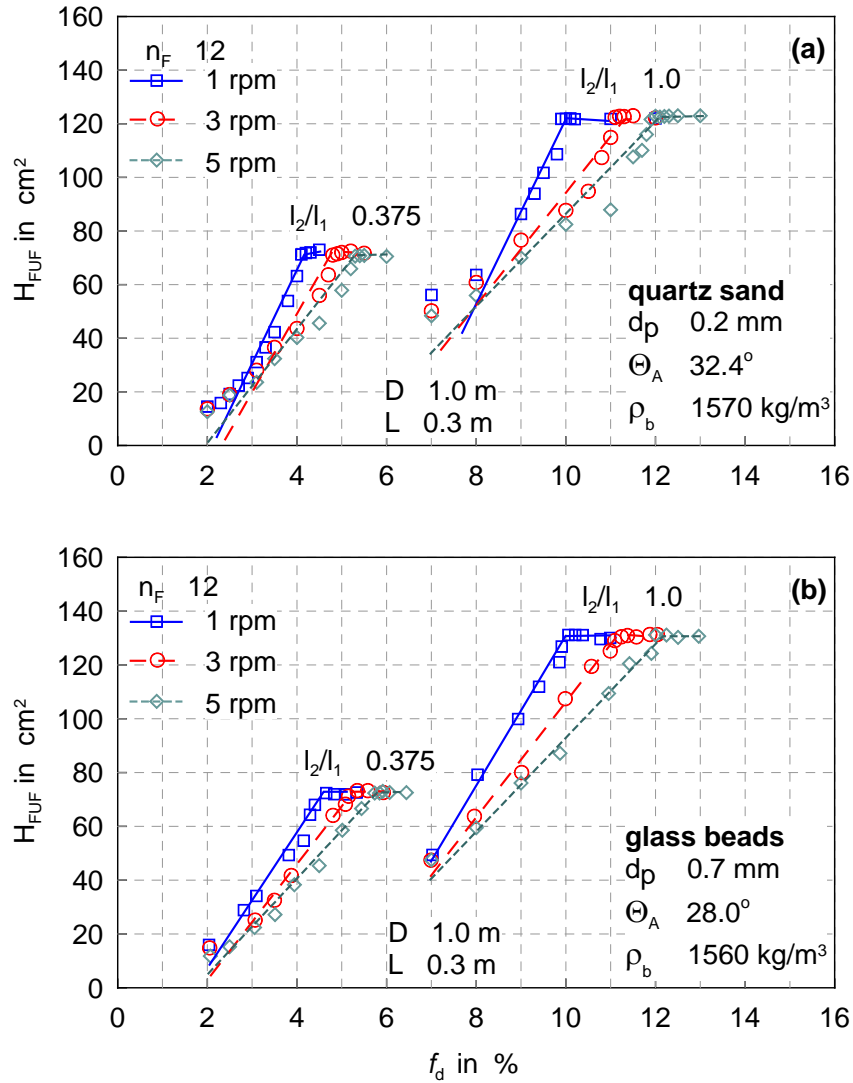


Figure 3.6: Measured FUF cross sectional area versus drum filling degree for various rotational speeds and flight length ratios at the same number of flights of 12 (a) quartz sand (b) glass beads.

3.4.3 Comparisons with models from literature

Table 3.2 lists all the experimental results performed on the large size drum of 1.0 m diameter including all of operating conditions. Also it shows the deviations from the design loading models of **Ajayi and Sheehan, 2012b** (Eq. (1.4)) and the developed model suggested by the current work (Eq. 2.1). The comparisons of the deviations from the models revealed that the current work model was the better to predict the design loading ($\pm 11\%$) than the one of Ajayi and Sheehan ($\pm 17\%$).

Table 3.2: Experimental results and deviation from models

No.	Material used	d_p (mm)	N (rpm)	n_F --	l_2/l_1 --	H_{FUF} (cm^2)	$f_{design\ load}$ (%)	Deviation from models (%)	
								Ajayi 2012	Karali 2015
1	Glass Beads	0.7	1	12	0.375	71.15 \pm 0.4	4.5	34.7	18.8
2	Glass Beads	0.7	3	12	0.375	72.21 \pm 0.6	5.2	18.3	4.4
3	Glass Beads	0.7	5	12	0.375	72.13 \pm 0.4	5.7	7.8	-4.9
4	Glass Beads	0.7	1	12	0.75	111.6 \pm 0.5	7.4	28.5	13.4
5	Glass Beads	0.7	3	12	0.75	110.3 \pm 0.3	8.1	16.0	2.4
6	Glass Beads	0.7	5	12	0.75	112.2 \pm 0.5	8.9	7.4	-5.2
7	Glass Beads	0.7	1	12	1.0	130.2 \pm 0.6	10	11.0	-2.1
8	Glass Beads	0.7	3	12	1.0	131.6 \pm 0.7	11.3	-0.8	-12.5
9	Glass Beads	0.7	5	12	1.0	131.0 \pm 0.5	12.1	-7.7	-18.6
10	Glass Beads	0.7	1	18	0.375	77.38 \pm 0.6	6.2	6.3	-6.2
11	Glass Beads	0.7	3	18	0.375	77.26 \pm 0.6	6.9	-4.6	-15.8
12	Glass Beads	0.7	5	18	0.375	77.98 \pm 0.6	7.8	-14.8	-3.8
13	Glass Beads	0.7	1	18	0.75	95.69 \pm 0.5	11.6	-29.7	-20.6
14	Glass Beads	0.7	3	18	0.75	95.73 \pm 0.4	12.7	-35.8	-27.4
15	Glass Beads	0.7	5	18	0.75	96.94 \pm 0.8	13.7	-39.7	-31.9
16	Quartz Sand	0.2	1	12	0.375	71.27 \pm 0.7	4.1	48.1	30.7
17	Quartz Sand	0.2	3	12	0.375	71.03 \pm 0.5	4.8	26.1	11.2
18	Quartz Sand	0.2	5	12	0.375	70.63 \pm 0.6	5.3	13.5	0.2
19	Quartz Sand	0.2	1	12	0.75	102.5 \pm 0.5	7.6	15.0	1.4
20	Quartz Sand	0.2	3	12	0.75	100.6 \pm 0.5	8.5	0.9	-11.0
21	Quartz Sand	0.2	5	12	0.75	101.7 \pm 0.4	9.5	-8.8	-19.5
22	Quartz Sand	0.2	1	12	1.0	121.8 \pm 0.5	9.9	4.8	-7.5
23	Quartz Sand	0.2	3	12	1.0	122.4 \pm 0.4	11.1	-6.0	-17.1
24	Quartz Sand	0.2	5	12	1.0	122.8 \pm 0.4	12	-12.8	-23.1

Table 3.2-continued: Experimental results and deviation from models

No.	Material used	d_p (mm)	N (rpm)	n_F --	l_2/l_1 --	H_{FUF} (cm ²)	$f_{\text{design load}}$ (%)	Deviation from models (%)	
								Ajayi 2012	Karali 2015
25	Quartz Sand	0.2	1	18	0.375	65.54 ±0.5	6	-6.9	-17.9
26	Quartz Sand	0.2	3	18	0.375	66.9 ±0.5	7	-18.6	-28.2
27	Quartz Sand	0.2	5	18	0.375	65.6 ±0.5	8	-30.1	-21.0
28	Quartz Sand	0.2	1	18	0.75	104.6 ±0.6	11	-19.0	-8.4
29	Quartz Sand	0.2	3	18	0.75	103.7 ±0.4	12.4	-28.7	-19.5
30	Quartz Sand	0.2	5	18	0.75	104.2 ±0.3	13.5	-34.2	-25.7

3.4.4 Scaling up the drum size

As described before the current chapter presented more experiments using a larger drum size as the scaling up process. Where the drum diameter increased from 0.5 m (old experiments in Ch. 2) to 1.0 m (new experiments). Figure 3.7 depicts the scaling up results based on comparing the required design loading filling degree of the new experiments to the old one at the same operating conditions. The comparison reveals that in most cases of operating conditions, the required filling degree for design loading of the higher drum diameter ($D=1.0$ m) is less than of the ($D=0.5$ m). Except for the cases of lower flight length ratio, both filling degrees were almost the same. The average of the deviation was about -9 % as shown with the shaded area in Fig.3.7. It should be mentioned that however the comparisons show decrease in the filling degree for the 1.0 m diameter drum rather than the 0.5 m diameter drum, but sure the total holdup (kg of solid) needed is much higher and in average was about 60%.

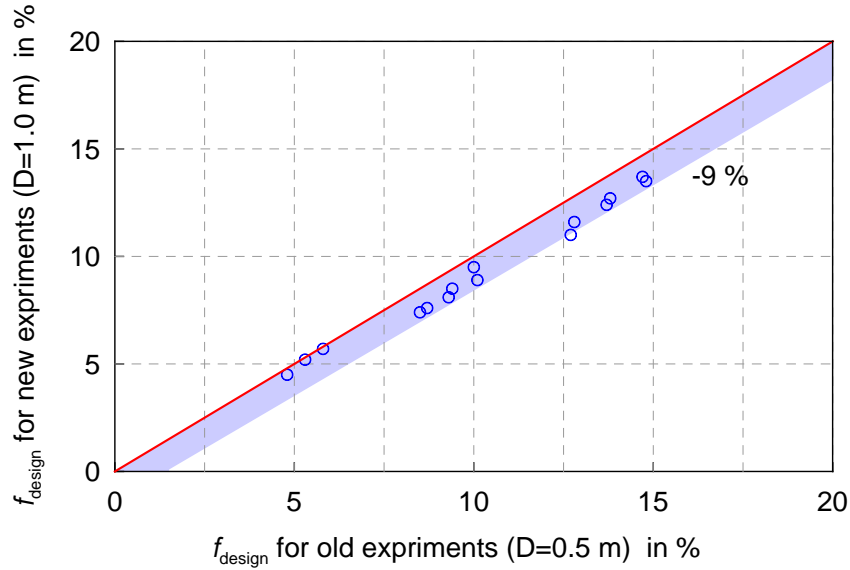


Figure 3.7: Comparison between the results of the experimental data from small drum ($D=0.5$ m) to ($D=1.0$ m) at the same operating conditions of design loading.

3.5 Correlation development

Based on all of the experimental data presented in Ch. 2 and Ch. 3 a correlation has been developed using the power function regression analysis as given in Eq. (3.1). Including all of the studied parameters, mostly in the form of dimensionless groups to help for the scaling up of the data (Froude number (Fr) was chosen to substitute the rpm). Table 4.2 lists all of the valid ranges of the correlation's parameters. The deviation of the calculated results from the correlation to the actual experimental results is shown in Fig. 3.8, where the shaded area represents the root mean square deviation (RMSD) with a factor of 3.4.

$$f_{\text{design load}} \% = 4.9 D^{-0.52} d_p^{0.043} (\tan \theta_A)^{0.351} \rho_b^{0.013} Fr^{0.052} n_F^{0.941} \left(\frac{l_2}{l_1} \right)^{0.839} l_1^{0.353} \quad (3.1)$$

By means of this correlation the point of under loading can be determined and avoided by changing some design parameters to the drum such; as the number of flights or the flight length ratio.

Table 3.2: Correlation valid ranges

	Parameter		Units	Valid Range
Drum characteristics	Drum diameter	D	m	0.5 - 1.0
	Drum length	L	m	0.15 - 0.3
	Drum length to Diameter ratio	L/D	–	0.3
	Rotational speed	N	rpm	1 - 5
	Froude Number	Fr	–	0.000279 - 0.013
Material properties	Particle diameter	d_p	m	0.0002 - 0.002
	Material dynamic angle of repose	θ_A	°	25.7 - 62.3
	Material consolidated bulk Density	ρ_b	kg/m ³	1550 - 4630
Flight characteristics (rectangular)	Total number of flights	n_F	–	12 - 18
	Flight tangential to radial length ratio	l_2/l_1	–	0.375 - 1.0
	Flight radial length	l_1	m	0.05 - 0.1

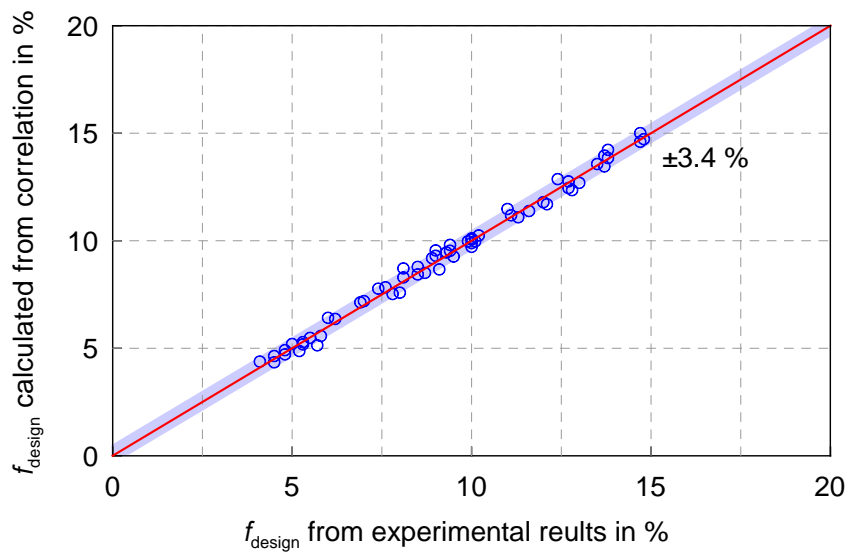


Figure 3.8: Deviation of correlation results from experimental results for the same operating conditions.

Chapter 4

Determination of the discharge characteristics

4.1 Overview

Previously In Ch. 2 and Ch. 3 a lot of experiments were performed to assess the optimum loading of a flighted rotary drum. Furthermore studies for the discharge characteristics of the solid which leaves the flights to the gas-borne area are needed. As they determines the amount of solid will present in the gas-borne phase and its disperse nature. Which influences the overall performance of the drum. The discharge characteristics to be studied in the present chapter are: kinetic angle of repose of the solid reside inside the flights, holdup of the solid carried by the flights, final discharge angle, height and time of fall. These discharge characteristics are to be determined as a continuous function of the flight angular position. Assuming a uniform distribution over the drum length (axial direction as described previously in Ch. 2).

The recorded videos of the design loading points from the experimental work presented in Ch. 2 and Ch. 3 are to be analyzed. The analysis relies on playing the recorded video then tracing one flight from the 9 o'clock position to the final discharge position (emptying point). The video has to be stopped arbitrarily at many positions in between to extract photos of interest. These photos are to be analyzed using a typical manual image analysis method described previously in Ch. 2 through measurement of solid areas of interest, angles and distances of fall. Some

geometrical parameters are needed in the present chapter and must first be defined as follows.

4.2 Geometrical parameters

Figure 4.1 shows some geometrical parameters of the flighted rotary drum needed for the present study: flight tip angle (discharge angle (δ)), final discharge angle (δ_L), dimensions of the flight; radial length (l_1) and tangential length (l_2) and effective radial distance (r_H) of the flight given by

$$r_H = R - l_1 \quad (4.1)$$

where R is the drum radius, the characteristic angle of the flight made by the tangential length (α) given by

$$\tan \alpha = \frac{l_2}{r_H}. \quad (4.2)$$

4.3 Kinetic angle of repose of the solid residing inside the flight

The kinetic angle of repose generally can be defined as the angle of stability of a granular (powder) material residing on a surface. For instance, if a granular material is poured onto a flat surface, it will form a pile whose stability angle with the horizontal plane is called the static angle of repose. This angle of repose is affected by the solid cohesivity.

Particles within a flight in a rotary drum will also form an angle of repose with the horizontal plane, which will depend on the angular position of the flight. Since the angle of repose is affected by the drum rotational speed, it is called the dynamic (kinetic) angle of repose (**J. Mellmann, 2001 and X. Liu et al., 2005**).

Sherritt et al., 1993; Wang et al., 1995; Van Puyvelde, 2009; Lee and Sheehan, 2010 and Sunkara et al., 2013b). It was stated by **Glikin, 1978** and followed by other researchers, that it is difficult to model the drum with a single relation for the flight holdup during the period of discharge. Hence, the discharge period should be divided into regions based on the range values of the kinetic angle of repose and the angular position.

Schofield and Glikin, 1962 (Eq. (4.3)) developed the first model to calculate the kinetic angle of repose of the solid residing inside the flight. The conventional two segment flight was used in the model by applying the force balance acting at the tip of the flight and assuming the material surface is smooth and approximately a straight line. The kinetic angle of repose from their model depends on the circumferential position of the flight (δ), the geometrical parameters (described previously in 4.1), the Froude number (Fr) given by

$$Fr = \frac{\omega^2 R}{g} \quad (4.3)$$

where ω is the drum angular velocity and μ is the dynamic friction coefficient.

$$\tan \gamma = \frac{\mu \cos \alpha + Fr \left(\frac{r_H}{R} \right) (\cos \delta - \mu \sin \delta)}{\cos \alpha - Fr \left(\frac{r_H}{R} \right) (\sin \delta + \mu \cos \delta)} \quad (4.4)$$

The dynamic friction coefficient (μ) can be taken as $\tan(\Theta_A)$, where Θ_A is the solid material property dynamic angle of repose (the angle of repose of the free bed surface at the bottom of the drum, **Sunkara, 2013**). Whereas in the present study it is estimated by iterative calculations using Eq. (3.4) based on known measured kinetic angles of repose (γ) at different flight discharge angles (δ). Finally, the calculated dynamic friction coefficient is used to calculate the **Schofield and Glikin, 1962** kinetic angle of repose (γ) and compare it with the experimental results.

The measured kinetic angle of repose of the solid residing inside the flight versus the angular position (flight discharge angle) is plotted in the following for different

materials and operating parameters at design loading conditions. The data points in all figures correspond to the experimental measurements and each point represents one image that was extracted from the video at a specific flight angular position.

Figure 4.2 depicts the influence of the discharge angle on the measured kinetic angle of repose for two rotational speeds (1 and 5 rpm) and two number of flights (12 and 18) at the same flight dimensions. The lines represent the fitting curves (polynomial fitting). It is observed that the kinetic angle of repose increases in average by $2-7^\circ$ during the initial period of discharge and then decreases in the last stage. This fact as discussed before is mainly attributed to the fluctuating avalanching behavior of the solid residing inside the flight. Also it is clear from Fig. 4.2 that changing the discharge angle has less influence on the kinetic angle of repose than lowering the speed of rotation (rpm). As the rpm increases, a shifting of the peak points is observed. It shown in Fig. 4.2 that increasing the number of flights from 12 to 18 at the same flight dimensions, increases the kinetic angle of repose. This can be attributed to the increase in the holdup carried by the flights which will increase the frequency of the avalanches relative to the smaller number of flights.

Figure 4.3 illustrates the influence of the discharge angle on the measured kinetic angle of repose for two rotational speeds (1 and 5 rpm) and two flight length ratios (0.75 and 0.375) for a constant number of flights. It can be seen that the change in the flight dimensions has nearly no influence on the kinetic angle of repose when compared to the speed of rotation.

In Figs. 4.2 and 4.3 it can be noted that the values of the kinetic angle of repose which were calculated based on **Schofield and Glikin, 1962** model (Eq. (4.4)) are almost constant for each case without fluctuation compared to experimental results. This fact is mainly attributed to the assumptions used in the model. Also it is worth noting that, because their model does not include the effect of the number of flights, the kinetic angles calculated based on their model and shown in Fig. 4.2 only consider the influence of the speed of rotation.

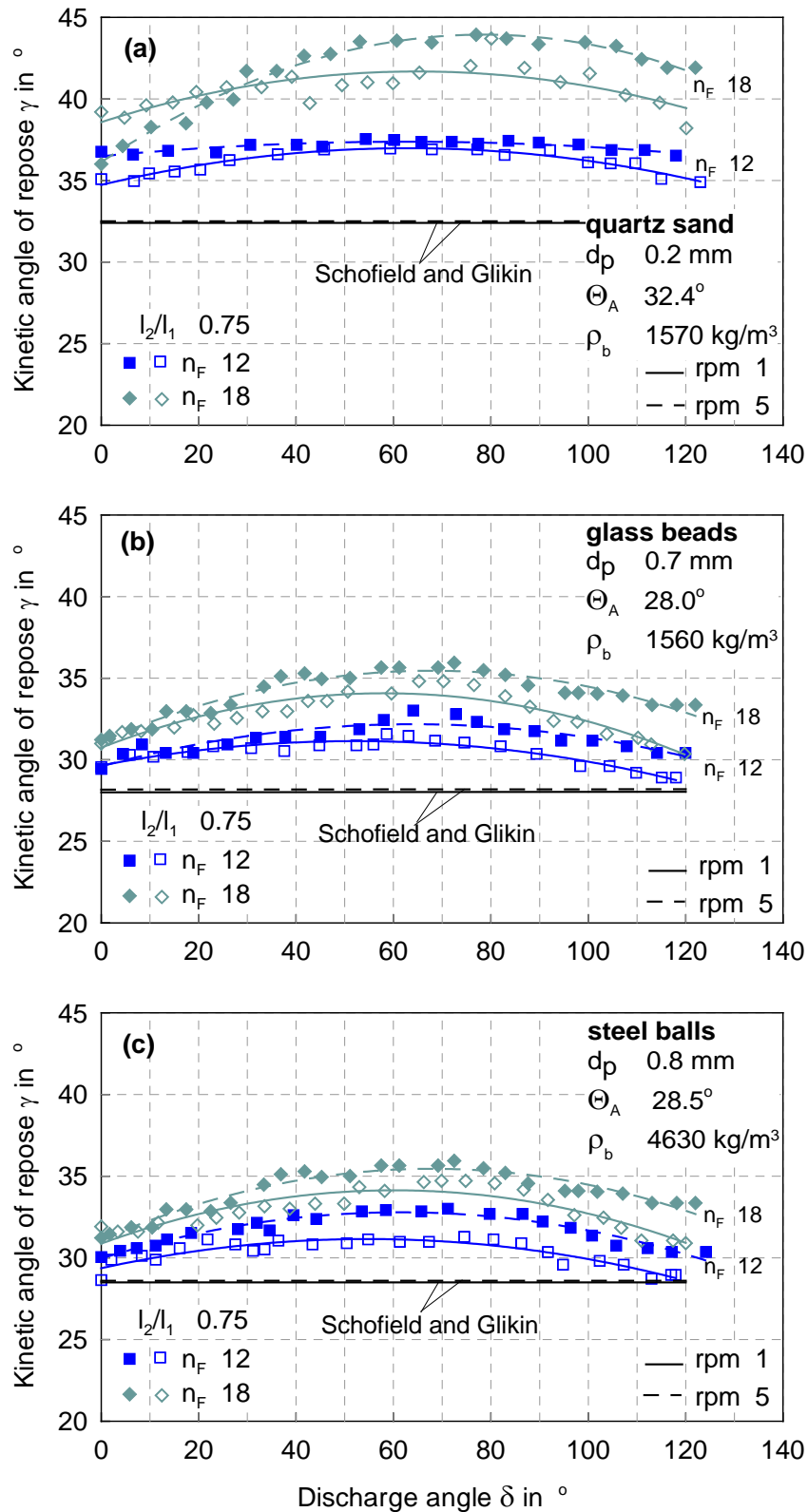


Figure 4.2: Variation of measured kinetic angle of repose of the solid reside inside a single flight against the flight discharge angle for various rotational speeds and number of flights at design loading conditions, (a) quartz sand (b) glass beads (c) steel balls.

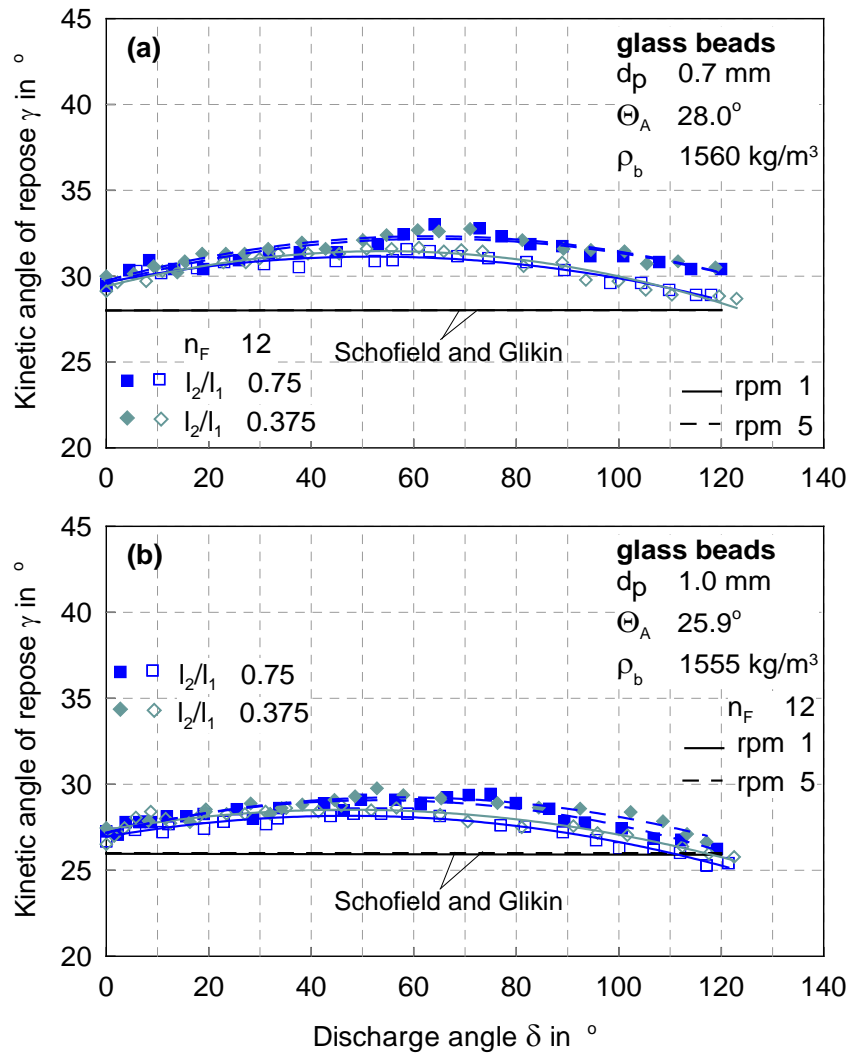


Figure 4.3: Variation of measured kinetic angle of repose of the solid residue inside a single flight against the flight discharge angle for various rotational speeds and flight length ratios at design loading conditions, (a) quartz sand (b) glass beads (c) steel balls.

4.4 Flight holdup

Studying the variation in the amount of solid material carried by the flight (flight holdup) is significantly important, in order to determine the cascading rate from the flight during the discharge period. This flight holdup can be determined theoretically rather than experimentally (Sunkara, 2013). The theoretical method as described before in section 4.2 is based on developing a geometrical mathematical model to predict the cross sectional area of the solid carried by the flight, depending on the definition of the kinetic angle of repose and assuming constant cross sectional area

along the drum. Experimentally there are mainly two methods: the first, by directly weighing the amount of solid carried by the flight at different discharge positions; in this method it is necessary to stop the drum at different arbitrary positions and collect the solid from the specified flight to directly measure its weight; the second, by tracking the boundary lines of the solid residing inside the flight to find the cross sectional areas. This tracking requires extraction of multiple images at different discharge positions from the recorded videos by stopping the footage at these positions then analyzing the images to calculate the areas. Then the calculated areas per unit drum length are converted to mass using the measured bulk density. Although the first method is more reliable as it measures the mass of the solid more precisely than the second method, this method requires suddenly interrupting the drum to collect the solid and can cause a kind of non-uniform distribution of the solid. In the present work, as described before, the calculation is experimentally determined based on tracking the boundary lines of the solid using the image analysis methods (described in Ch. 2). In the following, the measured flight holdup is plotted versus the discharge angle.

Figure 4.4 represents the effect of varying the discharge angle of the individual flight holdup for different rpm (1 to 5) and two numbers of flights (12 and 18) for constant flight dimensions and design loading conditions. Figure 4.4 shows that at any operating condition of the drum, the maximum holdup of the FUF is attained at 9 o'clock position (0° discharge angle) as the flight at that moment carries the largest amount of solid. Then, due to the rotation of the drum, the angular position of that flight (FUF) increases and the flight holdup decreases until the flight becomes empty. This fact is supported by the change in the kinetic angle of repose described before in Section 4.2. The final discharge angle can be estimated from the graphs as the amount of holdup reaches zero. The measured flight holdup can be noticed to have a curvilinear distribution, characterized by a dome its position varied according to the operating condition, where the dashed line represents the uniform distribution assumed by **Glikin, 1978** for only one case where the final discharge angle takes place at 180° . It can be seen from Fig. 4.4 that increasing the rpm or the number of flights yields an increase in the average flight holdup due to the increase of total holdup needed for the design loading.

Figure 4.5 represents the effect of varying the discharge angle on the individual flight holdup for different rpm (1 to 5) and two flight length ratios (0.75 and 0.375) for a constant number of flights and design loading conditions. From Fig. 4.5 it can be seen that changing the flight length ratio significantly affects the flight holdup, as increasing the flight length ratio from 0.375 to 0.75 causes an increase in the flight holdup by an average of 66%.

4.5 Final discharge angle of flight

The final discharge angle (δ_L see Fig. 4.1 (a)) represents the position of the flight at the end of the discharge period in the upper half of the drum. It can be determined directly from the recorded videos by stopping each video at the moment when a traced flight becomes totally empty and then extracting the image to measure the angle manually. Figures 3.4 and 3.5 give information about the final discharge angles for different solids and operating conditions of the drum. As the final discharge angles can be determined from Figs. 4.4 and 4.5 at the positions of zero flight holdup. The measured final discharge angles are plotted versus the change in the rpm in the following graphs.

Figure 4.6 (a) represents the variation of the final discharge angle with the change in the rpm for different solids and two numbers of flights (12 and 18) for a constant flight length ratio (0.75). It is shown from Fig. 4.6 (a) that the final discharge angle increases as the rpm increases, this related to the increase of the flight holdup which delays the emptying point at design loading conditions. Also it can be seen that the final discharge angle is decreased as the number of flights is increased.

Figure 4.6 (b) shows the variation of the final discharge angle with the change in the rpm for different solids and flight length ratios (0.375 and 0.75) for a constant number of flights (12). It is shown from Fig. 4.6 (b) that the final discharge angle increases as both the rpm and flight length ratio increases. When increasing the flight length ratio, the flight dimensions become bigger and carry more solid, which delays the emptying point at design loading conditions.

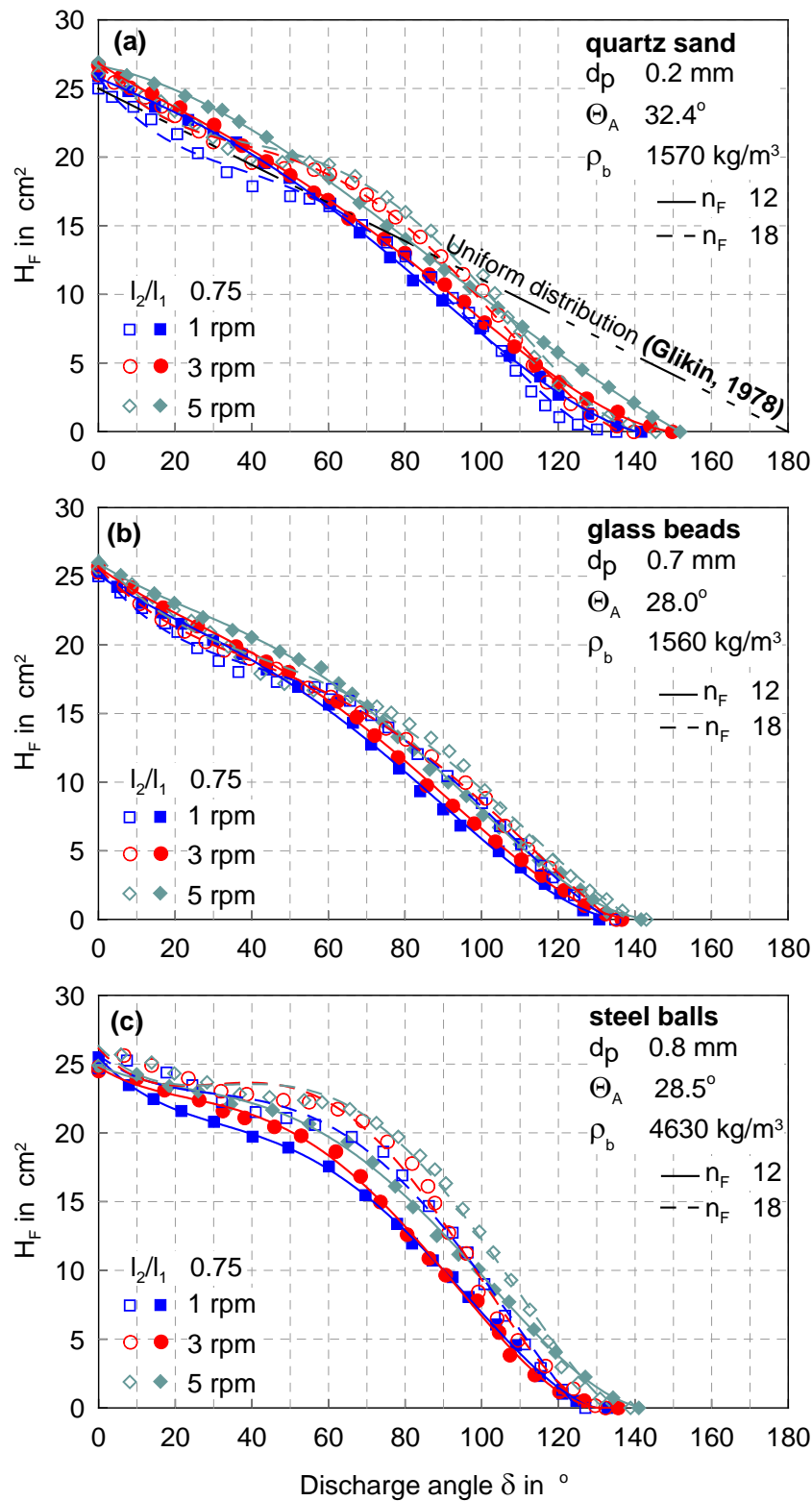


Figure 4.4: Influence of the flight discharge angle on the measured holdup of a single flight for various rotational speeds and number of flights at design loading conditions, (a) quartz sand (b) glass beads (c) steel balls.

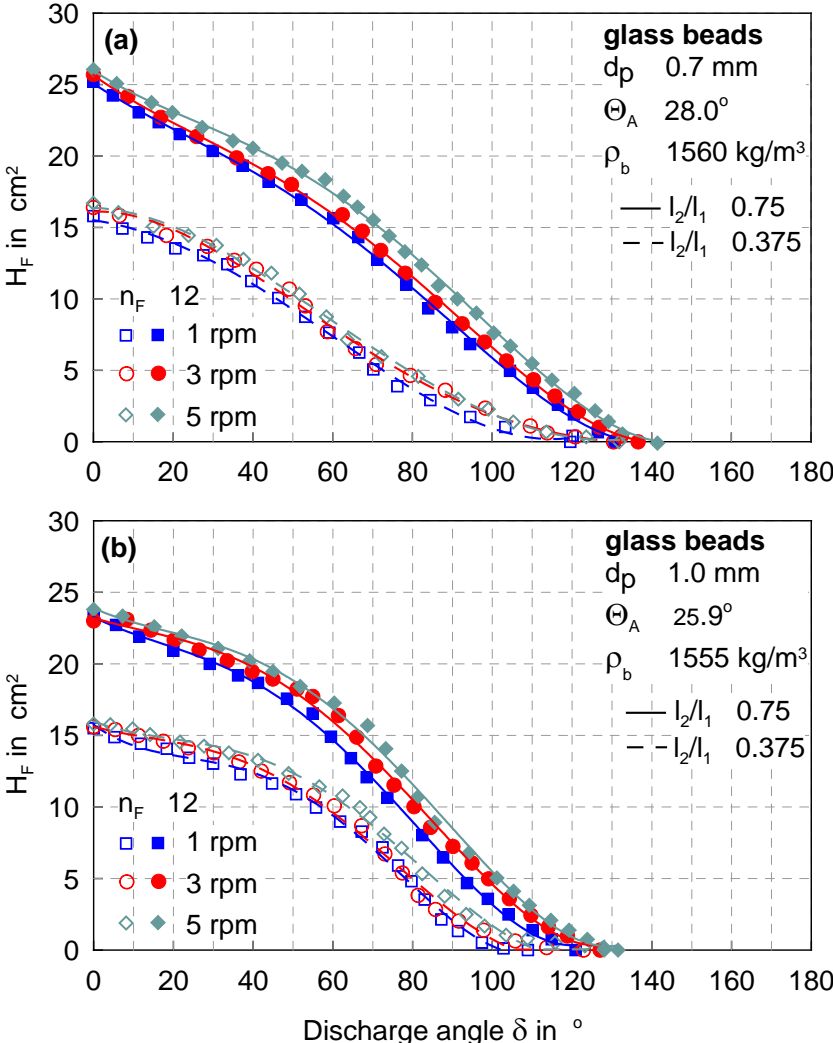


Figure 4.5: influence of the flight discharge angle on the measured holdup of a single flight for various rotational speeds and flight length ratios at design loading conditions (a) quartz sand (b) glass beads (c) steel balls.

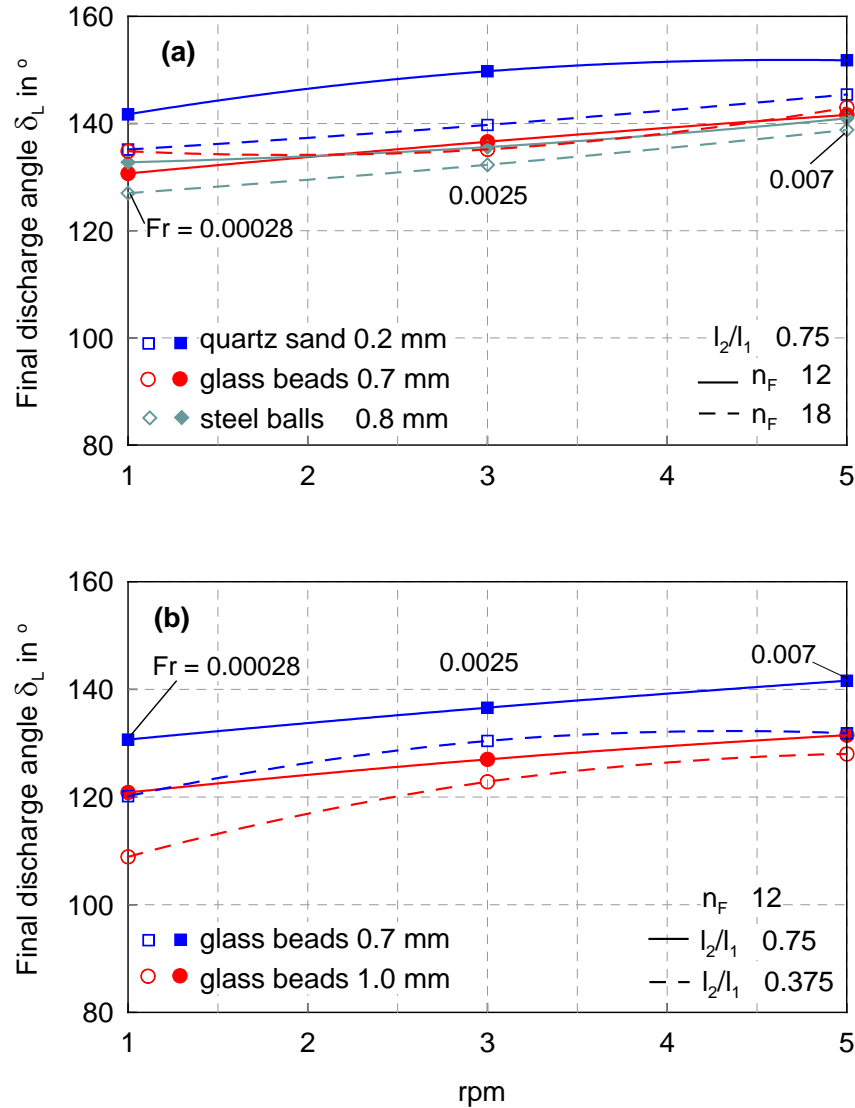


Figure 4.6: Variation of final discharge angle versus drum rpm for different materials and different operating conditions (a) different number of flights and same flight length ratio (b) different flight length ratios and same number of flights. At design loading conditions.

4.6 Flight cascading rate

The cascading rate from a flight can be represented as a dimensionless quantity by the changes of the flight filling degree ($f_{F(\delta)}$) with the discharge angle (δ) as noted in Eq. (4.6). Where the flight filling degree ($f_{F(\delta)}$) is the flight holdup per unit length ($H_{F(\delta)}$) divided by the total drum volume per unit length (V_{drum}) (Eq. (4.5)), ρ_b is the solid bulk density, ω is the drum angular velocity, and R and L are the drum

radius and length, respectively. The flight cascading rate ($\dot{m}_{F(\delta)}$) with units of kg/s can be drawn using Eqs. (3.5-3.6).

$$f_{F(\delta)} = \frac{H_{F(\delta)}}{V_{drum}} \quad (4.5)$$

$$-\left(\frac{d f_{F(\delta)}}{d \delta}\right) = \frac{\dot{m}_{F(\delta)}}{\rho_b \omega \pi R^2 L} \quad (4.6)$$

The calculated flight cascading rates over the periods of discharge are found to be with fluctuations, the fittings of the fluctuating curves are plotted against the discharge angle in Fig. 4.7. Figure 4.7 (a) shows the influence of the discharge angle on the flight cascading rate for quartz sand at two number of flights (12 and 18) and constant flight length ratio (0.75) and rpm (3). It can be seen from Fig. 4.7 (a) that the cascading rate is relatively high at the initial point of discharge as the flight has just left the large amount of solid bulk. Then the cascading rate decreases until it attains a minimum due to the decrease in the avalanching rate as the solid material returns again to stability. After that, as the flight elevates to higher positions, the cascading rate increases and attains a maximum at a certain point. Later the cascading rate sharply decreases until the emptying point. It could be noticed that the initial cascading rate for the case of drum with 18 flights is lower than the one of 12 flights. On the contrary the maximum peak of the cascading rate of 18 flights is higher than the one of 12 flights.

Figure 4.7 (b) depicts the influence of the discharge angle on the flight cascading rate for glass beads at two flight length ratios (0.375 and 0.75) at constant rpm (3) and number of flights (12). It can be seen from Fig. 4.7 (b) that the initial cascading rate for the lower flight length ratio (0.375) is higher than for the larger flight length ratio (0.75). Later it is noticed that the cascading rate is much higher for the larger flight length ratio (0.75) than the lower one (0.375). Overall, it could be concluded that increasing the flight dimension causes the cascading rate to increase.

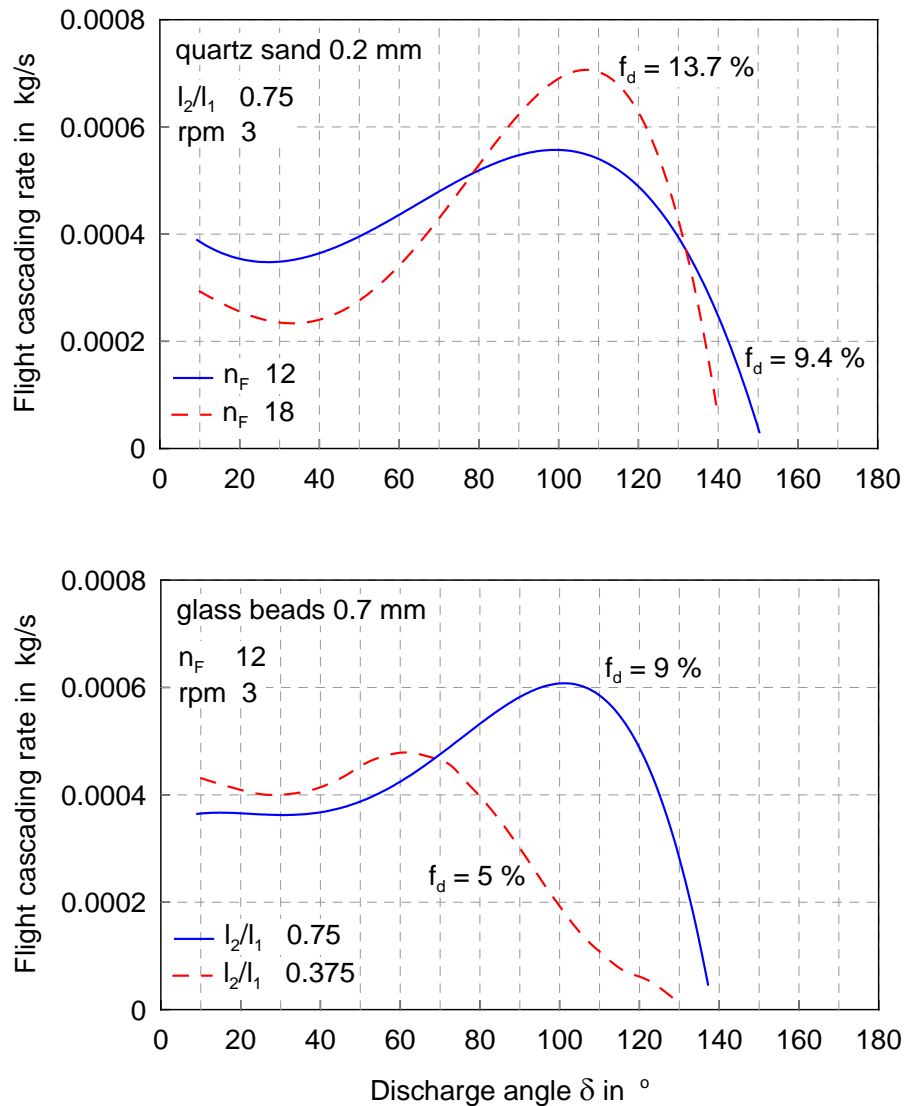


Figure 4.7: Variation of the flight cascading rate with the discharge angle at design loading conditions, (a) quartz sand at two number of flights and constant rpm and flight length ratio (b) glass beads at two flight length ratios and same number of flight and rpm.

4.7 Curtains height of fall

4.7.1 Measured height of fall

The cascading of the solid from the flights forms the same number of curtains as there are active flights. The height of a curtain can be measured directly from the photos as the vertical distance of a particle from the edge of the flight to the impact point at the bottom of the drum. This height of fall determines the amount of time the

particles reside in the gas-borne phase where they are exposed to the gas stream. The impact point differs according to the filling degree of the drum. For example, for an overloaded drum most of the impact points from falling are at the solid bed in the bottom of the drum, while for the case of design loaded drum the bottom solid bed no longer exists (see Fig. 4.1). However in some cases the impact point is located at the metal back side of an opposite flight. As a conclusion maximum falling height can be achieved when operated the drum at the design loading filling degree with varied locations of the impact points depend on the position of the flight (δ).

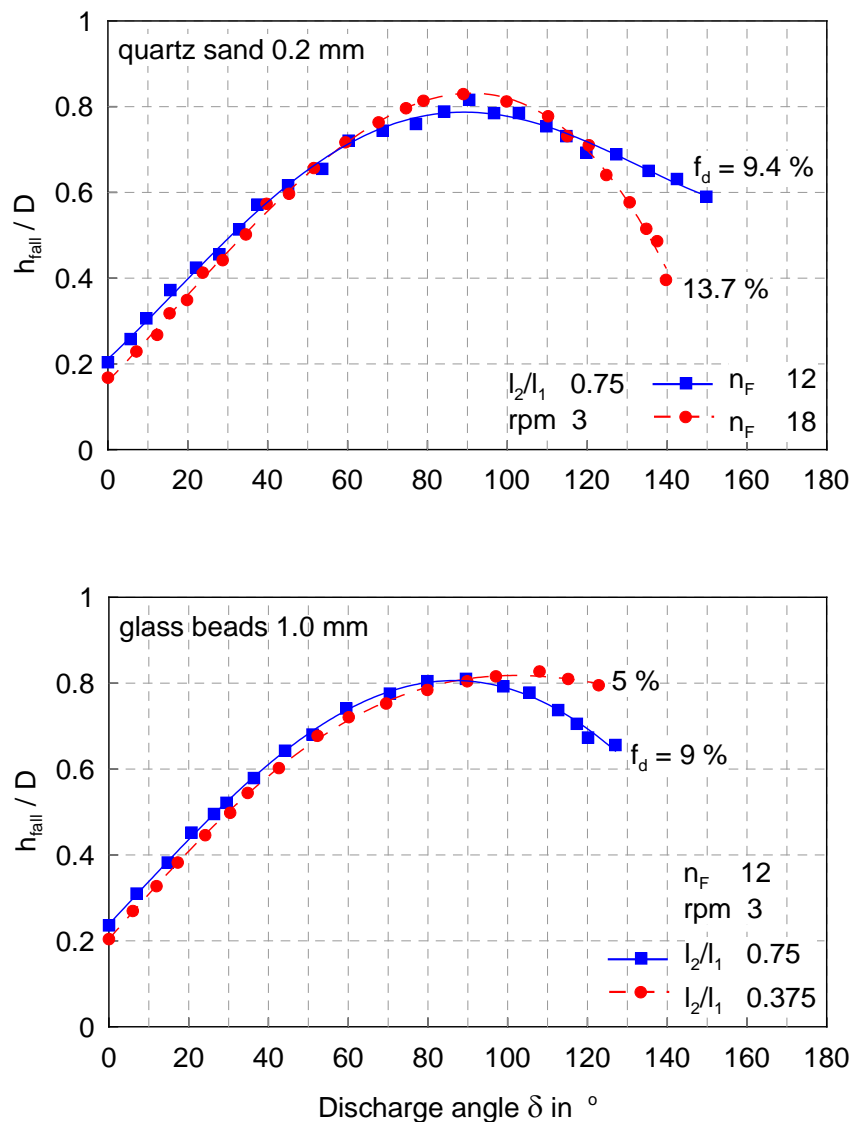


Figure 4.8: Variation of the measured curtains falling height against the discharge angle at design loading conditions, (a) quartz sand at two number of flights and constant rpm and flight length ratio (b) glass beads at two flight length ratios and same number of flights and rpm.

4.7.2 Mean height of fall

From literature, **Blumberg and Schlünder, 1996**, proposed a semi empirical relation (Eq. (4.7)) to estimate the mean height of fall (\bar{h}_{fall}) as a function of the drum filling degree (f), the solid material dynamic angle of repose (Θ_A) and the flight length ratio (l_2/l_1).

$$\bar{h}_{fall} = 0.85 R (1-f) (1+\Theta_A^2) \left(\frac{l_2}{l_1}\right)^{0.13} \quad (4.7)$$

However, the valid range of the filling degree was observed to be too high for industrial applications. $0.2 \leq f \leq 0.4$, $0.4 \leq \Theta_A \leq 0.8$ and $0.75 \leq l_2/l_1 \leq 1.0$.

In order to calculate and compare the measured mean height of fall of the current experimental results with correlations from literature, the following relation could be used.

$$\bar{h}_{fall} = \frac{1}{\delta_L} \int_0^{\delta_L} h_{fall}(\delta) d\delta \quad (4.8)$$

Table 4.1 outlines the comparison of the measured mean height of fall of the current experimental work with the one calculated using the correlation of **Blumberg and Schlünder, 1996**. It is shown that the correlation of **Blumberg and Schlünder, 1996** failed in the prediction of the measured height of fall with high deviation specially for the lower filling degree conditions. This is mainly due to that the correlation is valid for over-loaded drums.

Table 4.1: Mean measured height of fall and deviations from literature correlation

No.	Material used	d_p (mm)	N (rpm)	n_F --	l_2/l_1 --	Θ_A (°)	$f_{\text{design load}}$ (%)	\bar{h}_{fall} in (cm)		Dev. (%)
								Measured	Blumberg and Schlünder 1996	
1	Quartz Sand	0.2	3	12	0.75	32.4	9.4	30.2	24.4	23.4
2	Quartz Sand	0.2	3	18	0.75	32.4	13.7	28.2	23.3	21.0
3	Glass Beads	1.0	3	12	0.75	25.9	9	31.0	22.4	38.2
4	Glass Beads	1.0	3	12	0.375	25.9	5	30.2	21.3	41.1

Chapter 5

Axial transport

5.1 Introduction

The study of the axial transport of the solid through a flighted rotary drum aims to follow the motion behavior of the solid along the drum length under the effect of operating conditions. The axial transportation of the solid through a flighted rotating drum is influenced by: the drum slope to the horizontal, the drum rotational speed, the lifting of the solid by the flights, the disperse nature into the gas stream, the bouncing in the gas and rolling and the sliding of the particles on impact with the bottom of the dryer (**Britton et al., 2006** and **Rojas et al., 2010**). Hence the studying of the axial transport is much complicated and a lot of assumptions for simplifications are needed (**Duchesne et al., 1996** and **Renaud et al., 2000**). The main output results from studying the axial transport phenomena are: the estimation of the mean retention time (residence time) elapsed by the solid in the drum starting from the feed end to the discharge end and the solid mass feed rate.

The determination of the optimum residence time needed for the solid in a rotary drum (for example rotary dryer) is of importance which determines the quality of the product. Smaller residence time causes uneven drying of the feedstock, whereas the higher residence times lead to over drying of the material which involves unaccepted changes in the product shape and properties and moreover huge energy loss (**Friedman and Marshall, 1949; Tarhan et al., 2010** and **Sunkara, 2013**).

5.2 Physical description of the axial transport in a flighted rotary drum

Figure 5.1 gives information about the motion behavior of the solid in a flighted rotating drum. Considering a single particle of the solid transported through the drum, the particle is lifted up by the flight because of the rotation of the drum (from point A to B see Fig. 5.1 (a) and (b)) and then it is falling down (from B to C). After the particle leaving the flight it is travelling through the gas stream and subjected to drag force in a direction parallel to the axis of the drum and a drag force opposing the falling direction of the particle (see Fig. 5.1 (c)). The effect of the later is negligible compared to the accelerating force due to gravity. At the impact point at the bottom of the drum the particle can be rolling and sliding until it begin another cascade cycle (**Glikin, 1978** and **Cronin et al., 2011**).

Because of the slope of the drum (β) a successful axial advance (X) by the particle is observed during the fall. And the particle motion is forming a number of cascade cycles with an axial advance till it discharges from the drum. The number of cascades and the axial advance per cascade are determining the mean residence time of the solid inside the drum. To determine the axial advance (x) by the particle, the equation of motion should be applied as will be described in this chapter.

5.3 Models from literature

Many solid transport models of flighted rotary dryers have involved the development of empirical relationships for the mean residence time (τ) from pilot-scale experiments. While simplistic in nature, pilot-scale empirical relationships generally lead to under prediction of measured values of the mean residence time in industrial rotary dryers (Cao and Langrish, 1999). An alternative technique was employed by researchers to determine the mean residence time using geometric models arguments based on the holdup of flights over the discharge angle (Britton and Sheehan, 2006). The mean residence time of solid in a rotary drum is influenced by four components of particle movement along the drum: a) gravitational due to the slope of the drum, b) drag of the gas on the particles for counter-current flow (this is negative) c) bouncing of the particles on impact with the bottom of the dryer

and d) rolling of the particles in the bed at the bottom of the dryer, specially for overloaded dryers. The last two components are almost impossible to predict theoretically and are therefore evaluated experimentally for each type of material (Kemp and Oakley, 1997). Numerous equations have been proposed for the estimation of the mean residence time in rotary drums, in the following are some models from literature (Austin et al., 1978; Alvarez and Shene, 1994; Lisboa et al., 2007; Thibault et al., 2010 and Sunkara, 2013).

In many of these studies, only average holdups and solid feed rate were considered (**Kelly and O'Donnell, 1977**). The mean residence time for the particles (τ) in these cases is given by

$$\tau = \frac{H_{Tot}}{\dot{m}_s} \quad (5.1)$$

where H_{Tot} is the total drum holdup in kg, usually determined by suddenly stopping the drum and subsequently weighing its contents and \dot{m}_s is the solid feed rate in kg/s.

One of the most frequently used empirical equation for residence time estimation was proposed by **Friedman and Marshall, 1949**:

$$\tau = \frac{13.8 L}{\tan(\beta) N^{0.9} D} \pm \frac{0.59 L \dot{m}_a}{\sqrt{d_p \dot{m}_s}} \quad (5.2)$$

Here the upper plus sign refers to the counter-current flow and the lower minus sign refers to the co-current flow. β is the drum slope angle in degree, N is the rpm, L is the drum length in m, D is the drum diameter in m and d_p is the particle diameter in m and \dot{m}_a and \dot{m}_s are in kg/s.

Saeman and Mitchell, 1954 were the first to break away from the empirical approach to calculating rotary dryer holdups adopted by previous researchers. They analyzed material transport through the dryer in terms of incremental transport rates

associated with individual cascade paths to yield a transport-rate distribution function. By assuming a linear relationship between the horizontal displacement of the particles due to the air flow and its velocity, they derived the following equation for the mean residence time:

$$\tau = \frac{L}{f(H)DN(\tan(\beta) \pm m'u_g)} \quad (5.3)$$

Where $f(H)$ is a cascade factor with values typically between 2 and π that increase as solids holdup increases, and m' is an empirical parameter (dimensional) for a given material. The positive sign in Equation indicates the con-current flow and the negative sign indicates the counter-current flow.

Schofield and Glikin, 1962 derived the following residence time equation by considering the drag exerted by the air flowing counter-currently to the particles:

$$\tau = \frac{L}{y_{avg} \left(\sin(\beta) - \frac{k u_r^2}{g} \right)} \left[\left(\frac{2y_{avg}}{g} \right)^{0.5} + \frac{\delta_{avg}}{\pi N} \right] \quad (5.4)$$

where y_{avg} is the average falling height, u_r is the relative velocity between solid and gas, δ_{avg} is the average discharge angle corresponding to y_{avg} and k is a factor for the drag force (will be described in details later in Sec. 5.3).

In other publications the total residence time was calculated as the total number of cascades of a particle moving along the drum times the sum of the time of lifting and the time of falling per one cascade. Where the number of cascades can be estimated based on the calculated axial advance of the particle per cascade. For such reason a mathematical model was proposed by **Kamke and Wilson, 1986**. The axial advance of the particle (X) per cascade was given by the following expression

$$X = u_g t_{fall} + \frac{1}{k} \ln \left\{ \frac{\cos(\tan^{-1}(u_g/a_1))}{\cos(-a_1 K t_{fall} + \tan^{-1}(u_g/a_1))} \right\} \quad (5.5)$$

where a_1 and k are constants depending on the drum inclination and drag coefficient respectively, u_g is the gas velocity, t_{fall} is the falling time. The model has been validated with an experimental drum of 1.2 m in diameter and 5.5 m in length, with six centered flights and 12 flights installed to the outer shell of the dryer. The experiments were performed with wood particles having a sphericity of 0.75 and exposed to hot gas stream in con-current passion. The residence time was measured by injecting a radioactive tracer particles at the inlet along with the feed. They noticed that within a curtain, the particles may be effected by the other particles and shielding of the gas flow can also occur. Due to this the model over predicted the data collected, since the model assumes that the particles are independent to the gas flow. They noted that the particles may be attributed as a bulk material and the mean diameter can be used in order to measure the drag coefficient. It has been found that the root mean square error was 109.6% in the case of discrete particle size whereas, in case of mean diameter it was around 14.2%.

Recently, based on the analysis of a large amount of data found in the literature on the operation of rotary drums of many applications, both on a pilot and an industrial scale, **Perry and Green,1999** proposed the following general correlation for calculation of the mean residence time:

$$\tau = \frac{K L}{\tan(\beta) N^{0.9} D} \quad (5.6)$$

where K is a parameter that depends on the number and format of the flights.

In the present chapter, a mathematical model is developed for the axial transport based on applying the force balance on a falling particle from a flight in a rotary drum using the available experimental measurements of the holdups and height of fall over the discharge angle (described in Ch. 4).

5.3 Current work model description

5.3.1 Model assumptions

- Uniform discharge characteristics along the drum (discussed in Ch.3)
- Each particle spent the same amount of time over the drum
- The particle is of a spherical shape and it remains its dimensions and shape unchanged along the drum
- Neglect the rotational effect on the particle after leaving the flight
- Free and vertical fall of the particle (initially at zero velocity)
- Neglect the vertical drag force
- No slip condition of the gas on the particle surface
- Neglect transitional effects between the particle and the fluid
- Neglect the interactions between particles (free flowing - non cohesive)

5.3.2 Equationing

The free body diagram of the forces acting on a single particle falling freely from a flight of a rotary drum at a certain discharge angle (δ) and subjected to a gas flow (assumed air) is shown in Fig. 5.1 (c). Applying the equation of motion on the particle in the axial direction after considering the model assumptions (**Maxey and Riley, 1983**), reveals that;

$$m a_x = \sum Forces \quad (5.7)$$

$$m \frac{du_x}{dt} = mg \sin(\beta) \mp m k u_r^2 \quad (5.8)$$

$$\frac{du_x}{dt} = g \sin(\beta) \mp k u_r^2 \quad (5.9)$$

where the upper minus sign refers to air following counter-current flows and the lower positive is for co-current. β is the drum inclination angle, u_r is the relative velocity between the particle and the air as

$$u_r = u_a \pm u_x \quad (5.10)$$

u_a is the air velocity and u_x is the particle falling velocity component in x-direction. The upper positive sign refers to counter-current flows and the lower minus sign is for the con-current.

u_x can be obtained by applying the free fall equation on the particle assuming the fall from rest and then by resolving the falling velocity u_y .

$$\frac{u_y^2}{2g} = y \quad (5.11)$$

$$u_x(y) = \frac{1}{2} \sqrt{2gy} \sin(\beta) \quad (5.12)$$

The calculated u_x is a function of the falling distance (y) which is already varying with the flight position (δ).

In order to simplify the solution, an average value of the falling distance can be considered and calculated by the integration of the measured falling height over the flight discharge angle (see Ch.4 Eq. (4.8)) as

$$y_{avg} = \bar{h}_{fall} = \frac{1}{\delta_L} \int_0^{\delta_L} h_{fall}(\delta) d\delta \quad (5.13)$$

where δ_L is the measured final discharge angle at a specific operating conditions (see Ch. 4)

$$u_{x,avg} = \frac{1}{2} \sqrt{2gy_{avg}} \sin(\beta) \quad (5.14)$$

Then the average relative velocity can be calculated for known air velocity as

$$u_{r,avg} = u_a \pm \frac{1}{2} \sqrt{2gy_{avg}} \sin(\beta) \quad (5.15)$$

Back to Eq. (5.8), the term k (presented before in Eq. (5.4)) can be calculated based on the drag coefficient C_D . The drag coefficient was evaluated using the commonly used Schiller Naumann drag correlation (**Glikin, 1978, Kamke and Wilson, 1986** and **Karimi et al., 2012**) as stated in the following;

$$k = 1.5 \frac{C_D \rho_a}{d_p \rho_p} \quad (5.16)$$

$$C_D = \frac{12}{\text{Re}} \quad \text{Re} \leq 0.2 \quad (5.17)$$

$$C_D = \frac{12(1 + 0.15 \text{Re}^{0.687})}{\text{Re}} \quad 0.2 < \text{Re} \leq 1000 \quad (5.18)$$

$$C_D = 0.44 \quad \text{Re} > 1000 \quad (5.19)$$

$$\text{Re} = \frac{\rho_a u_{r,avg} d_p}{\mu_a} \quad (5.20)$$

where d_p is the particle diameter, ρ_p is the particle density, ρ_a is the fluid density, μ_a is the fluid dynamic viscosity and Re is a modified Reynolds number calculated based on the relative velocity between the fluid and the particle.

The final solution of Eq. (5.3) gives the axial advance of the particle per one cascade (lifting then falling) and it is found to be

$$X_{avg} = \frac{1}{2} (g \sin(\beta)) t_{fall(h,avg)}^2 \mp \frac{1}{2} (k u_{r,avg}^2) t_{fall(h,avg)}^2 \quad (5.21)$$

where $t_{fall(h,avg)}$ is the average falling time calculated based on the calculated average falling height as

$$t_{fall(h,avg)} = \sqrt{\frac{2 \bar{h}_{fall}}{g}} \quad (5.22)$$

Then the number of cascades can be drawn by dividing the total drum length by the axial advance per one cascade

$$C = \frac{L}{X} \quad (5-23)$$

During one cascade, the lifting time can be approximated as

$$t_{lift,avg} = \frac{2 \delta_{avg}}{\omega} = \frac{\delta_{avg}}{\pi N} \quad (5.24)$$

where δ_{avg} is the discharge angle (in radians) corresponding to the calculated average height of fall, ω is the angular velocity in rad/s and N is the rotational speed in rps

$$\delta_{avg} = \delta(\bar{h}_{fall}). \quad (5.25)$$

Thus the total average time elapsed by the particle in the drum (mean residence time τ in sec) can be estimated from the following relation

$$\tau = C(t_{lift,avg} + t_{fall(h,avg)}) \quad (5.26)$$

where $t_{lift,avg} + t_{fall(h,avg)}$ is the total time per one cascade.

In order to calculate the total solid mass flow rate passing through the drum a new average solid velocity should be introduced where the subscript (s) denotes the solid material as

$$\boxed{u_{avg,s} = \frac{L}{\tau}} \quad (5.27)$$

The total drum holdup H_{Tot} (in m³/m) can be estimated using one of two methods: the first is a direct way by using the proposed model that previously described in Ch. 2 (Eq. (2.1)) by the substitution of the measured flights holdups; the second is an indirect way depending on the measured design loading filling degree by using the following relation,

$$H_{Tot} = f_{design} \cdot \pi R^2 \cdot \quad (5.28)$$

The design loading filling degree at specific operating conditions is already known for the experimental work. However, it can be also estimated generally using the correlation proposed previously in Ch. 3 (Eq. (3.1)) by the direct substitution of the operating parameters.

By multiplying the total drum holdup H_{Tot} with the real drum length, the total solid volume (m^3) could be obtained

$$V_s = H_{Tot} L \quad (5.29)$$

hence the mass of solid (in kg) can be calculated using the solid bulk density (ρ_b) as

$$m_s = \rho_b V_s \quad (5.30)$$

The calculated solid average velocity and the total holdup can be used to calculate the average solid mass flow rate (in kg/s) as

$$\dot{m}_s = \rho_b H_{Tot} u_{avg,s} \cdot \quad (5.31)$$

In order to clarify the use of the current work experimental measurements (discussed in Ch. 2 and Ch. 3) with the described model, a case study is taken as in the followings.

5.4 Case study

5.4.1 Given data

The mathematical model described previously is applied using extracted data from the current work experimental measurements on a rotary dryer with the following specifications;

Drum dimensions: $D = 0.5$ m (taken exactly as the current work test-rig)

$$L = 2.5 \text{ m}$$

$$N = 3 \text{ rpm (0.05 rps), } \omega = 0.314 \text{ rad/s}$$

$$n_F = 12, l_2/l_1 = 0.75$$

$$\text{Drum slope } (\beta) = 4^\circ \text{ (0.0697 rad)}$$

Solid properties: glass beads

$$d_p = 1.0 \text{ mm}$$

$$\rho_p = 2650 \text{ kg/m}^3$$

$$\rho_b = 1555 \text{ kg/m}^3$$

Fluid properties: Air at 115°C (400 K) (**Cengle, 2003** and **Incropera and DeWitt, 2006**)

$$\rho_a = 0.8711 \text{ kg/m}^3$$

$$\mu_a = 0.000023 \text{ Pa.s}$$

$$u_a = \text{varied from 0.2 to 0.5 m/s.}$$

Required: calculate for both cases of fluid flows, counter-current and con-current and for the mentioned range of air velocity the followings; average axial advance per cascade, mean residence time of the solid in the drum and average solid mass flow rate at the design loading conditions. Using the current work experimental measurements mentioned in Ch. 2 and Ch. 3.

5.4.2 Results

The mathematical model is applied and the variation of the results with the air velocity for two types of flows; counter-current and con-current are illustrated in the following figures.

Figure 5.2 represents the variation of the axial advance per one cascade of falling particle with the air velocity for two types of flows counter-current and con-current. It is obviously shown from Fig. 5.2 that the average axial advance of the case of counter-current flow type is lower than the one of the con-current flow type. This is mainly attributed to the higher drag coefficient (k) achieved by the counter-current

flow. From Fig. 5.2 it can be seen that increasing the air flow rate causes a decrease in the axial advance for the case of counter-current flow type where the air is resisting the particle advance. While for the case of con-current flow type the axial advance increases as the air flow rate increases.

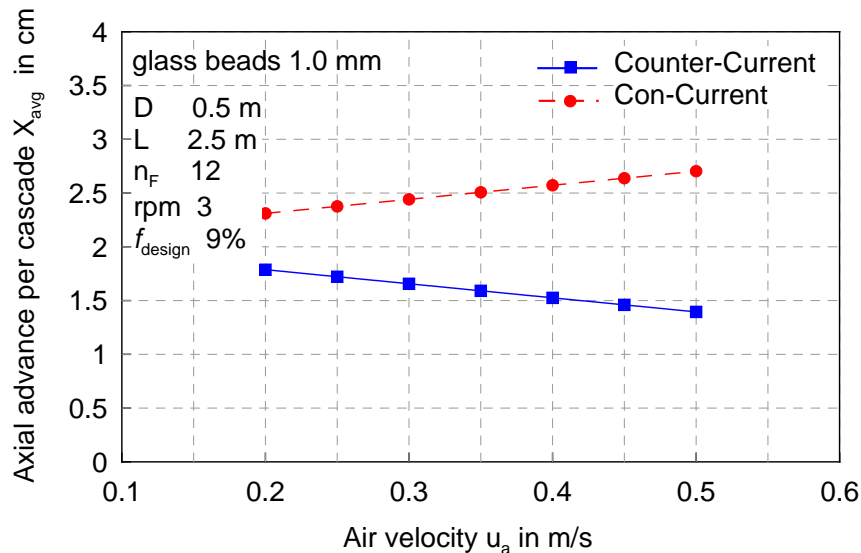


Figure 5.2: Variation of the axial advance per one cascade of falling particle with the air velocity for two types of flows counter-current and con-current.

Figure 5.3 depicts the variation of the mean residence time against the air velocity for two types of flows counter-current and con-current. It is obviously shown from Fig. 5.3 that the mean residence time elapsed by the solid in the drum of the case of counter-current flow type is higher than the one of the con-current flow type. This is related to the higher drag coefficient characterized the by the counter-current flow. From Fig. 5.3 it can be seen that increasing the air flow velocity causes the mean residence time to increase for the case of counter-current flow type as the drag force increased. While for the case of con-current flow type the mean residence time decreases as the air flow velocity increases as the drag force decreases.

Figure 5.4 illustrates the variation of the solid flow rate with the air velocity for two types of flows counter-current and con-current. It is obviously shown from Fig. 5.4 that the average solid flow rate of the case of counter-current flow type is lower than the one of the con-current flow type. This is mainly because of the higher residence time and the hence the lower solid average velocity of the case of the counter-current

flow. Figure 5.4 shows that increasing the air flow rate causes a decrease in the solid flow rate for the case of counter-current flow type. While for the case of con-current flow type the solid flow rate increases as the air flow rate increases.

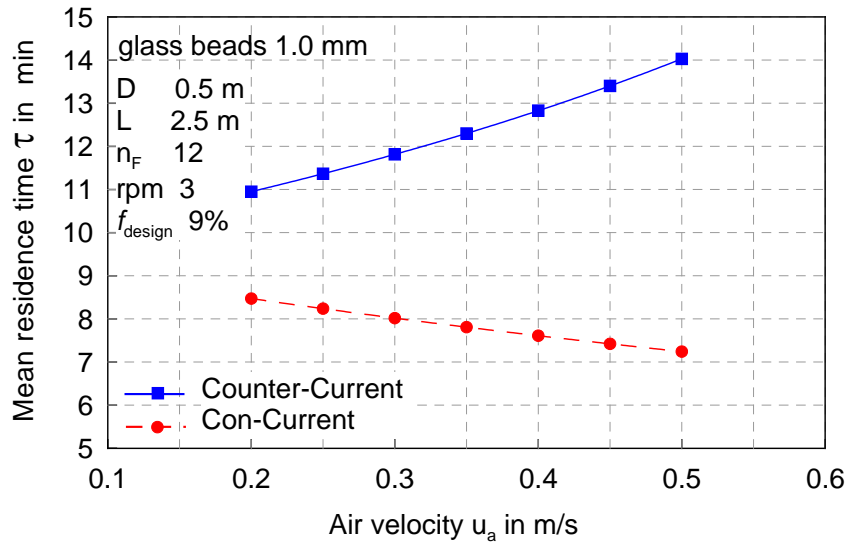


Figure 5.3: Variation of the mean residence time with the air velocity for two types of flows counter-current and con-current.

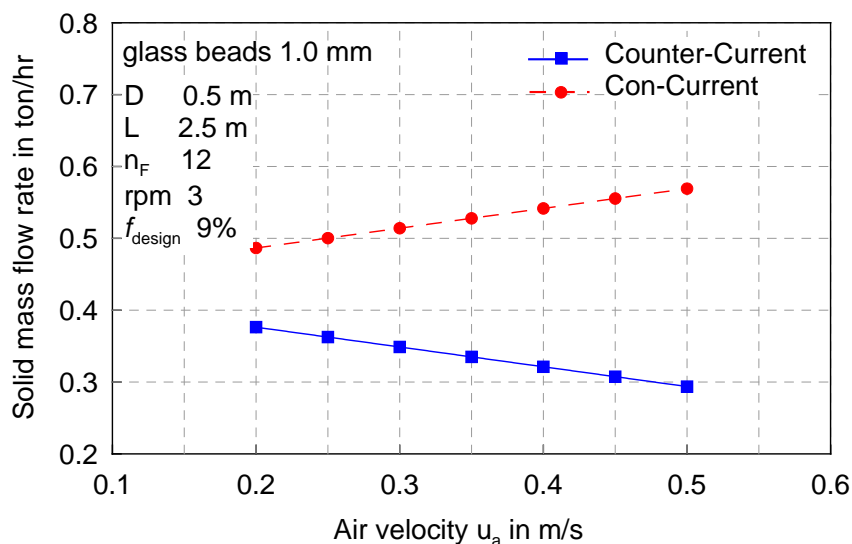


Figure 5.4: Variation of the solid mass flow rate with the air velocity for two types of flows counter-current and con-current.

In order to validate the calculated mean residence time, the results is compared with the commonly used correlations from literature; correlation of **Friedman and Marshall, 1949** and later modified by **Foust et al., 1960** described previously by Eq. (5.2). The comparison is shown in Table 5.1 and reveals that the correlation of **Friedman and Marshall, 1949** failed in the prediction of the current work mean residence time. As presented by the high deviations also shown in Table 5.1, same conclusion found by many previous studies (**Iguaz et al. 2003** and **Abbasfard et al., 2013**). Hence it is of importance to carry out experiments to determine the time taken by the solid through the drum.

Table 5.1: Comparison of residence time with correlation from literature

v_a in m/s	τ in min					
	Counter-current flow			Con-current flow		
	Karali, 2015 Eq. (5.26)	Friemann and Marshall, 1949	deviation %	Karali, 2015 Eq. (5.26)	Friemann and Marshall, 1949	deviation %
0.20	10.94	6.38	-41.67	8.46	5.85	-30.84
0.25	11.36	6.46	-43.11	8.23	5.77	-29.83
0.30	11.81	6.55	-44.55	8.01	5.69	-28.96
0.35	12.29	6.64	-45.99	7.80	5.60	-28.24
0.40	12.82	6.74	-47.43	7.60	5.50	-27.68
0.45	13.39	6.85	-48.88	7.41	5.39	-27.30
0.50	14.02	6.96	-50.32	7.23	5.27	-27.15

Fitting of the current work results of the mean residence time using the model of **Perry and Green,1999** (Eq. (5.6)) reveals the fitting factor (K) equals to 22.7 in average (see Eq. (5.32)).

$$\tau = \frac{22.7 L}{\tan(\beta) N^{0.9} D} \quad (5.32)$$

5.5 Direct application of the model (using in industry)

The described model for the axial transport can be a useful tool to be used in industry to help for the design of rotary drums operated at optimum loading. The model can estimate the total holdup needed for the drum to be operated at optimum loading and also the mean residence time will elapsed by the solid as follows;

Design loading filling degree in %

$$f_{design\ load} \% = 4.9 D^{-0.52} d_p^{0.043} (\tan \theta_A)^{0.351} \rho_b^{0.013} Fr^{0.052} n_F^{0.941} \left(\frac{l_2}{l_1} \right)^{0.839} l_1^{0.353} \quad (5.33)$$

Total holdup of the drum at design loading in m²

$$H_{Tot} = \pi R^2 \left(4.9 D^{-0.52} d_p^{0.043} (\tan \theta_A)^{0.351} \rho_b^{0.013} Fr^{0.052} n_F^{0.941} \left(\frac{l_2}{l_1} \right)^{0.839} l_1^{0.353} \div 100 \right) \quad (5.34)$$

Total holdup of the drum at design loading in kg

$$m_s = \rho_b L \left(\pi R^2 \left(4.9 D^{-0.52} d_p^{0.043} (\tan \theta_A)^{0.351} \rho_b^{0.013} Fr^{0.052} n_F^{0.941} \left(\frac{l_2}{l_1} \right)^{0.839} l_1^{0.353} \div 100 \right) \right) \quad (5.35)$$

Total mass flow rate at design loading in kg/s

$$\dot{m}_s = \rho_b H_{Tot} u_{avg,s} \quad (5.36)$$

Average passing velocity (in m/s) can be calculated from

$$u_{avg,s} = \frac{L}{\tau} \quad \text{the mean residence time } (\tau) \text{ has its model described} \quad (5.37)$$

previously (Eqs. 5.21 - 5.26).

Check for the calculated mean residence time

$$\tau = \frac{m}{\dot{m}_s} \quad (5.38)$$

Chapter 6

Heat Transfer

6.1 Introduction

As described previously, the performance evaluation of a rotary drum depends on; the drum loading at a specific operating conditions of: drum dimensions, flights number and dimensions, rpm, slope angle to the horizontal, the solid material property. Where the drum loading and operating conditions determines the discharge characteristics: the cascading rate, final discharge angle and height of fall, these characteristics determines the amount of solid will presented in the gas-borne area and subjected to the gas flow for a certain process in the drum. Using all of the mentioned parameters to study the axial transport of the solid through the drum, information about the mean residence time along the drum and the solid feeding rate needed for such conditions could be obtained. Finally, all of these estimated parameters are used to evaluate the performance of the drum through the calculation of the heat and mass transfer between the solid and the gas.

Several authors have carried out investigations on the steady state modeling of the rotary dryer and the rotary cooler processes. Static models are in general differential equations and they are suitable for investigation of static distributions. **Porter, 1963** and **Turner, 1966** were the first in considering heat transfer within a rotary cooler as an intermittent phenomenon constituted by a number of cooling and soaking periods. **Turner, 1966** developed an expression for the mean temperature of

spherical particles after a number of cooling and soaking periods. **Miller et al., 1942** present the first extensive study of heat transfer in rotary dryers and conclude that the total rate of heat transfer is affected by the number of flights. **Myklestad, 1963** was the first to obtain an expression to predict product moisture content throughout a rotary dryer based on drying air temperature, initial moisture content and product feed rate. **Sharples et al., 1964** developed a steady state model of a con-current fertilizer rotary dryer using a set of four differential equations to describe the heat and mass transfer and the material and energy balances. Considering that heat transfer depended on dryer rotational speed and flights holdup, they constructed an overall model but no results were presented to verify the accuracy of the model. **O'Donnell, 1975** developed a new equation to calculate retention time which was coupled with heat transfer equations to construct an overall complex and laborious dryer model. A simplified drying model was proposed by **Kisakurek, 1982** who assumed a constant solid temperature and neglected sensible heat effects. **Kamke and Wilson, 1986** studied wood particles rotary drying using a retention time equation similar to that of **Kelly and O'Donnell, 1977** and **Ranz and Marshall, 1952** equation to predict heat transfer. The model agreed with experimental values. They found that initial product moisture content and drying air temperature had the greatest effect on outlet product moisture content. **Rastikian et al., 1999**, developed a mathematical model describing sugar drying in a counter-current cascading rotary dryer from stationary profiles of temperature and moisture in order to determine the optimal values of heat and mass transfer coefficients. Mathematical modeling of woody biomass drying was developed by **Xu and Pang, 2008** and a new correlation between the theoretical maximum drying rate and the actual constant drying rate for the wood chips was proposed from the drying experiments. It was also found that the drying curve from the wood chips is within a falling rate drying period below the critical moisture of 55%. **Wardjiman et al., 2008** and **Wardjiman and Rhodes, 2009**, reported a study of the behavior of a curtain of particles falling through a horizontal flowing gas stream in a flighted rotary drum and later continued their research by studying the heat transfer. A steady and uniformly distributed stream of cold particles was fed through a rectangular slit and allowed to fall to form a curtain to investigate the heat transfer characteristic. Particle temperatures within the curtain and air temperatures outside the curtain were measured as a function of vertical position in the duct. A simple model based on single particle behavior was developed. The predicted solid temperatures agreed well

with the experimental results. However, the predictions for the gas temperatures were less satisfactory. **Afshar and Sheehan, 2012**, used a 3-D Eulerian-Eulerian CFD to simulate the convective heat transfer in free falling particle curtains. Total heat loss for curtaining particles falling a fixed distance was compared to heat loss for isolated single particles. Hot spherical silica particles with density of 2634 kg/m^3 at 400K of different particle diameters of 200 μm , 400 μm and 600 μm were examined at flow approximately 0.041 kg/s to 0.2 kg/s through a narrow slot in a rectangular box (0.45m \times 0.9m \times 0.225 m) filled with ambient air. The slot sizes through which the particles enter the rectangular box were 10mm, 30mm, 60mm and 80mm. Mesh dependency was performed by comparing the average properties of the falling curtain such as total heat loss per unit mass, as a function of mesh size. Mesh dependency was found to be independent of convergence and divergence of particle curtains and a 4mm mesh size was selected. The results for total heat loss at different slot sizes in the particle curtain simulations were compared to commonly used single particle heat transfer models. The results showed that modifying the inlet slot width at 0.041kg/s for 400 μm particles can lead to 13% increases in rates of convective heat transfer per unit mass. **Abbasfard et al., 2013**, mathematically modeled a rotary dryer used in the production of ammonium nitrate (AN) of concurrent flow studying the heat and mass transfer between solid and air. New correlations were proposed for AN equilibrium moisture and drying rate. The model was checked against the industrial data which showed a good agreement. The model predicts air and product moisture and temperature depending on working conditions of the rotary dryer. Regardless of the slope and speed of the dryer, inlet AN moisture and air temperature have been shown to be the variables that have the greatest effect, on the outlet moisture content of the product. **Le Guen et al., 2013**, experimentally studied the heat transfer analysis from an apparatus installed in a large-scale rotary drum reactor applied to the asphalt materials production. The equipment including in-situ thermal probes and external visualization by mean of infrared thermography gives rise to the longitudinal evaluation of inner and external temperatures. The assessment of the heat transfer coefficients were by an inverse methodology resolved in order to accomplish a fin analysis of the convective mechanism inside baffled (or flights) rotary drum. The results are discussed and compared with major results of the literature. They concluded that, the aggregates-to-wall contact (aggregates in the bed and into the baffles) can be considered as an

important convective transfer, similar to the gases-to-wall transfer. More investigations about convective mechanisms (aerothermal phenomena and aggregates-to-wall contact) are relevant to determine the wall thermal losses in order to design new equipments including power recovery for hot-mix asphalt processes.

The studies on dynamic simulation of rotary dryers and coolers are not so numerous in literature. In these models the system variables are dependent on both time and space. **Douglas et al., 1993** developed a dynamic model for sugar drying in a counter-current flow rotary dryer. Dryer was divided into 10 sections and dynamic heat and mass balances were set up in each section. Time retention and heat transfer were calculated after **Friedman and Marshall, 1949** and equilibrium was supposed to be reached in each elementary section. They validated the model with industrial data and studied dynamic behavior of the dryer when perturbations in several inlet variables were introduced. **Wang, 1993**, presented a non-equilibrium distributed-parameter model for rotary drying process based on the model of **Douglas et al., 1993**. The model consisted in a set of partial differential equations and they used different methods to predict heat transfer. Static and dynamic simulation studies were carried out. **Cao and Langrish, 2000** developed an overall system model for a counter-current rotary dryer. The model was based on heat and mass balances combined with two subsidiary models, one describing particle transport and heat transfer within the dryer and the other describing material drying kinetic. Six partial differential equations have been set up to evaluate six state variables: solids moisture content and temperature, air humidity and temperature, and solid and air hold up as functions of time and rotary dryer length. The model was validated in a pilot scale counter-current rotary dryer using sorghum and reasonable agreement between predicted and experimental values was found. **Iguaz et al., 2002** and **Iguaz et al., 2003**, developed a dynamic model to simulate the dehydration process of wastes of vegetable from a wholesale market in a rotary dryer. The dryer was divided into 10 sections and mass and energy balances were established in each of them. The results have been validated in a semi-industrial dryer. The model predicts air and product moisture and temperature depending on working conditions of the rotary dryer. Inlet air temperature has been shown to be the variable that has the greatest effect, on both outlet moisture content of the product and on outlet air temperature.

It is observed that, although several models have been proposed, there is not a general theory to describe the mechanism of heat and mass transfers of rotary drying and rotary cooling. It seems that specific models for an equipment and material are more useful than general models.

In the present study, a steady state model to solve for the temperature profiles in a rotary cooler (the case study described in Ch. 5) is proposed. This proposed model based on using experimental measurements from the current work: the estimated mean residence time and solid feed rate under the effect of varying the air flow rate.

6.2 Model description

The mechanism of heat transfer of an infinitesimal volume element of a rotary cooler operating at a counter-current flow is shown in Fig. 6.1. Where the solid material (to be cooled) is the source of heat, this heat content distributed mainly in to two parts the first is to the cold air stream (dQ_{sa}) and the second is to the wall of the drum (dQ_{sw}) that surrounded by the ambient air. The first part is dominant by convection, while the second part is dominant by radiation. Later on the heat transferred to the wall will leaks outside the drum as a heat loss to the surrounding air, its amount is determined according to the material type of the drum wall (drum wall thermal conductivity). After reaching steady state the drum wall will be able to give amount of heat to the interior air as shown by the part (dQ_{wa}).

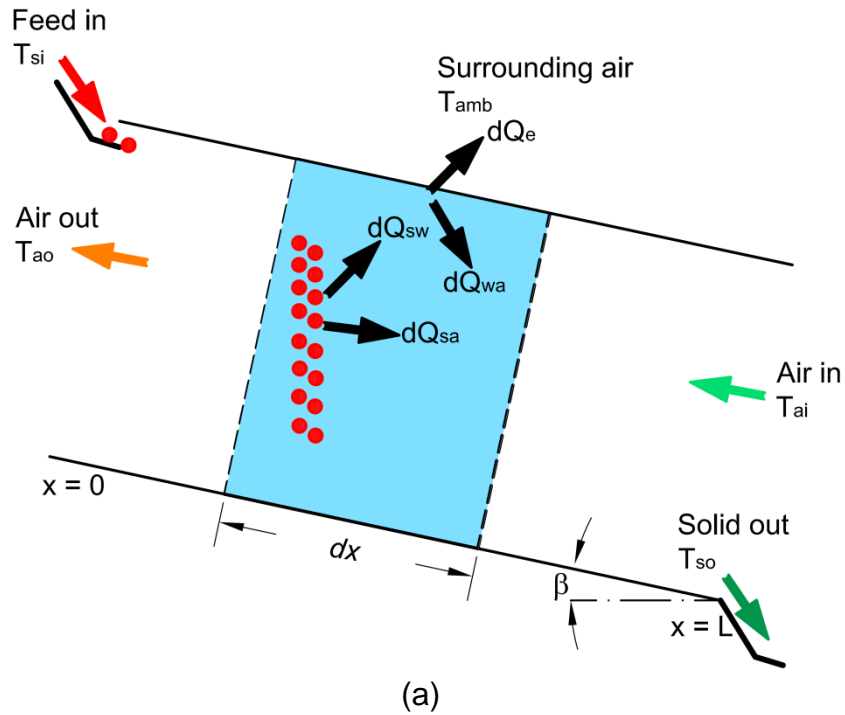


Figure 6.1: Heat transfer mechanism for an element in a rotary cooler with counter-current flow.

Applying the conservation of mass for the shown element in Fig. 6.1, at steady state and assuming no moisture content within the solids (dry solid material) reveals that;

$$\dot{m}_{si} = \dot{m}_{so} = \dot{m}_s \quad (6.1)$$

$$\dot{m}_{ai} = \dot{m}_{ao} = \dot{m}_a \quad (6.2)$$

where the subscript (s) refers to the solid and (a) to the air and (i) and (o) are inlet and outlet ports, respectively.

Applying the conservation of energy for the control volume by the solid material of the element shown in Fig. 6.1 considering; the total amounts of heat transfer, and assuming steady state, no moisture content with the solid, a set of two first order ordinary differential equations can be derived as will be shown in the followings;

$$-\dot{m}_s c_s dT_s = -dQ_s = dQ_a + dQ_e \quad (6.3)$$

where the subscript (e) refers to the heat transfer loss from the drum to the surrounding air. dQ_s is the **total** change in the heat rate of the solid material, \dot{m}_s is the solid mass flow rate, (c_s) is the solid material specific heat and dT_s is the change of the solid temperature along the drum.

The **total** change in the heat rate of the air (dQ_a) is given by

$$dQ_a = \dot{m}_a c_{p_a} dT_a = U_v dV (T_s - T_a) \quad (6.4)$$

where \dot{m}_a is the air mass flow rate, (c_{p_a}) is the air specific heat at constant pressure, dT_a is the change of the air temperature along the drum, dV is the element volume given by $dV = A dx$ where A is the drum cross section area $A = \pi R^2$ and U_v is the volumetric overall heat transfer coefficient between solid and air (in kW/m³K) it can be given from literature (**Foust et al., 1960 and Myklestad, 1963**) by

$$U_v = 0.52 \left(\frac{\dot{m}_a}{A} \right)^{0.8} \quad (6.5)$$

where A is the drum cross sectional area in m².

The **total** change in the loss heat rate from the drum to the surrounding can be estimated from the following relation

$$dQ_e = U_e 2\pi R dx (T_a - T_{amb}) \quad (6.6)$$

where (T_{amb}) is the surrounding air temperature and U_e is the overall heat loss coefficient in kW/m²K taken as (**Douglas at al., 1993 and Aruda et al., 2009**)

$$U_e = 0.022 \left(\frac{\dot{m}_a}{A} \right)^{0.879} \quad (6.7)$$

By the substitution of all of the parameters in Eqs. (6.3) and (6.4), and dividing by dx , two first order ordinary differential equations could be obtained and expressed as;

for solid,

$$\frac{dT_s}{dx} = \frac{-1}{\dot{m}_s c_s} \left[U_V \pi R^2 (T_s - T_a) + U_e 2\pi R (T_a - T_{amb}) \right] \quad (6.8)$$

and for air.

$$\frac{dT_a}{dx} = \frac{1}{\dot{m}_a c_{p_a}} \left[U_V \pi R^2 (T_s - T_a) \right] \quad (6.9)$$

The solution of the derived two ordinary differential equations will give information about the temperature profiles of solid and air along the drum length, respectively. In the present work, the two ordinary differential equations are to be solved simultaneously numerically using **Matlab ode - bvp solver** at known inlet conditions of temperatures and mass flow rates of solid and air.

6.3 Case study

6.3.1 Case study description

A real case study from industry was taken as an example to show the application of the heat transfer model. All technical specifications of the case study are shown in Fig. 6.2 and Table 6.1. The given data of the case study are fed to the heat transfer model in order to get information about the temperature profiles.

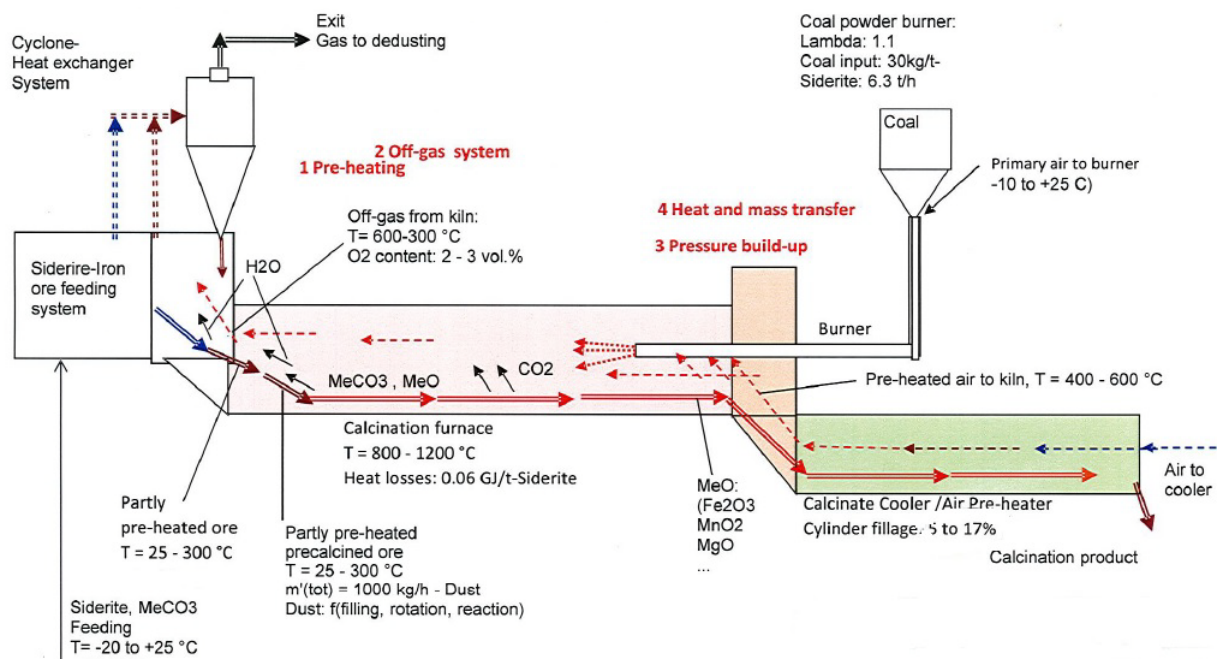


Figure 6.2: Cooler design from industry (Client Bilim Makina, Siderite calcinations project, Turkey).

Table 6.1: Technical specifications of the case study

Cooler dimensions:	Rotary cooler with $D = 5$ m; $L = 40$ m; $n_F = 18$; $l_2/l_1 = 0.75$ ($l_1 = 0.5$ m).
Solid material:	Siderite, $\dot{m}_s = 140$ t/hr (38.8 kg/s), $\rho_b = 2200$ kg/m ³ , $c_s = 1.4$ kJ/kg.K, $T_{Si} = 800^\circ\text{C}$.
Cooling gas:	Air $\dot{m}_a = 34.7$ kg/s (counter-current) $\rho = 1.29$ kg/m ³ , $cp_a = 1.007$ kJ/kg.K, $T_{ai} = 30^\circ\text{C}$.

6.3.2 Results

The results from solving Eqs. (6.8) and (6.9) gives information about the temperature profiles of the solid and air along the cooler for the prescribed operating conditions as shown in the following figures. Where z is a dimensionless length (position (x) / total cooler length (L))

Figure 6.2 illustrates the resulted temperature profiles of the solid and air along the cooler at two velocities of 0.2 and 0.5m/s. Figure 6.2 (a) depicts the case of counter current flow while Fig. 6.2 (b) depicts the case of con-current flow. It is obviously shown from Fig. 6.2 (a) for counter current flow case that the solid temperature is decreased over the length of the drum (cooling process), while the air temperature is increased in the opposite direction (heating process) because of the exchange of heat comes from the solid to the air. Also it can be seen that increasing the air velocity from 0.2 to 0.5 m/s increases the solid temperature difference due to the decrease in the solid mass flow rate. In contrary it decreases the air temperature difference due to the increase of the air mass flow rate.

Figure 6.2 (b) for the con-current flow type shows that the solid temperature is decreased over the length of the drum (cooling process), while the air temperature is increased in the same direction (heating process) because of the exchange of heat comes from the solid to the air. Also it can be seen that increasing the air velocity from 0.2 to 0.5 m/s increases the solid temperature difference due to the decrease in the solid mass flow rate. In contrary it decreases the air temperature difference due to the increase of the air mass flow rate. Full details of the results are outlined in Table 6.1 (a) and (b) including the varied parameters. Table 6.1 (a) shows the temperatures of both solid and air at inlet and outlet ports of the cooler and its differences including the calculations of the LMTD. While Table 6.1 (b) shows the heat transfer rate amounts of the solid and air and the heat loss to the surrounding. The comparison between the counter and con current flow types reveals that; the counter current flow type is better for the heat exchange between the solid and air in the cooler. As using the counter type flow type yields to much cooled solid temperature and much heated air temperature over the con-current flow type.

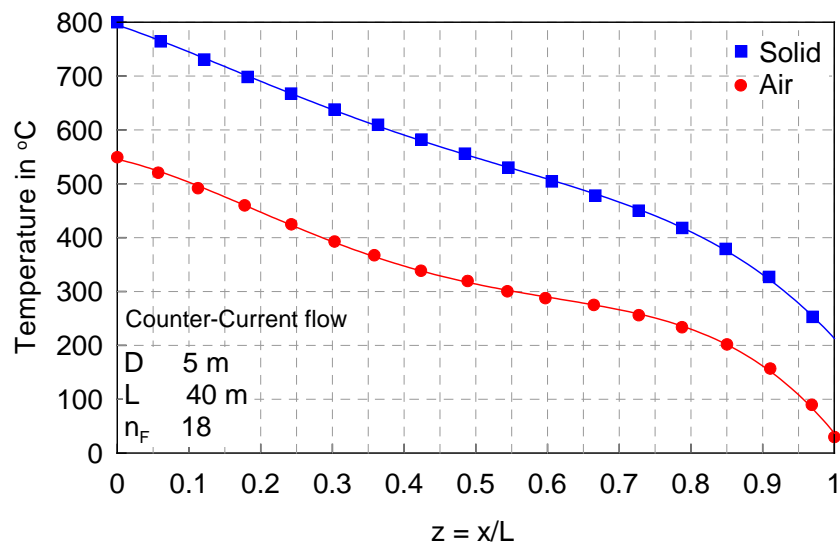


Figure 6.3: Temperature profiles of solid and air along the cooler.

Table 6.2: Results for heat transfer analysis

(a) temperatures

\dot{m}_a kg/s	\dot{m}_s kg/s	T_{si} °C	T_{so} °C	ΔT_s °C	T_{ai} °C	T_{ao} °C	ΔT_a °C	LMTD °C
34.7	38.8	800	202	598	30	540	510	213

Hint: For counter-current flow T_{si} and T_{ao} @ $z=0$ and T_{so} and T_{ai} @ $z=1$.

Table 6.2: (b) heat rates

U_v kW/m ³ .K (Eq. 6.5)	Q_s kW (Eq. 6.3)	Q_a kW (Eq. 6.4)	UA_{sur} kW/K ($Q_a/LMTD$)	Q_e kW ($=Q_s-Q_a$)	Q_e/Q_s %
0.75	32592	20750	111	11841.4	36.3

Hint: U is the overall heat transfer coefficient W/m².K

A_{sur} is the heat transfer surface area.

6.4 Defining the heat transfer area

The surface area responsible for heat transfer in a flighted rotary drum operated at optimum loading, mainly affected by the area of the solid material represented in the gas borne phase that contained within the cascaded curtains from the active flights.

The present work assumed two approaches for the estimation of the solid area contained in the curtains: the first is assuming the curtains are dense enough that may consider it as a rigid flat plate where the air is following over, thus the area here will be the sum of curtains surfaces; the second is assuming the curtains having less volume fraction of the solid particles, thus the air can penetrates between particles and the flow is like over sphere where the area here is the sum of all particles surface areas. In the following are application of the two approaches on the previously described case study in Sec. 6.3 using all the given data and material properties. It is worth noting that the two approaches neglect the part of heat transfer by radiation from the solid to the air, hence only convection were processed using known Nusselt correlations for each case (**Cengel, 2003** and **Incropera and DeWitt, 2006**). In order to proceed with the calculations to estimate the heat transfer area, the curtains dimensions should first be defined for the case study. Table 6.3 outlines the curtains specifications of the case study rotary drum.

Table 6.3: Curtains specifications

No. of curtains (No. of active flights)	8
Curtain length (drum length)	40 m
Average height of fall (\bar{h}_{fall})	3.1 m
Average thickness	0.18 m

6.4.1 First approach (flow over flat plate)

For the case of forced convection over flat plate (turbulent flow), the following Nusselt correlation can be used;

$$Nu_L = 0.037 Re_L^{0.8} Pr^{0.33} \quad (6.10)$$

where Pr is the Prandtl number (for air at 400 K, $Pr = 0.69$) and Re is the Reynolds number which can be calculated as follows;

$$Re_L = \frac{\rho_a u_a L}{\mu_a} \quad (6.11)$$

Thus the convection heat transfer coefficient could be estimated as follows;

$$h_{conv} = \frac{Nu k_a}{L} \quad (6.12)$$

k_a is the air thermal conductivity ($k_a = 0.0338$ W/m.K).

The heat transfer area here is the sum of the curtains surfaces parallel to the air flow;

$$A_{sur\ total} = \text{No. of curtains} \times \bar{h}_{fall} \times L \quad (6.13)$$

Then the product of h_{conv} and A_{sur} could be obtained and compared with values of UA_{sur} presented before in Table 6.2 (b).

6.4.2 Second approach (flow over a spherical particle)

This approach is assuming a certain solid volume fraction of the curtain volume (assumed = 0.8). For the case of forced convection over a sphere, the following Nusselt correlation (Ranze Marshal) can be used;

$$Nu_{dp} = 2 + 0.6 Re_{dp}^{0.5} Pr^{0.33} \quad (6.14)$$

where Reynolds number can be calculated as follows;

$$Re_{dp} = \frac{\rho_a u_r dp}{\mu_a} \quad (6.15)$$

u_r is the relative velocity discussed in details before in Ch. 5.

Thus the convection heat transfer coefficient could be estimated as follows;

$$h_{conv} = \frac{Nu k_a}{dp} \quad (6.16)$$

The heat transfer area in this case is the sum of all particles surface areas inside the curtains;

$$A_{sur\ total} = \text{No. of particles} \times \pi dp^2 \quad (6.17)$$

and the number of particles could be obtained as;

$$\text{No. of particles} = \text{No. of curtains} \times \frac{V_{solid, Curtain}}{V_{particle}} \quad (6.18)$$

$V_{solid, Curtain}$ is the volume of particles in one curtain which can be calculated using the assumed solid volume fraction as,

$$V_{solid, Curtain} = 0.8 \times \bar{h}_{fall} \times L \times \text{thickness} \quad (6.19)$$

and $V_{particle}$ is the particle volume which is the volume of a sphere $\frac{4}{3}\pi r_p^3$. Finally the product of h_{conv} and A_{sur} could be calculated.

Table 6.4 outlines the results of the calculated average heat transfer area based on the previously described two approaches. The calculated average area was estimated at different air velocities from 0.2 to 0.5 m/s for the same rotary cooler described in Sec 6.3. Also the product of $h_{conv}A_s$ is presented Table 6.4 and compared to the values of UA_s presented before in Table 6.2 (b). The comparison revealed that the current Nusselt correlations failed in the prediction of the heat transfer coefficients and a new fitting factor should be applied. The new factors for Nusselt correlations are listed in Table 6.4.

Table 6.4: Heat transfer area calculations

		First approach (flow over a flat plate)	Second approach (flow over a sphere)
A_{sur}	in m ²	1984	620944
$h_{conv}A_{sur}$	in kW/K	8	22
Nusselt factor		0.546	11.7

6.4.3 New suggested factors for Nusselt correlations

For dealing the curtains as flat plate

$$Nu_L = 0.546 Re_L^{0.8} Pr^{0.33} \quad (6.20)$$

For dealing with spherical particles in the curtains

$$Nu_{dp} = 11.7 (2 + 0.6 Re_{dp}^{0.5} Pr^{0.33}) \quad (6.21)$$

Chapter 7

Conclusions and Outlook

7.1 Conclusions

The new experimental technique that is presented in this thesis (Ch. 3) which is associated with carrying out experiments for rotary drums studies. Was found to be a good tool in assessing the optimum loading (design loading) of flighted rotary drums contrary to the traditional technique found from literature. This proved through the use of both image analysis methods:- manual and automated. However the manual method is reliable and may be more precise than the automated method, but it is more time consuming. The correlation developed based on all of the experimental results, including results from scaling up the size of the drum. Is useful to assess the design loading of a flighted rotary drum by directly substituting the operating parameters. The model developed for the axial transport can be used to determine the mean residence time of the solid through the drum depending on the current experimental results. The model described for the heat transfer can be used to obtain information about the temperature profiles of the solid and air along the drum. The new Nusselt factors proposed can be useful for the actual representation of the heat transfer inside a flighted rotary drum, but this needs a validation.

It is recommended based on the experimental results that a flight length ratio of 0.0 is not useful for the drums operated at design loading. In this case the solid amount is much less and the drum should be operated at overloading conditions. Also, special

care should be taken when using flight length ratio of 1.0 while using large number of flights as the experiments showed a formation of a solid bed at the bottom of the drum, which is inconsistent with the definition of design loading.

Based on the experimental results the following observations can be drawn: the required filling degree for the design loading point is more strongly influenced by the change in the number of flights and the flight length ratio than by other operating parameters of rotational speed or material properties. As an example, for glass beads of 0.7mm diameter the required f_D for design loading increased by about 48% when the n_F increased from 12 to 18 at the same l_2/l_1 , and it increased by about 75% when the l_2/l_1 increased from 0.375 to 0.75 at the same n_F , while the increase in the f_D w.r.t. the increase in the rpm was about 15%. The FUF cross sectional area of saturation is more influenced by the change in the flight dimensions than by other parameters. For example, glass beads of 0.7mm diameter the FUF area was observed to be nearly constant with the change in rotational speed and n_F , while the FUF area increased by about 65% when using a l_2/l_1 of 0.75 instead of 0.375. Finally, over the investigated ranges of operating parameters and based on the experimental results. It can be suggested that in order to ensure design loading, the volume occupied by the solid in a flighted rotary drum should be between 5-15% of the total drum volume.

7.2 Outlook

1. This study was focused only on dry particulate solid materials (free flowing). However in industry, many of the available particulate solid materials contains moisture and are to be processed and dried using different rotary drums. Thus it is recommended to examine cohesive solid materials.
2. Comparing the results of the calculated mean residence time, the present work axial transport model significantly deviated from available models from literature. That means the models from literature failed in the prediction of the current work mean residence time. As consequence, it is important to carry out further experiments to determine the mean residence time achieved by the solid through a real flighted drum.
3. It is recommended to validate the results from the model of the heat transfer by conducting experiments including the measurements of the temperature profiles of both the solid and the gas.

Bibliography

Abbasfard, H., Rafsanjani, H.H., Ghader, S., and Ghanbari, M. Mathematical modeling and simulation of an industrial rotary dryer: A case study of ammonium nitrate plant. *Powder Technology*, 239:499-505, 2013.

Afshar, S., and Sheehan, M.E. Using CFD to simulate heat transfer in particle curtains. *Proceeding of the Ninth International Conference on CFD in the Minerals and Process Industries*, CSIRO, Melbourne, Australia, 10-12, 2012.

Ajayi, O.O., and Sheehan, M.E. Application of image analysis to determine design loading in flighted rotary dryers. *Powder Technology*, 223:123-130, 2011.

Ajayi, O.O., and Sheehan, M.E. Design loading of free flowing and cohesive solids in flighted rotary dryers. *Chemical Engineering Science*, 73:400-411, 2012.

Alvarez, P.I., and Shene, C. Experimental study of residence time in a direct rotary dryer. *Drying Technology*, 12 (7):1629-1651, 1994.

Arruda, E.B., Lobato, F.S., Assis, A.J., and Barrozo, M.A.S. Modeling of fertilizer drying in roto-aerated and conventional rotary dryers, *Drying Technology*, 27:1192-1198, 2009.

Austin, L.G., Shoji, K., Hogg, R., and Carlson, J. Flow rates of dry powders in inclined rotating cylinders under open ended discharge conditions. *Powder Technology*, 20:219-225, 1978.

- Bagnold, R.A. Experiments on a gravity-free dispersion of large solid spheres in a Newtonian fluid under shear. 225(1160):49-63, 1954.
- Baker, C.G.J. The design of flights in cascading rotary dryers. *Drying Technology*, 6:4:631-653, 1988.
- Bierwisch, C.S. Numerical Simulations of Granular Flow and Filling. PhD thesis, University of Freiburg, Germany., 2009.
- Blumberg, W., and Schlünder, E.U. Transversale Schüttgut bewegung und konvektiver Stoffübergang in Drehrohren. Teil 2: Mit Hubschaufeln. *Chemical Engineering and Processing: Process Intensification*, 35(6):405-411, 1996.
- Boateng, A. Boundary layer modeling of granular flow in the transverse plane of a partially filled rotating cylinder. *International Journal of Multiphase Flow*, 24(3):499-521, 1998.
- Britton, P., Sheehan, M.E., and Schneider, P. A physical description of solids transport in flighted rotary dryers. *Powder Technology*, 165(3):153-160, 2006.
- Canales, E. Steady state modelling and simulation of an indirect rotary dryer. *Food Control*, 12(2):77-83, 2001.
- Cao, W.F., and Langrish, T.A.G. Comparison of residence time models for cascading rotary dryers. *Drying Technology*, 17(4):825-836, 1999.
- Cao, W.F., and Langrish, T.A.G. The development and validation of a system model for a counter-current cascading rotary dryer. *Drying Technology*, 18 (1 and 2):99-115, 2000.
- Cengel, Y.A. Heat transfer-A particle approach. International Ed., New York: McGraw-Hill, 2003.

- Cronin, K., Catak, M., Bour, J., Collins, A., and Smee, J. Stochastic modelling of particle motion along a rotary drum. *Powder Technology*, 213(1-3):79-91, 2011.
- de Gennes, P.G. Granular matter: a tentative view. *Reviews of Modern Physics*, 71(2):374-382, 1999.
- Douglas, P.L., Kwade, A., Lee, P.L., and Mallick, S.K. Simulation of a Rotary Dryer for Sugar Crystalline. *Drying Technology*, 11(1):129-155, 1993.
- Duchesne, C., Thibault, J., and Bazin, C. Modeling of the solids transportation within an industrial rotary dryer: A simple model. *Industrial and Engineering Chemistry Research*, 35(7):2334-2341, 1996.
- Duran, J. *Sands, Powders, and Grains: An Introduction to the Physics of Granular Materials* (translated by A. Reisinger). Springer-Verlag New York, Inc., New York, 1999.
- Elperin, T., and Vikhansky, A. Granular flow in a rotating cylindrical drum. *Europhysics Letters*, 42(6):619-624, 1998.
- Evesque, P. Shaking Dry Powders and Grains. *Contemporary Physics*, 33:245-261, 1992
- Foust, A.S., Wenzel, L.A., Clump, C.W., Maus, L., and Andersen, L.B. *Principles of Unit Operations*. Wiley, New York, 1960.
- Frette, V., Christensen, K., Malthé-Sørensen, A., Feder, J., Jøssang, T., and Meakin, P.. Avalanche dynamics in a pile of rice. *Nature*, 379(6560):49-52, 1996.
- Friedman, S.J., and Marshall, W.R. Studies in rotary drying: Part 1 - holdup and dusting. *Chemical Engineering Progress*, 45:482- 573, 1949.

Geng, F., Yuan, Z., Yan, Y., Luo, D., Wang, H., Li, B., and Xu, D. Numerical simulation on mixing kinetics of slender particles in a rotary dryer. *Powder Technology*, 193(1):50-58, 2009.

Gerhartz, W. *Ullmann's Encyclopedia of Industrial Chemistry*, 2:243–252, 1985.

Glikin, P.G. Transport of solids through flighted rotating drums. *Trans. Inst. Chem. Eng.*, 56:120-126, 1978.

Gray, J.M.N.T. Granular flow in partially filled slowly rotating drums. *Journal of Fluid Mechanics*, 441:1-29, 2001.

Heffels, C., Willemse, A., and Scarlett, B. Possibilities of near backward light scattering for characterizing dense particle systems, *Powder Technol.* 86:127-135, 1996.

Henein, H., Brimacombe, J.K., and Watkinson, A.P. Experimental study of transverse bed motion in rotary kilns. *Metallurgical Transactions B*, 14B:191-205, 1983.

Iguaz, A., Esnoz, A., Martinez, G., López, A., and Vírveda, P. Mathematical modeling and simulation for the drying process of vegetable wholesale by-products in a rotary dryer, *Journal of Food Engineering* 59:151-160, 2003.

Iguaz, A., Lopez, A., and Vírveda, P. Influence of air recycling on the performance of a contiguous rotary dryer for vegetable wholesale by-products. *Journal of Food Engineering* 54:289-297, 2002.

Incropera, F.P., and DeWitt, D.P. *Fundamental of heat and mass transfer*. 6th Ed., New York: Jone Wiley & Sons, 2006.

Jaeger, H.M., and Nagel, S.R. Physics of the granular state. *Science*, 255:1523-1531, 1992.

- Jop, P., Forterre, Y., and Pouliquen, O. A constitutive law for dense granular flows. *Nature*, 441(7094):727-30, 2006.
- Kadanoff, L.P. Built Upon Sand: Theoretical Ideas Inspired by Granular Flows. *Reviews of Modern Physics*, 71: 435-444, 1999.
- Kamke, F.A., and Wilson, J.B. Computer simulation of a rotary dryer. Part II: Heat and mass transfer. *American Institute of Chemical Engineers Journal*. 32:269-275, 1986.
- Kamke, F.A., and Wilson, J.B. Computer simulation of a rotary dryer. Part I: Retention time. *AIChE Journal*, 32(2):263-268, 1986.
- Karimi, M., Akdogan, G., Dellimore, K., Bradshaw, H., and Steven, M. Comparison of different drag coefficient correlations in the CFD modeling of a laboratory-scale Rushton-turbine flotation tank. Ninth International Conference on CFD in the Minerals and Process Industries CSIRO, Melbourne, Australia, 10-12, 2012..
- Keey, R.B. *Drying: Principles and Practice*. Pergamon Press, Oxford, UK, 1972.
- Kelly, J.J. Flight design in rotary dryers. *Drying Technology*, 10 (4): 979-993, 1992.
- Kelly, J.J., and O'Donnell, J.P. Residence time model for rotary drums. *Trans. IChemE*, 55:243-252, 1977.
- Kemp, I.C., and Oakley, D.E. Simulation and scale-up of pneumatic conveying and cascading rotary dryers. *Drying Technology*, 15(6-8):1699-1710, 1997.
- Khakhar, D.V., Orpe, A.V., Andresen, P., and Ottino, J.M. Surface flow of granular materials: model and experiments in heap formation. *Journal of Fluid Mechanics*, 441:255-264, 2001.

- Kim, K., Siegel, N., Kolb, G., Rangaswamy, S., and Moujaes, S.F. A study of solid particle flow characterization in solar particle receiver, *Solar Energy*, 83:1784-1793, 2009.
- Kisakurek, B. Retention time in a rotary dryer in: J.C. Ashworth (Ed.). *Proc. Int. Drying Symp.* Wolver Hampton, England, 1982.
- Krokida, M., Marinos-Kouris, D., and Mujumdar, Arun S. Handbook of industrial drying. In A.S. Mujumdar, editor, *Rotary Drying*, pages 151-172. Taylor & Francis Group, 3rd edition, 2007.
- Kröll, K. Trockner und Trocknungsverfahren. In *Trocknungstechnik*, volume 2, chapter 2, pages 444-461. Springer-Verlag, Berlin, 1978.
- Le Guen, L., Huchet, F., Dumoulin, J., Baudru, Y., and Tamagny, P. Convective heat transfer analysis in aggregates rotary drum reactor, *Applied Thermal Engineering* 54:131-139, 2013.
- Lee, A., and Sheehan, M.E. Development of a geometric flight unloading model for flighted rotary dryers. *Powder Technology*, 198(3):395-403, 2010.
- Lisboa, M.H., Vitorino, D.S., Delaiba, W.B., Finzer, J.R.D., and Barrozo, M.A.S. A study of particle motion in rotary dryer. *Brazilian Journal of Chemical Engineering*, 24(3):365-374, 2007.
- Liu, X., Specht, E., and Mellmann, J. Experimental study of the lower and upper angles of repose of granular materials in rotating drums. *Powder Technology*, 154 (2-3):125-131, 2005.
- Liu, X., Zhang, C., and Zhan, J. Quantitative comparison of image analysis methods for particle mixing in rotary drums. *Powder Technology*, 282:32-36, 2015.
- Longo, S. and Lamberti, A. Grain shear flow in a rotating drum. *Experiments in Fluids*, 32(3):313-325, 2002.

Massana, R., Gasol, J., Bjørnsen, P., Blackburn, N., Hagström, Å.S.H., Hygum, B., Kuparinen, J., and Pedrós-alió, C. Measurement of bacterial size via image analysis of epifluorescence preparations: description of an inexpensive system and solutions to some of the most common problems. *Scientia Marina* 61 (3), 397-407, 1997.

Matchett, A.J., and Baker, J. Particle residence times in cascading rotary dryers. part 1-derivation of the two-stream model. *J Separ Proc Technol*, 8:11-17, 1987.

Matchett, A.J., and Baker, J. Particle residence times in cascading rotary dryers. part 2-application of the two-stream model to experimental and industrial data. *J Separ Proc Technol*, 9:5-13, 1988.

Maxey, M.R., and Riley, J. Equation of motion for a small rigid sphere in a turbulent fluid flow. *Phys. Fluids* 26:883-889, 1983.

Mellmann, J. The transverse motion of solids in rotating cylinders-forms of motion and transition behavior. *Powder Technology*, 118(3):251-270, 2001.

Mellmann, J. Zonales Feststoffmassenstrommodell für ammenbeheizte Drehrohrreaktoren. PhD thesis, TU Magdeburg, Germany, 1989.

Mellmann, J., and Specht, E. Mathematical modeling of the transition behavior between the various forms of transverse motion of bulk materials in rotating cylinders. *ZKG International*, 54: 281-296 and 380-402, 2001.

Menon, N. and Durian, D.J. Particle Motions in a Gas-Fluidized Bed of Sand. *Physics Review*, 79:3407-3410, 1997.

Midi, GDR. On dense granular flows. *The European Physical Journal E*, 14(4):341-365, 2004.

Miller, C.O., Smith, B.A., and Schuette, W.H. Factors influencing the operation of rotary dryers. part ii. the rotary dryer as a heat exchanger. *Transaction, American Institution of Chemical Engineers*, (38):841-864, 1942.

Miskell, F., and Marshall, W.R. A study of retention time in a rotary dryer. *Chemical Engineering Progress*, 52(1):35-38, 1956.

Moyers, C.G., and Baldwin, G.W. Psychrometry, evaporative cooling, and solids drying. In D. W. Green, editor, *Perry's Chemical Engineers Handbook*, chapter 12. McGraw-Hill, 7th edition, 1997.

Mujumdar, Arun S. Principles, classification, and selection of dryers. In A. S. Mujumdar, editor, *Handbook of Industrial Drying*, pages 4-31. Taylor & Francis Group, 3rd edition, 2007.

Myklestad, O. Heat and mass transfer in rotary dryers. *Chemical Engineering Progress Symposium Series*, 59(41):129-137, 1963.

Obadiat, T.M., Al-Masaeid, H.R., Gharaybeh, F., and Khedaywi, T.S. An innovative digital image analysis approach to quantify the percentage of voids in mineral aggregates of bituminous mixtures, *Canadian Journal of Civil Engineering* 25 (6): 1041-1049.1998 ,

O'Donnell, P. Heat transfer studies in rotary coolers, Ph.D. thesis, University College, Dublin, 1975.

Papadakis, S.E., Langrish, T.A.G., Kemp, I.C., and Bahu, R.E. Scale-up of cascading rotary dryers. *Drying Technology*, 12(1):259-277, 1994.

Perron, J., and Bui, R.T. Rotary cylinders: transverse bed motion prediction by rheological analysis. *The Canadian Journal of Chemical Engineering*, 70:223-231, 1992.

Perry, R.H., and Green, D.W. *Chemical Engineers Handbook*. McGraw-Hill, New York, 1999.

Porter, S.J. The design of rotary driers and coolers. *Trans. Inst. Chem. Eng.*, 41:272-280, 1963.

Raghavan, G.S.V., Rennie, T.J., Sunjka, P.S., Orsat, V., Phaphuangwittayakul, W., and Terdtoon, P. Overview of new techniques for drying biological materials with emphasis on energy aspects. *Brazilian Journal of Chemical Engineering*, 22(2):195-201, 2005.

Ranz, W.E., and Marshall, W.R. Evaporation from drops. I, II. *Chemical Engineering Progress*. 48(3):141-173, 1952.

Rastikian, K., Capart, R., and Benchimol, J. Modelling of sugar drying in a countercurrent cascading rotary dryer from stationary profiles of temperature and moisture. *Journal of Food Engineering*, 41:193-201, 1999.

Renaud, M., Thibault, J., and Trusiak, A. Solids transportation model of an industrial rotary dryer. *Drying Technology*, 18(4):843-865, 2000.

Revol, D., Briens, C.L., and Chabagno, J.M. The design of flights in rotary dryers. *Powder Technology*, 121(2-3):230-238, 2001.

Rodhes, M. *Principles of powder technology*. John Wiley & Sons, 1997.

Rojas, R., Pina, J., and Bucala, V. Solids transport modeling in a fluidized drum granulator. *Industrial and Engineering Chemistry Research*, 49:6986-6997, 2010.

Savaresi, S.M., Bitmead, R.R., and Peirce, R. On modelling and control of a rotary sugar dryer. *Control Engineering Practice*, 9(3):249-266, 2001.

Shahhosseini, S., Cameron, I.T., and Wang, F. A simple dynamic model for solid transport in rotary dryers, *Drying Technol.* 18, 867-886, 2000.

Sharples, K., Glikin, P.G., and Warne, R. Computer simulation of rotary dryers. *Transactions of the Institute of Chemical Engineers*, 42:T275-T284, 1964.

Sheehan, M.E., Britton, P., and Schneider, P. A model for solids transport in flighted rotary dryers based on physical considerations. *Chemical Engineering Science*, 60 (15):4171-4182, 2005.

Shene, C., Cuhillos, F., Perez, R. and Alvarez, P.I. Modelling and simulation of a direct contact rotary dryer. *Drying technology*, 14(10):2419-2433, 1996.

Sherritt, R.G., Caple, R., Behie, L.A., and Mehrotra, A.K. The movement of solids through flighted rotating drums. part i: Model formulation. *The Canadian Journal of Chemical Engineering*, 71(3):337-346, 1993.

Shirley, A.R., Nunnally, L.M., and Carney, F.T. Melt granulation of urea by the falling-curtain process. *Industrial & Engineering Chemistry Product Research and Development*, 21:617-620, 1982.

Smith, B.A. Factors influencing rotary dryer performance. *Transactions, American Institution of Chemical Engineers*, 38:251-257, 1942.

Song, Y., Thibault, J., and Kudra, T. Dynamic characteristics of solids transportation in rotary dryers. *Drying Technology*, 21(5):755-773, 2003.

Sullivan, J.D., Maier, C.G., and Ralston, O.C. Passage of solid particles through rotary cylindrical kilns. U.S. Bureau of Mines Tech Paper 384, page 44, 1927.

Sunkara, K.R. Granular flow and design studies in flighted rotating drums. PhD thesis, Otto von Guericke University Magdeburg, Germany, 2013.

Sunkara, K.R., Herz, F., Specht, E., and Mellmann, J. Influence of flight design on the particle distribution of a flighted rotating drum. *Chemical Engineering Science*, 90:101-109, 2013.

Sunkara, K.R., Herz, F., Specht, E., and Mellmann, J. Transverse flow at the flight surface in flighted rotary drum. *Powder Technology*, 275:161-171, 2015.

Sunkara, K.R., Herz, F., Specht, E., Mellmann, J., and Erpelding, R. Modeling the discharge characteristics of rectangular flights in a flighted rotary drum. *Powder Technology*, 234:107-116, 2013.

- Tarhana, S., Telci, I., Tuncay, M.T., and Polatci, H. Product quality and energy consumption when drying peppermint by rotary drum dryer. *Industrial Crops and Products* 32:420-427, 2010.
- Thibault, J., Alvarez, P.I., Blasco, R. and ,Vega, R. Modelling the Mean Residence Time in a Rotary Dryer for Various Types of Solids, *Drying Technology: An International Journal*, 28(10):1136-1141, 2010.
- Tscheng, S.H. Convective heat transfer in a rotary kiln. PhD thesis, The University of British Columbia, 1978.
- Turner, G.A. The thermal history of a granule in a rotary cooler. *Canadian Journal of Chemical Engineering*, 44:13-16, 1966.
- Van Puyvelde, D.R. Modelling the hold up of lifters in rotary dryers. *Chemical Engineering Research and Design*, 87(2):226-232, 2009.
- Van Puyvelde, D.R., Young, B.R., Wilson, M.A., and Schmidt, S.J. Experimental determination of transverse mixing kinetics in a rolling drum by image analysis. *Powder Technology*, 106:183-191, 1999.
- Van't Land, C.M. *Industrial Drying Equipment Selection and Application*. Marcel Dekker, Inc., 1991.
- Wang, F.Y., Cameron, I.T., and Litsler, J.D. Further theoretical studies on rotary drying processes represented by distributed systems. *Drying Technology*, 13(3):737-751, 1995.
- Wang, F.Y., Cameron, I.T., Lister, J.D., and Douglas, P.L. A distributed parameter approach to the dynamics of rotary drying processes. *Drying Technology*. 11(7):1641-1656, 1993.
- Wardjiman, C., and Rhodes, M. Heat transfer in a particle curtain falling through a horizontally-owing gas stream. *Powder Technology*, 191(3):247-253, 2009.

Wardjiman, C., Lee, A., Sheehan, M.E., and Rhodes, M. Behaviour of a curtain of particles falling through a horizontally-owing gas stream. *Powder Technology*, 188(2):110-118, 2008.

Williams-Gardner, A. Industrial drying. In *Rotary Dryers*, chapter 7, pages 121-150. Chem. & Proc. Eng. Ser., London Hill, 1971.

Xu, Q., and Pang, Sh. Mathematical modeling of rotary drying of woody biomass, *Drying Technology* 26:1344-1350, 2008.

Internet web links

- [1] https://en.wikipedia.org/wiki/Granular_material
<http://cliparts.co/hourglass-clipart>
<http://www.physicscentral.com/explore/action/granular.cfm>
- [2] http://www.diytrade.com/china/pd/12133668/cement_rotary_kiln_wit_h_ISO.html
<http://www.cementplantmanufacturer.com/rotary-kiln-751462.html>

List of publications of the current work

Mohamed A. Karali, Koteswara Rao Sunkara, Fabian Herz and Eckehard Specht, 2015. "Experimental analysis of a flighted rotary drum to assess the optimum loading", *Chemical Engineering Science*, under review.

Mohamed A. Karali, Fabian Herz and Eckehard Specht, July, 2015, "Experimental Determination of the Discharge Characteristics of a Flighted Rotary Drum Operated at Optimum Loading. Proceedings of joint conference of 5th UK-China and 13th UK Particle Technology Forum, Leeds - United Kingdom.

Mohamed A. Karali, Fabian Herz, Eckehard Specht and Jocken Mellmann, 2015. "Comparison of image analysis methods to determine the optimum loading of flighted rotary drums", *Powder Technology*, under review.

Curriculum Vitae

First Name Mohamed
Father Name Ahmed Mahmoud
Family name Karali
Nationality Egyptian
Date of birth 01.12.1979
Place of birth Kalyobiya, Ägypten
Marital status Married with a child
Email mohamedkarali@yahoo.com
karali@ovgu.de



Current position Lecturer at the faculty of Engineering and Technology, Future University, Cairo, Egypt.
Studying

1996-2001 B.Sc. in Mechanical Engineering, Helwan University, faculty of Engineering - Mataria, Cairo, Egypt.

2003-2007 M.Sc. in Mechanical Engineering, Helwan University, faculty of Engineering - Mataria, Cairo, Egypt. Thesis entitled "Performance evaluation a vapor compression refrigeration system using R22 alternatives".

2009-2011 PhD study in Mechanical Engineering, Helwan University, faculty of Engineering - Mataria, Cairo, Egypt.

PhD topic registration "Heat transfer augmentation using water - based Nano-fluids containing different metallic Nano-particles".

2012-2015 PhD study, Otto-von-Guericke Universität Magdeburg, Fakultät für Verfahrens und Systemtechnik, Institut für Strömungstechnik und Thermodynamik, Germany.

PhD topic "Analysis study of the axial transport and heat transfer of a flighted rotary drum operated at optimum loading".

Mohamed A. Karali

***Magdeburg,
06.07.2015***